COLOR ENHANCEMENT OF TOURMALINE BY ELECTRON BEAM IRRADIATION

Miss Waratchanok Suwanmanee

จุฬาลงกรณ์มหาวิทยาลัย
CHULALONGKORN UNIVERSITY

A Thesis Submitted in Partial Fulfillment of the Requirements

for the Degree of Master of Science in Geology

Department of Geology

Faculty of Science

Chulalongkorn University

Academic Year 2019

Copyright of Chulalongkorn University

การปรับปรุงสีของทัวร์มาลีนโดยวิธีการฉายรังสีจากเครื่องเร่งอนุภาคอิเล็กตรอน

น.ส.วรัตน์ชนก สุวรรณมณี

จุฬาลงกรณ์มหาวิทยาลัย
CHULALONGKORN UNIVERSITY

วิทยานิพนธ์นี้เป็นส่วนหนึ่งของการศึกษาตามหลักสูตรปริญญาวิทยาศาสตรมหาบัณฑิต
สาขาวิชาธรณีวิทยา ภาควิชาธรณีวิทยา
คณะวิทยาศาสตร์ จุฬาลงกรณ์มหาวิทยาลัย
ปีการศึกษา 2562
ลิขสิทธิ์ของจุฬาลงกรณ์มหาวิทยาลัย

Thesis Title	Color Enhancement of Tourmaline by Electron Beam Irradiation
By	Miss Waratchanok Suwanmanee
Field of Study	Geology
Thesis Advisor	Professor Dr. Chakkaphan Sutthirat, Ph.D.
Thesis Co Advisor	Dr. Bhuwadol Wanthanachaisaeng, Ph.D.

Accepted by the Faculty of Science, Chulalongkorn University in Partial Fulfillment of the Requirement for the Master of Science

..... Dean of the Faculty of Science
(Professor Polkit Sangvanich, Ph.D.)

Thesis Committee

..... Chairman
(Assist. Professor Dr. Vichai Chutakositkanon, Ph.D.)

..... Thesis Advisor
(Professor Dr. Chakkaphan Sutthirat, Ph.D.)

..... Thesis Co-Advisor
(Dr. Bhuwadol Wanthanachaisaeng, Ph.D.)

..... Examiner
(Dr. Alongkot Fanka, Ph.D.)

..... External Examiner
(Dr. Chatree Saiyasombat, Ph.D.)

จุฬาลงกรณ์มหาวิทยาลัย
Chulalongkorn University

วรัตน์ชนก สุวรรณมณี: การปรับปรุงสีของทัวร์มาลีนโดยวิธีการฉายรังสีจากเครื่องเร่งอนุภาคอิเล็กตรอน. (Color Enhancement of Tourmaline by Electron Beam Irradiation). อาจารย์ที่ปรึกษาวิทยานิพนธ์หลัก: ศ. ดร. จักรพันธ์ สุทธิรัตน์, อาจารย์ที่ปรึกษาวิทยานิพนธ์ร่วม: ดร. ภูวดล วรรธนะชัยแสง, 128 หน้า

ทัวร์มาลีนเป็นพลอยเนื้ออ่อนที่ค่อนข้างได้รับความนิยมในตลาดอัญมณี โดยเฉพาะทัวร์มาลีนสีแดงที่เรียกว่า รูเบลไลท์ ปัจจุบันผู้ประกอบการนิยมนำทัวร์มาลีนสีชมพูไปฉายรังสีแกมมาเพื่อเพิ่มความเข้มสี ในการศึกษานี้จึงเลือกวิธีในการปรับปรุงคุณภาพสีทัวร์มาลีนด้วยการฉายด้วยรังสีอิเล็กตรอนพลังงานสูง จากเครื่องเร่งอนุภาคอิเล็กตรอน และการฉายรังรังสีแกมมา เพื่อทำการเปรียบเทียบสีที่เข้มขึ้นจากรังสีทั้งสองชนิด ที่ปริมาณรังสี 3 ระดับได้แก่ 400, 800 และ 1,200 กิโล-เกรย์ โดยตัวอย่างทัวร์มาลีนที่นำมาทดลองมาจากประเทศไนจีเรีย มีสีชมพูและสีเขียว โดยแต่ละตัวอย่างจะถูกตัดแบ่งออกเป็น 2 ส่วนสำหรับการฉายรังสีสองชนิด จากการศึกษาองค์ประกอบทางเคมีของตัวอย่างทัวร์มาลีนพบว่าเป็นทัวร์มาลีนชนิดเอลเบไอต์ สเปกตรัมการดูดกลืนแสงในช่วงแสงอัลตราไวโอเลต-แสงมองเห็นที่ตำแหน่งการดูดกลืน 300-850 นาโนเมตร ทัวร์มาลีนสีชมพูพบการดูดกลืนแสงเด่นชัดในช่วงแสงสีน้ำเงิน-เขียว ที่ตำแหน่งประมาณ 515 นาเมตร สัมพันธ์กับการเกิดสีชมพูเนื่องจากอิทธิพลของ Mn^{3+} และแถบการดูดกลืนรองในช่วงแสงสีม่วงที่ตำแหน่งประมาณ 395 นาโนเมตร สัมพันธ์กับสีเหลืองเนื่องจากอิทธิพลของ Mn^{2+} ภายหลังการนำตัวอย่างไปฉายรังสีอิเล็กตรอนและรังสีแกมมา พบว่าทัวร์มาลีนสีชมพูที่ผ่านการฉายรังสีอิเล็กตรอนแสดงการเปลี่ยนแปลงสีที่เข้มขึ้นกว่า ความเข้มแถบการดูดกลืนแสงที่ตำแหน่งประมาณ 515 และ 395 นาโนเมตรเพิ่มขึ้นสูงกว่าทัวร์มาลีนสีชมพูที่ผ่านการฉายรังสีแกมมา ประกอบกับทัวร์มาลีนสีชมพูที่มีค่าสัดส่วนระหว่างแมงกานีสต่อเหล็กสูงกว่าจะให้สีชมพูเข้มขึ้นกว่า ทั้งนี้ภายหลังการฉายรังสีสำหรับทัวร์มาลีนสีชมพูพบสัญญาณศูนย์กลางการเกิดสี 2 แบบ ได้แก่ O^- center (hole color center) และ H^0 center (electron color center) สำหรับทัวร์มาลีนสีเขียวที่ผ่านการฉายรังสีแสดงเฉดสีเหลืองเพิ่มขึ้นเล็กน้อยโดยสัญญาณศูนย์กลางการเกิดสี O^- center ชนิดเดียว ดังนั้นสามารถสรุปได้ว่าสีที่เกิดขึ้นภายหลังการฉายรังสีมีสาเหตุจาก color center โดยสีชมพูที่เข้มขึ้นสอดล้องกับ H^0 center ร่วมกับมลทินธาตุแมงกานีส ขณะที่เฉดสีเหลืองที่เกิดขึ้นมีอิทธิพลมาจาก O^- center

ภาควิชา	ธรณีวิทยา	ลายมือชื่อนิสิต	_____
สาขาวิชา	ธรณีวิทยา	ลายมือชื่อ อ.ที่ปรึกษาวิทยานิพนธ์หลัก	_____
ปีการศึกษา	2562	ลายมือชื่อ อ.ที่ปรึกษาวิทยานิพนธ์ร่วม	_____

6072094523: MAJOR GEOLOGY

Keywords: Irradiation / Color Enhancement / Tourmaline/ EPMA / UV-Vis spectroscopy / Color Center

Waratchanok Suwanmanee: Color Enhancement of Tourmaline by Electron Beam Irradiation. Advisor: Professor Dr. Chakkaphan Sutthirat, Ph.D., Co-advisor: Dr. Bhuwadol Wanthanachaisaeng, Dr. rer. Nat., 128 pp.

Tourmaline is a semi-precious stone that is quite popular in gem market. Red-purple tourmaline, so-called “Rubellite”, is particularly famous. Consequently, pink tourmalines have recently been enhanced by gamma radiation to intensify color as rubellite. In this study, an electron beam technique was applied for experimental treatment. Moreover, gamma ray irradiation was also applied to treat the same sample collection for comparison. Color enhancement was designed for both radiations at three levels of doses, i.e., 400, 800, and 1,200 kilogreys. Pink and green tourmalines from Nigeria were collected for the experiment. Each sample was cut into two tablets for experimental irradiations using e-beam and gamma ray. Based on chemical compositions, these samples were identified as elbaite. The UV-Vis absorption spectra (300-850 nm) of pink tourmalines showed the maximum absorption band in blue-green range around 515 nm, which was caused by Mn^{3+} yielding pink color. The minor absorption band was also observed in purple range (about 395 nm) causing yellow which related to Mn^{2+}. As the results, electron beam irradiation produced more intense pink which absorption bands at 395 and 515 nm were intensified after irradiation. Therefore, e-beam irradiation provides more efficiency for intensification of pink color in tourmaline. Moreover, higher Mn/Fe ratio in sample yielded more intense pink after irradiation. Two color centers, O^- center (hole color center) and H^0 center (electron color center), appeared in pink tourmalines after irradiation . For green tourmalines, yellow shade appeared slightly after both irradiation techniques. The irradiated green tourmalines after both types of radiation presented only O^- center signal in EPR spectra. Therefore, it can be assumed that the intense pink color after irradiation is probably related to H^0 center (electron color center) with involvement of Mn impurity. On the other hand, yellow tonality produced after irradiation is caused by O^- center (hole color center).

จุฬาลงกรณ์มหาวิทยาลัย
CHULALONGKORN UNIVERSITY

Department:	Geology	Student’s signature	_____
Field of study:	Geology	Advisor’s signature	_____
Academic of year:	2019	Co-advisor’s signature	_____

ACKNOWLEDGEMENTS

I would like to acknowledge thesis advisors, Professor Dr. Chakkaphan Sutthirat and Dr. Bhuwadol Wanthanachaisaeng for their patience, guidance and mentorship throughout my graduate education and completion of thesis.

Special acknowledgements are sent to: Dr. Bhuwadol Wanthanachaisaeng, College of Creative Industry, Srinakarintrawirot University, for providing samples used in this research; Assistant Professor Dr. Somruedee Satitkhun, Department of Earth Sciences, Faculty of Science, Kasetsart University, for technical supervision in UV-Vis-NIR spectrophotometry; Mr. Thanapong Lhuaamporn of the Gem and Jewelry Institute of Thailand (GIT) for assistance in Fourier Transform Infrared (FTIR) spectrometry; Mrs. Sopit Pumpuang, Department of Geology, Chulalongkorn University, for assistance in Electron Probe Microanalysis (EPMA). Gem Irradiation Center, Thailand Institute of Nuclear Technology, provided electron accelerator and gamma laboratory for the gem treatment experiment.

Faculty of Science, Chulalongkorn University provide for partial exemption of tuition fee. This research was funded by the 90th Anniversary of Chulalongkorn University Fund (Ratchadaphiseksomphot Endowment Fund).

Finally, my special appreciation is delivered to friends in Burapha University and Chulalongkorn University as well as my family for their support, understanding, friendship, and trustfulness which really encouraged me to pass through all the stress and difficulty during the last two years. I could not have done this without all of them.

Waratchanok Suwanmanee

จุฬาลงกรณ์มหาวิทยาลัย
Chulalongkorn University

TABLE OF CONTENT

Page

THAI ABSTRACT..... IV

ENGLISH ABSTRACT..... V

ACKNOWLEDGEMENTS..... VI

CONTENTS..... VII

LIST OF TABLES..... IX

LIST OF FIGURES..... X

CHAPTER I..... 1

INTRODUCTION..... 1

1.1 Background and Significance of Research..... 1

1.2 Research objectives..... 2

1.3 Scope of study..... 3

1.4 Research methodology..... 3

1.5 Expected results..... 5

CHAPTER II..... 6

LITERATURE REVIEWS..... 6

2.1 Tourmaline..... 6

2.2 Tourmaline formation..... 16

2.3 Irradiation..... 18

CHAPTER III..... 22

MATERIAL AND METHODOLOGY..... 22

3.1 Material..... 22

3.2 Methodology..... 22

CHAPTER IV..... 43

PHYSICAL AND GEMOLOGICAL PROPERTIES..... 43

จุฬาลงกรณ์มหาวิทยาลัย
CHULALONGKORN UNIVERSITY

Page

4.1 Physical Properties..... 43
4.2 Microscopic Internal Feature..... 44
4.3 Chemical Compositions..... 46
4.4 Structural Analysis with Raman Shift..... 50
4.5 Hydroxyl group..... 55
4.6 UV-Vis spectroscopy..... 59
4.7 Oxidation states of Manganese and Iron..... 61

CHAPTER V..... 63
IRRADIATION EXPERIMENT..... 63
5.1 Color Modification..... 63
5.2 UV-Vis spectroscopy..... 65
5.3 XAS spectroscopy..... 69
5.4 EPR spectroscopy..... 71

CHAPTER VI..... 75
DISCUSSION AND CONCLUSIONS..... 75
6.1 Discussion..... 75
6.2 Conclusions..... 80

REFERENCES..... 81

APPENSICES..... 85

APPENDIX A..... 86
APPENDIX B..... 87
APPENDIX C..... 91

CURRICULUM VITAE..... 114

จุฬาลงกรณ์มหาวิทยาลัย
Chulalongkorn University

LIST OF TABLES

		Page
2.1	The classification of tourmaline according to type of trace elements that is chemical compositions in the structure	9
2.2	Correlation between color absorbed and color perceived	12
2.3	Mechanism of color causing in various tourmaline shades	15
3.1	Nigerian tourmaline samples (Group 1) collected for electron beam irradiation	22
3.2	Nigerien tourmaline samples (Group 2) for gamma irradiation	26
3.3	Measurement parameters and configurations of UV-Vis spectro-photometer applied for this study	33
3.4	Analytical parameters and configurations of FTIR spectrometer in this study	34
4.1	Summary of physical properties of tourmaline samples from Nigeria	43
4.2	EPMA analysis representing chemical compositions of all tourmaline samples	48
4.3	Assignment of Raman shift (cm^{-1}) associated with the OH bands and environments in Nigerian tourmaline	53
4.4	Assignment of infrared absorption band (cm^{-1}) related to hydroxyl group for pink and green tourmalines from Nigeria source	57
5.1	Calculated g-factor values from EPR signals	72
6.1	Raman frequency (cm^{-1}) of ^{V}OH and ^{W}OH stretching modes assignment	76
6.2	Price of service fees for tourmaline irradiation	80
A.1	The basic properties analysis results of all tourmaline samples before irradiated	86

LIST OF FIGURES

		Page
1.1	presentation of diagram about the methodology of this thesis study.....	4
2.1	Tourmalines in various colors.....	6
2.2	(A) The difference of tourmaline crystal forms (B) Different characteristic of crystal along C-axis (antilogous-analogous).....	7
2.3	The crystal structure of tourmaline	7
2.4	Tourmaline structure consist of chemical compositions in oblique view.....	8
2.5	Species and varieties of tourmaline.....	11
2.6	Electron center in fluorite.....	13
2.7	Hole color center in Amethyst.....	14
2.8	Fe^{2+}-Fe^{3+} intervalence charge transfer.....	14
2.9	The crystallization process of tourmaline.....	17
2.10	Decay of isotopes cobalt-60 (60Co) as a source of gamma ray at two levels of energy.....	19
2.11	Linear electron accelerators.....	20
2.12	Thai research reactor 1 modification 1 (TRRM1/M1).....	21
3.1	Nigerian tourmaline samples.....	22
3.2	Optic character of tourmaline samples under polariscope displaying alternate dark and bright during rotation of the sample every 45 degree.....	31
3.3	Uniaxial optic Figure of samples, cross-shape, shown under polariscope with conoscope supplementary.....	31
3.4	Refractive indices of tourmaline samples read under refractometer.....	31
3.5	UV-Vis-NIR spectrophotometer, LAMBDA 900.....	33
3.6	Nicolet iS50 FTIR spectrometer.....	34
3.7	T64000 JOBIN YVON HORIBA Raman spectrometer.....	35
3.8	JEOL JXA-8100 model of EPMA spectrometer.....	36

จุฬาลงกรณ์มหาวิทยาลัย
Chulalongkorn University

		Page
3.9	Beam line 1.1W: Multiple X-ray Techniques (BL1.1W: MXT).....	37
3.10	Preparing samples for XAS technique analysis.....	38
3.11	Bruker EMX Electron Paramagnetic Resonance.....	39
3.12	Schematic presentation of electron spin state splitting.....	39
3.13	Source of electron beam and control room of electron beam irradiation operation system.....	40
3.14	Sample preparation for electron beam irradiation.....	41
3.15	Sample preparation for gamma irradiation.....	41
3.16	Control room of gamma irradiation.....	42
4.1	Orientated pink tourmaline in parallel and perpendicular to c-axis yielding clearly different shades of pink color.....	44
4.2	Significant inclusions are commonly found in tourmalines.....	45
4.3	Growth tube inclusions.....	46
4.4	Na^{+}+K^{+}-Ca^{2+}-Vacancy ternary classification diagram indicating all tourmaline samples belong to alkali group.....	50
4.5	Absorption Raman spectra within range between 100-3800 cm^{-1} of pink tourmaline.....	54
4.6	Absorption Raman spectra within range between 100-3800 cm^{-1} of green tourmaline.....	55
4.7	Absorption Infrared spectra within range of 8000-2500 cm^{-1} of pink tourmaline.....	58
4.8	Absorption Infrared spectra within range of 8000-2500 cm^{-1} of green tourmaline.....	59
4.9	UV-Vis absorption spectra of representative pink and green tourmalines showing absorption coefficients in oriented directions compared between parallel and perpendicular to C-axis.....	60
4.10	Normalized Mn *K*-edge XANES spectra of natural tourmalines.....	61
4.11	Normalized Fe *K*-edge XANES spectra of natural tourmalines.....	62
5.1	Color modification after 3 steps of irradiation treatments, viewed in the direction parallel to c-axis.....	64

จุฬาลงกรณ์มหาวิทยาลัย
Chulalongkorn University

Page

.5.2 Color modification after 3 steps of irradiation treatments, viewed in the direction perpendicular to c-axis..... 64
5.3 Correlation a* and b* diagram of pink tourmalines in parallel to C-axis..... 66
5.4 Correlation a* and b* diagram of pink tourmalines in perpendicular to C-axis..... 66
5.5 Correlation a* and b* diagram of green tourmalines in parallel to C-axis..... 67
5.6 Correlation a* and b* diagram of green tourmalines in perpendicular to C-axis..... 67
5.7 UV-Vis absorption spectra of Pk03 sample showing increasing absorption coefficients in oriented directions compared between natural and irradiated colors with different dosages..... 68
5.8 UV-Vis absorption spectra of DG02 sample showing increasing absorption coefficients in oriented directions compared between natural and irradiated colors with different dosages..... 69
5.9 Normalized XANES spectra of Mn *K*-edge for Nigerian tourmalines before and after irradiation..... 70
5.10 Normalized XANES spectra of Fe *K*-edge for Nigerian tourmalines before and after irradiation..... 71
5.11 Room temperature EPR spectra of representative pink tourmaline sample (Pk03)..... 73
5.12 Room temperature EPR spectra of representative green tourmaline sample (DG02)..... 74
6.1 Comparison IR spectra of pink tourmaline along to different crystal direction..... 77
6.2 Comparison the oxidation state of Mn between MnO (Mn^{2+}) and Mn_2O_3 (Mn^{3+}) for tourmaline samples derived from the *K*-edge energy..... 78

จุฬาลงกรณ์มหาวิทยาลัย
Chulalongkorn University

Page

6.3 Comparison the oxidation state of Fe between FeO (Fe^{2+}) and Fe_2O_3 (Fe^{3+}) for green tourmalines derived from the *K*-edge energy..... 78

B.1 Color modification after 3 steps of irradiation treatments; all samples are viewed in the direction parallel to c-axis..... 87

B.2 Color modification after 3 steps of irradiation treatments; all samples are viewed in the direction perpendicular to c-axis..... 89

C.1 UV-Vis spectra of natural tourmalines and after irradiation..... 91

จุฬาลงกรณ์มหาวิทยาลัย
CHULALONGKORN UNIVERSITY

CHAPTER I

INTRODUCTION

1.1 Background and Significance of Research

Thailand is the world leading gem trading market and one of famous gem producer. Currently, amount of gemstone from Southeast Asia deposits, including Thailand, is decreasing continuously because gem mining activity is almost run out. The raw gem materials that used in Thailand gem and jewelry industry have been imported from foreign sources, particularly African countries.

Gemstones have various species, color varieties and perhaps phenomena. Price of any gem depends on popularity, rarity, durability, and beauty. Nowadays, natural gemstones without treatment called “untreated gems” are rarely found with beautiful color and good quality. Therefore, most of good quality gems have been undertaken enhancement process to improve color quality, and clarity. Tourmaline is among those gemstones which have been enhanced to meet the market’s demand.

Tourmaline is classified as a semi-precious stone which is now popular in the market. It has a wide variety of colors such as red, pink, blue, sky-blue, green, yellow, brown, black, colorless, and also bi-colored, tri-colored or even multicolored in single crystals. Their colors are caused by variation of trace elements during crystallization. Tourmaline crystal shows color combination between green and pink parts and perhaps forming as green crust surrounding pink core that is known as watermelon tourmaline. All colored tourmalines usually display dichroism which their colors change or shift in different directions. Trading names have been given for color varieties of tourmalines such as: Verdelite for green, bluish green or yellowish green; Chrome tourmaline for intense green; Indicolite for intense blue; Paraiba for neon blue or greenish blue to blue-green; Pink tourmaline for pink or orangy pink; Canary for yellow to brown; Rubellite for red, purplish red, reddish purple to red-purple or purple-red. It

จุฬาลงกรณ์มหาวิทยาลัย
CHULALONGKORN UNIVERSITY

should be notified that Paraiba is the rarest variety and extremely high price whereas Rubellite is the secondary high price and rather popular (Gem Reference Guide, 1995).

Tourmaline can also be treated by irradiation to improve color quality to Rubellite. There are three radiation techniques which are gamma radiation, electron beam radiation and neutron radiation for color enhancement.

Based on experimental radiation service of the Gem Radiation Center (GIC), Thailand Institute of Nuclear Technology (Public organization), GIC has been using gamma radiation to irradiate tourmaline turning to pink color with various shades, e.g., orangy pink, pinkish orange, and intense pink to red which are depended different trace elements in stone (Henry et al., 2011). However, the cause of color in tourmaline is still ambiguous. reported that trace of manganese included with color center may cause pink color in tourmaline. Nevertheless, there might be other trace elements are slightly related, for example, iron, titanium, gallium, zinc, lead, and bismuth, which can cause various shades in the pink color of tourmaline.

This research is focused on color enhancement of tourmaline using an electron beam irradiation from the electron particle accelerator with an energy of 10 MeV which this technique provides higher energy than the gamma radiation. This facility belongs to Thailand Institute of Nuclear Technology (Public organization). Using high energy to irradiate gemstones, it would spend shorter time of irradiation and provide a better color quality. Color modifications of electron beam irradiation and gamma irradiation are comparable. However, disadvantage of electron beam radiation is that it can produce radioactive isotopes of gemstone after radiation. Therefore, the treated tourmaline must be last on the basis of decay time until the residual radioactivity meets the safe level (less than two nanocuries per gram).

จุฬาลงกรณ์มหาวิทยาลัย
Chulalongkorn University

1.2 Research objectives

1. To study the cause of color modification of tourmaline undertaken electron beam radiation.

2. To compare the colors of tourmaline affected between electron beam radiation and gamma radiation.

1.3 Scope of study

The scope of this work will be study of tourmaline sample from Nigeria that is unknown source. Twenty-five samples were selected included pink and green color. They will be subjected to irradiation with an electron beam and gamma radiation at three level of doses, such as 400, 800, and 1,200 kilogreys.

1.4 Research methodology

The methods of this work, were planned to achieve the objective, are observed in Figure 1.1. Details of each step are as follows:

1. Study and review related literatures.
2. Buy and select tourmaline samples; provide samples into group followed by a cut in two pieces for both kind of radiations and register the sample code.
3. Prepare the samples, cut the stones into a square shape and polish surface as a tablet.
4. Analyze the physical properties of tourmaline with basic gemological tools such as polariscope, refractometer, hydrostatic weighing balance, UV lamp, and gemological microscope to take the inclusion image before radiations.
5. Analyze tourmaline samples using advanced instrumental techniques, for example, UV-Vis-NIR spectroscopy, FTIR spectroscopy, Raman spectroscopy, and Electron Probe Micro-analyzer (EPMA) before irradiation.
6. Analyze the oxidation state transition of manganese and iron before irradiation using X-ray Absorption spectroscopy (XAS).
7. Analyze the signal of paramagnetic ions environment in tourmaline samples before irradiation using electron paramagnetic resonance (EPR) spectroscopy.
8. Enhance tourmaline samples with electron beam and gamma radiation.
9. Check the radiation strength or radioactivity, preliminary, with survey meter.

จุฬาลงกรณ์มหาวิทยาลัย
Chulalongkorn University

10. Correlate the altering color after irradiated tourmaline samples with UV-Vis spectroscopy and calculate color value in CIE L*a*b* system of the tourmaline samples.

11. Analyze the oxidation state transition of manganese and iron after irradiated tourmaline samples using X-ray Absorption spectroscopy (XAS)

12. Analyze the signal defect, known as color center, after irradiated tourmaline samples with EPR technique.

13. Discuss experimental results.

14. Conclude and write a thesis.

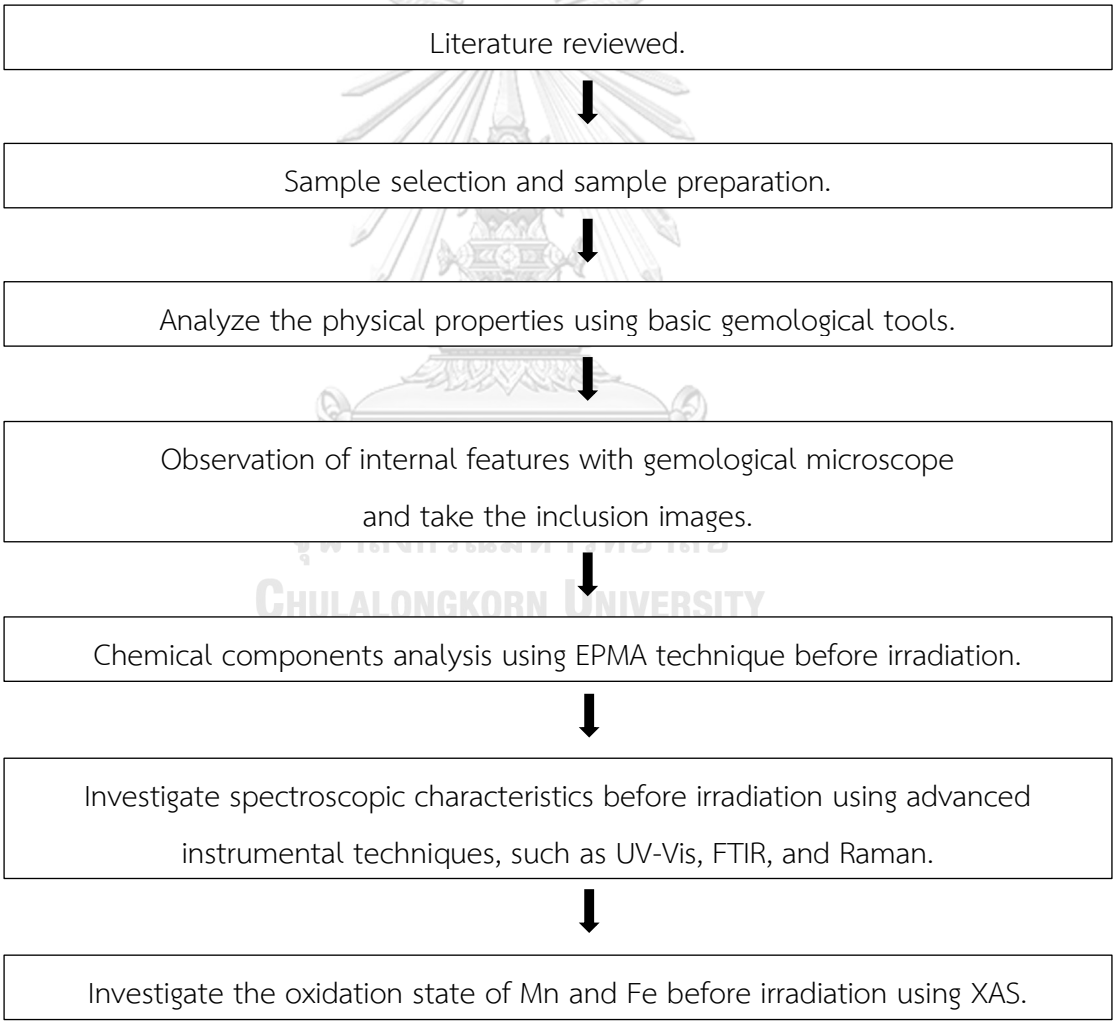

Figure 1.1 presentation of diagram about the methodology of this thesis study.

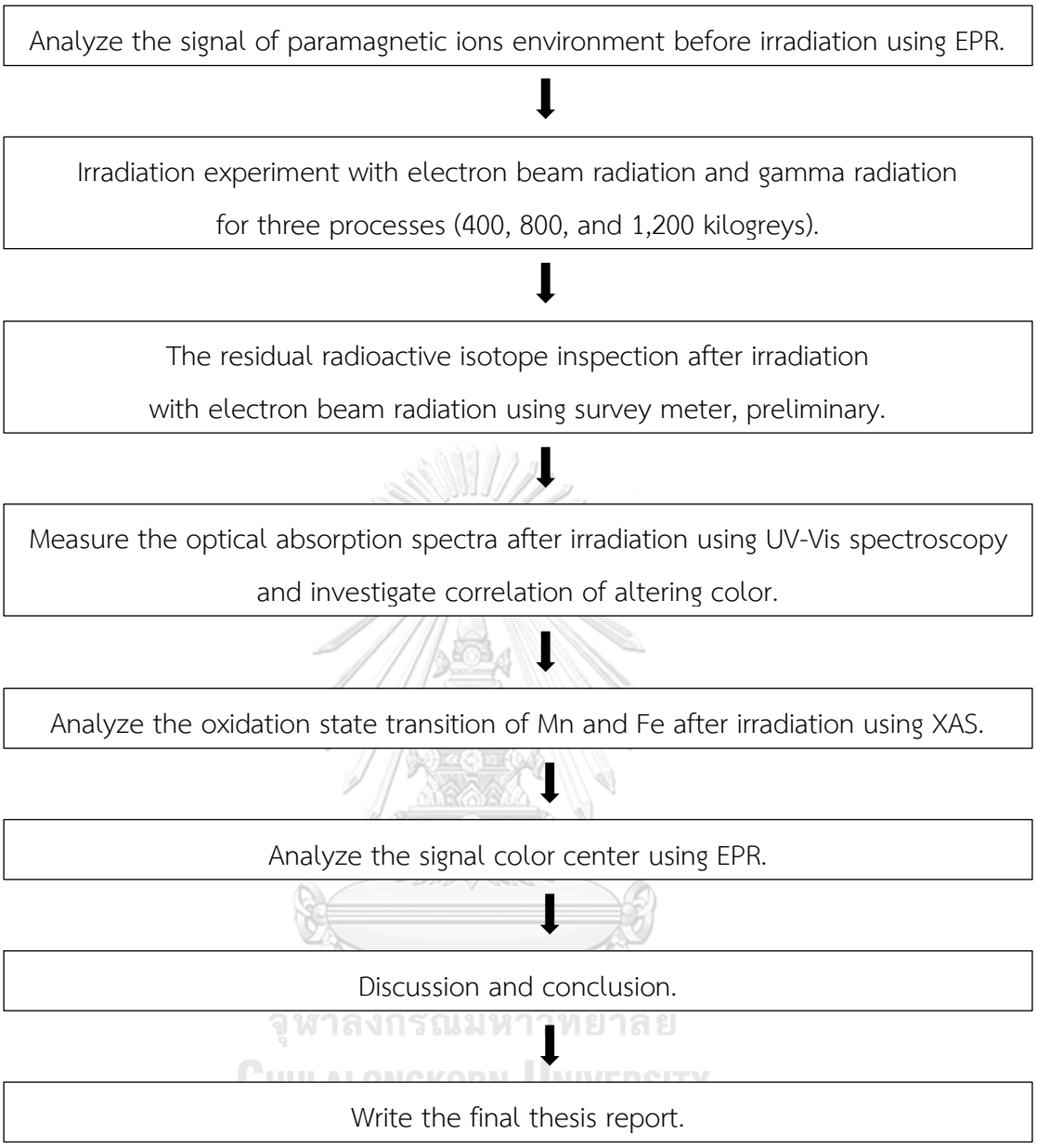

Figure 1.1 (continued)

1.5 Expected results

This work can be guideline in choosing the appropriate type of radiation and determining suitable dosage of radiation to improve color of tourmaline and developing color enhancement further technique.

CHAPTER II

LITERATURE REVIEWS

2.1 Tourmaline

Tourmaline is semi- precious gemstone with hardness around 7 to 7.5 according to Mohs scale. It is distinctive and very popular gem, which due to beauty and wide colors variety. Color of tourmaline is provided in Figure 2.1, such as red, pink, blue, green, yellow, brown, black, colorless. Sometimes it could be two color or multi-colored in same stone. Tourmaline was discovered in many deposits. For example, Afghanistan, Russia, Myanmar, India, Sri Lanka, Brazil, Madagascar, Nigeria, Mozambique, Tanzania, Malawi, Zambia and Zimbabwe etc.

Figure 2.1 Tourmalines in various colors (Photo from GIA).

Tourmaline is a group of boron silicate mineral having a trigonal crystal system. It was consisted of trigonal prism and second order hexagonal prism. Triangle shape was appeared when looking through cross-section (⊥ C-axis) and sometimes tourmaline is probably displayed curved edges that are specific features of tourmaline (Figure 2.2A). Crystal forms of tourmaline are mostly occurred as perfect single crystal (prismatic crystal). It could be formed as small crystals with long rods, which are needles-like. Due to it is non-centrosymmetric mineral that caused the dipole, as electric dipole

moment, causing the pyroelectric and piezoelectric properties, and caused polar axis, as c^+ axis (Antilogous) with a slender shape and c^- axis (Analogous) with a shallow shape (Figure 2.2B)

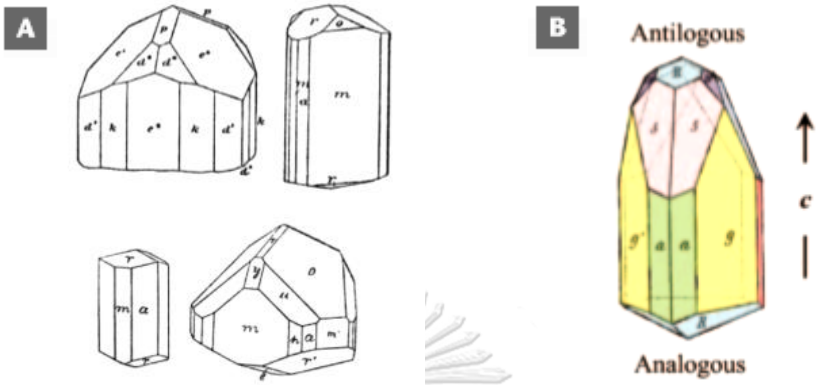

Figure 2.2 (A) The difference of tourmaline crystal forms (B) Different characteristic of crystal along C-axis (antilogous-analogous)

The crystal structure of tourmaline consists of six-membered ring cyclosilicate (Figure 2.3) has a complicated chemical formula as $XY_3Z_6[T_6O_{18}][BO_3]_3V_3W$. The symbols, shown in the chemical formula, represented the position of elements into the structure.

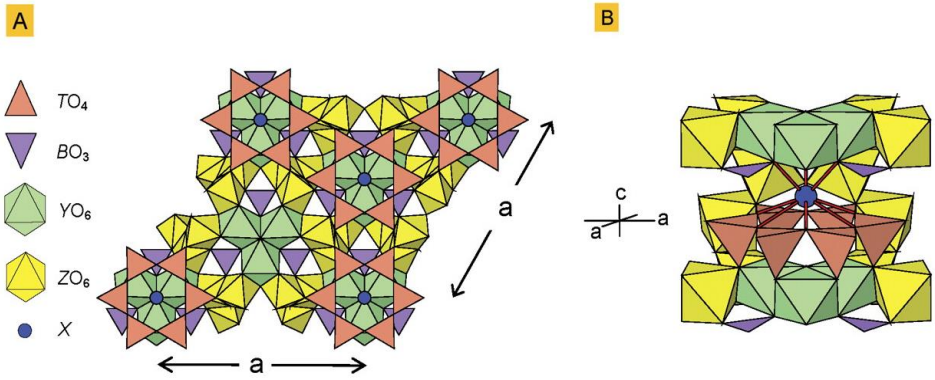

Figure 2.3 The crystal structure of tourmaline (A) viewpoint along (001) (B) oblique view (Hawthorne and Dirlam, 2011)

where: X-site = □ (vacancy), Na^{+}, K^{+}, Ca^{2+}

Y-site = Li^{+}, Mg^{2+}, Fe^{2+}, Mn^{2+}, Cu^{2+}, Al^{3+}, V^{3+}, Cr^{3+}, Fe^{3+}, Mn^{3+}, Ti^{4+}

Z-site = Mg^{2+}, Fe^{2+}, Al^{3+}, V^{3+}, Cr^{3+}, Fe^{3+}

T-site = Si^{4+}, B^{3+}, Al^{3+}

V-site = Hydroxyl group (OH^{-}), O^{2-}

W-site = Hydroxyl group (OH^{-}), F^{-}, O^{2-}

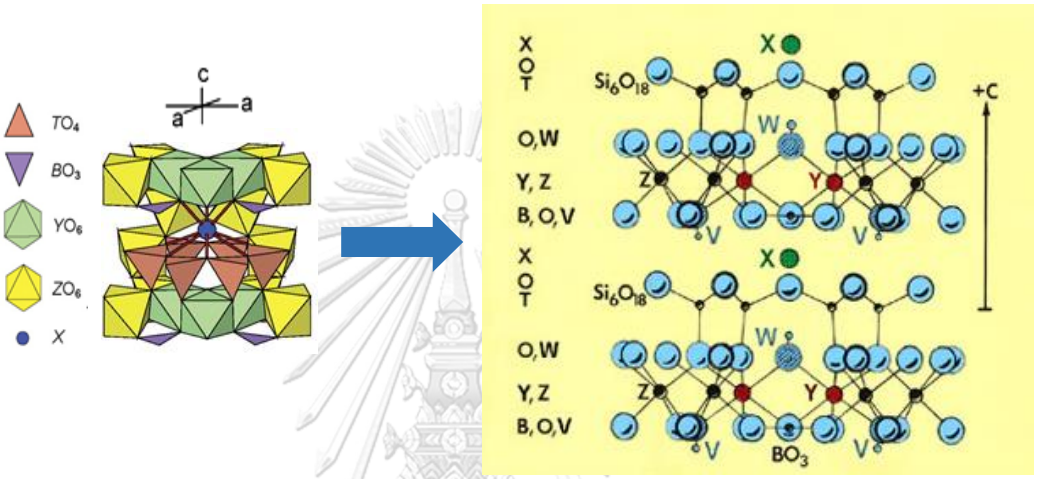

Figure 2.4 Tourmaline structure consist of chemical compositions in oblique view (Hawthorne et al., 1993)

The major compositions (Figure 2.3) consisted of silicon tetrahedra (SiO_4), boron triangular (BO_3), and alumina octahedra. SiO_4 is in T-site position connected with six-member rings and connected with Y-site and Z-site positions. In the Y-site position include cations were occupied by Li^{+}, Mg^{2+}, Al^{3+} and this site could replace by other elements: Fe^{2+}, Mn^{2+}, Cu^{2+}, V^{3+}, Cr^{3+}, Fe^{3+}, Mn^{3+}, Ti^{4+}, etc., as trace elements that act as important color-causing in tourmaline. In the Z-site mainly comprised of trivalent cations: Al^{3}, V^{3+}, $Cr^{3+}$and Fe^{3+}, sometimes it also has divalent cation of elements such as Mg^{2+}, Fe^{2+}, etc. Another one is the X-site, center of the cyclosilicate, has the principle component, which could be Na^{+}, Ca^{2+} or vacancy (Hawthorne and Dirlam, 2011).

In the two positions that included anions composition, are given in Figure 2.4): W-site commonly included with hydroxyl group (OH^{-}), F^{-}, and O^{2-}; V-site generally consisted of hydroxyl (OH^{-}), but it also enclosed with O^{2-} (Hawthorne and Henry, 1999).

จุฬาลงกรณ์มหาวิทยาลัย
Chulalongkorn University

2.1.1 Tourmaline species

As structure of tourmaline is generally of very complex, resulting in a variety of chemical compositions. Also, tourmaline could classify into various species based on the substitution of principle elements and trace elements in each site, observed in Table 2.1. Most tourmalines, as a valuable gem, are specie of elbaite, dravite, and liddicoatite.

Table 2.1 The classification of tourmaline according to type of trace elements that is chemical compositions in the structure (Pezzotta and Laurs, 2011).

General Formula	X	Y3	Z_6	T_6O_{18}	$(BO_3)_3$	V_3	W
Alkali Group							
Dravite	Na	Mg_3	Al_6	Si_6O_{18}	$(BO_3)_3$	$(OH)_3$	(OH)
"Fluor-Dravite"	Na	Mg_3	Al_6	Si_6O_{18}	$(BO_3)_3$	$(OH)_3$	F
"Chromium-Dravite"	Na	Mg_3	Cr_6	Si_6O_{18}	$(BO_3)_3$	$(OH)_3$	(OH)
"Vanadium-Dravite"	Na	Mg_3	V_6	Si_6O_{18}	$(BO_3)_3$	$(OH)_3$	(OH)
"Oxy-Dravite"	Na	Mg_2Al	Al_6	Si_6O_{18}	$(BO_3)_3$	$(OH)_3$	O
Schorl	Na	Fe^{2+}_3	Al_6	Si_6O_{18}	$(BO_3)_3$	$(OH)_3$	(OH)
"Fluor-Schorl"	Na	Fe^{2+}_3	Al_6	Si_6O_{18}	$(BO_3)_3$	$(OH)_3$	F
"Oxy-Schorl"	Na	Fe^{2+}_2Al	Al_6	Si_6O_{18}	$(BO_3)_3$	$(OH)_3$	O
Elbaite	Na	$Li_{1.5}Al_{1.5}$	Al_6	Si_6O_{18}	$(BO_3)_3$	$(OH)_3$	(OH)
"Fluor-Elbaite"	Na	$Li_{1.5}Al_{1.5}$	Al_6	Si_6O_{18}	$(BO_3)_3$	$(OH)_3$	F
Povondraite	Na	Fe^{3+}_3	$Mg_2Fe^{3+}_4$	Si_6O_{18}	$(BO_3)_3$	$(OH)_3$	O
"Chromo-Alimino-Povondraite"	Na	Cr_3	Mg_2Al_4	Si_6O_{18}	$(BO_3)_3$	$(OH)_3$	O
Fluor-buergerite	Na	Fe^{3+}_3	Al_6	Si_6O_{18}	$(BO_3)_3$	$(O)_3$	F
Olenite	Na	Al_3	Al_6	Si_6O_{18}	$(BO_3)_3$	$(O)_3$	(OH)

จุฬาลงกรณ์มหาวิทยาลัย
Chulalongkorn University

Table 2.1 (continued).

General Formula	X	Y3	Z_6	T_6O_{18}	$(BO_3)_3$	V_3	W
Calcite Group							
Uvite	Ca	Mg_3	Al_5Mg	Si_6O_{18}	$(BO_3)_3$	$(OH)_3$	(OH)
"Fluor-Uvite"	Ca	Mg_3	Al_5Mg	Si_6O_{18}	$(BO_3)_3$	$(OH)_3$	F
Feruvite	Ca	$Fe^{2+}{}_3$	Al_5Mg	Si_6O_{18}	$(BO_3)_3$	$(OH)_3$	(OH)
"Fluor-Feruvite"	Ca	$Fe^{2+}{}_3$	Al_5Mg	Si_6O_{18}	$(BO_3)_3$	$(OH)_3$	F
Liddicoatite	Ca	Li_2Al	Al_6	Si_6O_{18}	$(BO_3)_3$	$(OH)_3$	(OH)
"Fluor-Liddicoatite"	Ca	Li_2Al	Al_6	Si_6O_{18}	$(BO_3)_3$	$(OH)_3$	F
Vacancy Group							
Foitite	□	$Fe^{2+}{}_2Al$	Al_6	Si_6O_{18}	$(BO_3)_3$	$(OH)_3$	(OH)
Magnesio-Foitite	□	Mg_2Al	Al_6	Si_6O_{18}	$(BO_3)_3$	$(OH)_3$	(OH)
Rossmanite	□	$LiAl_2$	Al_6	Si_6O_{18}	$(BO_3)_3$	$(OH)_3$	(OH)

Due to Tourmaline has very complex chemical composition, causing various color from colorless, red, pink, green, blue, yellow brown, black and multi-color in same crystal. Each tourmaline species have a special name as trade name which is differed by color (Figure 2.5): Achroite, colorless that without trace element; Pink tourmaline, caused by Mn^{2+}; Rubellite, intense pink to red color that caused by Mn^{3+}/ Mn^{2+}-Mn^{3+} IVCT or irradiated; Canary, yellow to brown color that caused by Mn^{2+} or Mn^{2+}-Ti^{4+} IVTC; Verdelite, yellowish green to green or bluish green that caused by Fe^{2+}/ Fe^{3+} or Fe^{2+}-Fe^{3+} IVTC; Chrome tourmaline, intense green color that caused by Cr^{3+} or V^{3+}; Indicolite, blue color that caused by Fe^{2+} or Fe^{2+}-Fe^{3+} IVTC; and Paraiba, greenish blue to neon blue color that cause by Cu^{2+} and sometimes can contained with Mn^{2+} (Pezzotta and Laurs, 2011).

Figure 2.5 Species and varieties of tourmaline (Pezzotta and Laurs, 2011).

2.1.2 Cause of tourmaline color.

The visibility of gem color caused by absorption and reflection of light in visible range (white light). Visible light is some part within the electromagnetic spectrum, which consisted of wavelengths ranging from 400 nanometers (violet-purple light) to 700 nanometers (red light). When white light transmitted through gemstone, some part of light was reflected out, and some was absorbed by gemstone, so allowed us to see various colors of gem.

จุฬาลงกรณ์มหาวิทยาลัย
Chulalongkorn University

Generally, there are two types of cause of color in gemstones that are idiochromatic and allochromatic. Idiochromatic is self-colored of minerals caused by their chemical formula. Allochromatic is color of minerals due to trace elements that contaminated in their chemical structure. The theory that described the mechanism of color causing in gemstones could be divided into three theories as followed:

Table 2.2 Correlation between color absorbed and color perceived.

Wavelengths of visible light (nanometer, nm.)	Color of light absorbed	Color of light transmitted (visible color of objects)
380-420	violet	green-yellow
420-440	violet-blue	yellow
440-470	blue	orange
470-500	blue-green	red
500-520	green	purple
520-550	green-yellow	violet
550-580	yellow	violet-blue
580-620	orange	blue
620-680	red	blue-green
680-780	purple	green

1. Crystal field theory (CFT):

1.1) Substitution of transition metal, as allochromatic, which involved energy in d-shell orbit of transition metal ions replaced in chemical structure. When gemstones absorbed light in visible range, electrons of transition metal jump from its ground state (t_{2g}) to a higher energy level (e_g). The energy of light was absorbed by gemstones is equal to the different energy between t_{2g} and e_g orbitals. Thus, the energy level of light could be calculated from Planck's equation as equation 1:

$$\Delta E = h\nu = \frac{hc}{\lambda} \qquad \text{(1)}$$

ΔE = different energy of light absorbed between t_{2g} and e_g orbitals

h = Planck's constant equal 6.626×10^{-34} Joule. second (J.s)

ν = frequency of light absorbed (Hertz, Hz)

C = speed of light equal 3×10^{8} meter/second (m/s)

λ = wavelength of light absorbed (nanometer, nm)

จุฬาลงกรณ์มหาวิทยาลัย
Chulalongkorn University

In case of ruby, it is red corundum gemstone with a chemical formula as Al_2O_3. In general, virtuous corundum that without transition metal, it will be a colorless. Due to Al^{3+} ion in Al_2O_3 lattice was substituted by Cr^{3+} ion, causing of red. Cr^{3+} ions arranged electrons as d^3 under the octahedral field that caused energy level divided into t_{2g} and e_g levels. When Cr^{3+} ion received energy, electron in t_{2g} level will be stimulated to the energy level of e_g.

1.2) Color center is structural defect in gemstones, as a result of obtaining radiation that it probably occurred in nature. This defect caused by reaction in nature between rare earth elements and structural elements of gemstones and it could be caused by radiation in laboratory to enhancement gemstone. Color center produced unstable color that it probably yielded to fading of color when gemstones were heated or exposed to sunlight.

Defect center could be divided into two cases, first is an electron color center. For example, purple color in fluorite caused by disappearance of fluorine ion that is missing from particular site in the crystal structure then an unpaired electron trapped in this vacancy, so called "F-center (Figure 2.6). Another defect center is hole color center caused by the one electron of oxygen atoms removed and left behind a hole when obtained radiation. Hole color center is usually described about causing color in smoky quartz and amethyst (Figure 2.7). Defect color of both gemstones are more stability than white light, so they could be reduced or disappeared their color by heating and returned their color by irradiation.

จุฬาลงกรณ์มหาวิทยาลัย
Chulalongkorn University

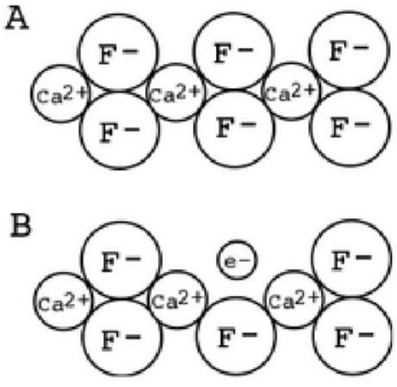

Figure 2.6 Electron center in fluorite (Nassau, 1978).

$$[FeO4]^{-5} \rightarrow [FeO4]^{-4} + e^{-}$$

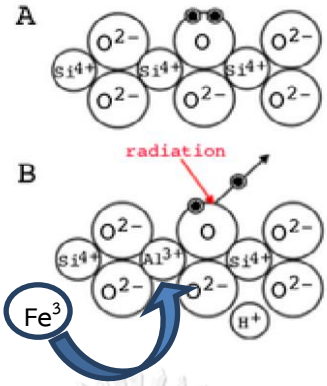

Figure 2.7 Hole color center in Amethyst (Nassau, 1978).

2. Intervalence charge transfer (IVTC) is electrons transformation of transition metal ions that contained different charges. When electrons received a certain amount of energy, causing one electron of transition metal transferred to another transition metal. If the essential energy for transfer electron correspond to the energy of visible light, it will be causing of color in gemstone. For example, blue color in Iolite caused by one electron of Fe^{2+} ion that located at outer energy level transferred to Fe^{3+} ion. Then resulting in the oxidation state of Fe^{3+} changed to Fe^{2+} and oxidation state of Fe^{2+} also changed to Fe^{3+} (Figure 2.8) as equation 2:

$$Fe^{2+} + Fe^{3+} \longrightarrow Fe^{3+} + Fe^{2+} \qquad (2)$$

จุฬาลงกรณ์มหาวิทยาลัย
CHULALONGKORN UNIVERSITY

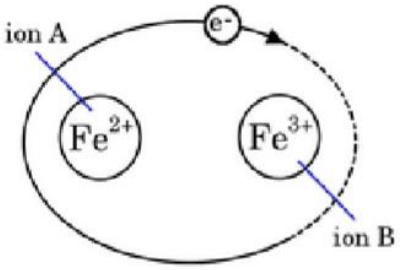

Figure 2.8 Fe^{2+}-Fe^{3+} intervalence charge transfer (Nassau, 1978).

3. The physical properties theory is an optical phenomenon of gemstones caused by a reaction between light and internal features of gemstone, such as

inclusion. Gemstones phenomenon, such as iridescence, adularescence, Aventurescence, chatoyancy, etc.

Causing of tourmaline color is the case of allochromatic with a wide various color causing mechanisms. (table 2.3) that resulting in tourmaline being a various color of gemstones.

Table 2.3 Mechanism of color causing in various tourmaline shades. (Zang and da Fonseca-Zang, 2002[1], Henry et al., 2011[2], Rossman, 1991[3])

Color	Variety Name / Trade Name	Transition metal ions / Cause of color	Tourmaline Species[2]
Colorless	Achroite	No or Minor Chromophores[3]	Elbaite, "Fluor-Elbaite", Fluor-Liddicoatite, Rossmanite
Pink	Pink Tourmaline	- Mn^{2+} CFT[3] - Mn^{3+} CFT	Elbaite, "Fluor-Elbaite", Fluor-Liddicoatite, Rossmanite
Red Purple-Red	Rubellite	- Mn^{3+} CFT - Mn^{2+}- Mn^{3+} IVTC[3] - Color center by natural radiation	Elbaite, "Fluor-Elbaite", Fluor-Liddicoatite, Rossmanite
Yellow, Yellow-Green	Canary	- Mn^{2+} CFT - Mn^{2+}-Ti^{4+} IVTC[3]	Elbaite, "Fluor-Elbaite", Fluor-Liddicoatite
Green	Verdelite Green Tourmaline	- Fe^{2+}-Ti^{4+} IVTC[3] - Fe^{3+} CFT[3]	Elbaite, "Fluor-Elbaite", Fluor-Liddicoatite
Intense Green	Chrome Tourmaline	V^{3+}, Cr^{3+} CFT[3]	Dravite
Blue	Indicolite	- Fe^{2+} CFT[3] - Fe^{2+}-Fe^{3+} IVTC[3]	Elbaite, *"Fluor-Elbaite"*, Fluor-Liddicoatite
Blue (Neon)	Paraiba	Cu^{2+} CFT	Elbaite, Liddicoatite
Orange, Brown,	Golden Tourmaline Brown Tourmaline	- Fe^{2+}-Ti^{4+} IVTC[3]	Dravite, Elbaite, Liddicoatite
Black	Black Tourmaline [1] (Schorl)	- High concentrations of Fe^{2+}, Mn^{2+} and/or Ti^{4+} CFT [1]	Schorl, Elbaite, Liddicoatite

จุฬาลงกรณ์มหาวิทยาลัย
CHULALONGKORN UNIVERSITY

2.1.3 Physical properties of tourmaline

Physical properties are characteristics and basic knowledges that could be classified preliminary gemstones. The physical properties of tourmaline are as follows:

Chemical formula: $XY_3Z_6[T_6O_{18}] [BO_3]_3V_3W_3$ **Crystal system:** Trigonal

Refractive index (R.I.): 1.624 – 16.44 (+0.011/-0.009) **Specific gravity:** 3.06 (+0.20/-0.06)

Birefringence: 0.018-0.020 **Pleochroism:** dichroism (moderate to strong)

Optic character: Double refraction **Optic Figure:** cross

Hardness: 7-7.5 **Luster:** vitreous

Transparency: transparent to opaque **Fluorescence:** inert

Color: many color

2.2 Tourmaline occurrence

Tourmaline is silicate mineral group with various chemical components. It could be occurred in many types of rocks included igneous rock, sedimentary rock, metamorphic rock, and ore. Mostly, tourmaline often occurred in igneous rock, which is magmatic. Investigation of tourmaline is able to understand in significant factors during tourmaline crystallization, such as temperature and pressure included geological crystallization. Tourmaline occurrence will describe the crystallization process with three types of rocks, such as igneous rocks, sedimentary rocks, and metamorphic rocks, are given in Figure 2.9 (Van Hinsberg et al., 2011).

Figure 2.9 (B) stage 1, displayed the crystallization of tourmaline in the pegmatite gap from products of magma that consisted of boron, an important composition in its structure, which is suitable for crystallized tourmaline and accumulated in host rock. Then, resulting in crystal growth in host magma, surfaced on the Earth, and cooled

down. Thus, it provided a first-order of composition from magma included major components, such as Fe, Mg, and Mn.

Due to tourmaline is mineral with very complex structure and diverse chemical composition. Therefore, crystallization of tourmaline with different chemical constituents resulted in tourmaline could be classified to many species (Table 2.1).

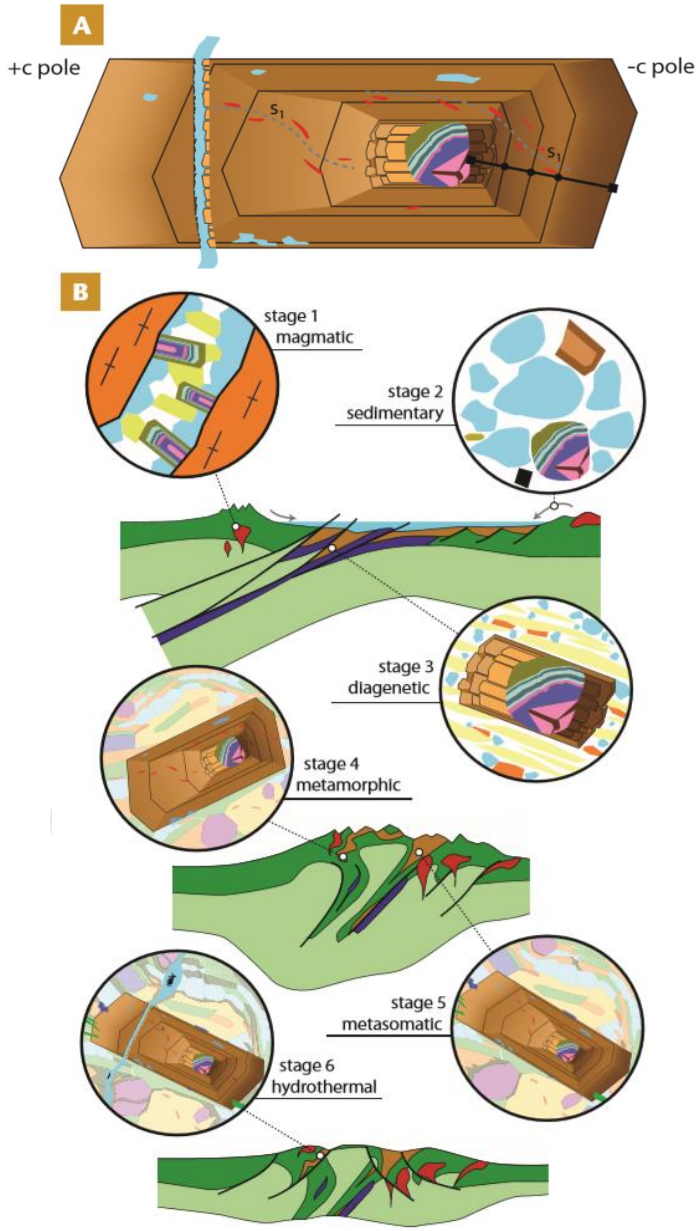

Figure 2.9 (A) Perfect crystal form of tourmaline. (B) Diagram of the tourmaline crystallization in various geological processes and environments (Van Hinsberg et al., 2011) .

Stage 2, when the tourmaline exposed to the earth's surface, causing fracture and transportation to accumulate with sediments of other rocks. For the reason that tourmaline is a mineral that has an identity of chemical composition could be used fragments of stone contained with tourmaline as an indicator of sediments source. Lithification process involved with heat and pressure that causing crystallization of tourmaline again. This process is monopolar crystallization, called “diagenetic process”, stage 3. Namely, crystal would be grown towards the +c pole (Figure 2.9 A), this growth could be indicated temperature of the crystallization.

Stage 4, tourmaline occurrence in metamorphic rock would be formed progressive metamorphism in subduction of the earth's crust with high pressure and high temperature. If there is an appropriate amount of boron in the area more than 100 ppm, it will cause tourmaline crystallization. Stage 5, crystallization of tourmaline during cooled as retrograde growth process, it would be caused metasomatism process (Figure 2.9 B).

The hydrothermal process is provided in Figure 2.9 (B), resulted the exchange between minerals in crystallization, stage 6. If this process was replaced by boron, it could be caused tourmaline crystallization. Growth of tourmaline in final step caused extensional brittle fractures, which has fibrous nature and could be generally found. Besides, this growth resulted different shapes of both +c and -c poles, which contained a high zinc content (Zn) and high ratio of sodium to calcium.

จุฬาลงกรณ์มหาวิทยาลัย
Chulalongkorn University

2.3 Tourmaline irradiation

Radiation is an energy released from source in particles forms or electromagnetic waves. It could be classified to many types depended on radiation sources, radiation energy, and energy forms. Radiation that usually used to improving color divided to, radiation in electromagnetic wave forms included x-ray and gamma ray, and another one is radiation in particle forms, such as high energy electron beam and neutron radiation. These radiations could be caused defect in chemical structure of gemstones, which related to the color transformation, called color center.

2.3.1 Gamma ray radiated from a cobalt-60 source with a half-life of 5.27 years and energies of 1.17 and 1.33 MeV (Figure 2.10). Due to gamma ray is electromagnetic energy, so irradiation by gamma ray does not make gemstone radioactive because it decays all the time during irradiated. Therefore, it considered the safest gems irradiation, but the changing color will be less effective than other types of radiation because of low energy.

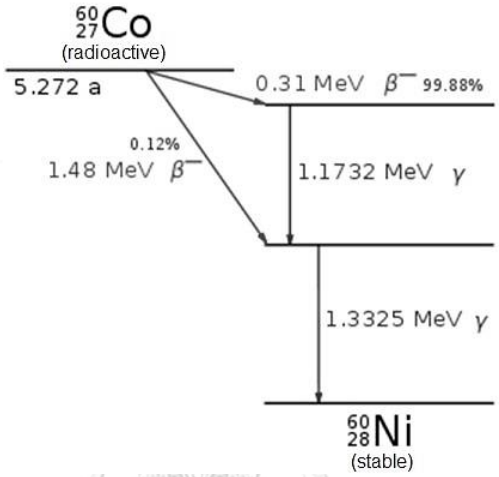

Figure 2.10 Decay of isotopes cobalt-60 (^{60}Co) as a source of gamma ray at two levels of energy (Preoteasa et al., 2012).

2.3.2 High-energy electron radiation is radiation that produced from linear accelerators (Figure 2.11), generally used an electron beam radiation with a high energy of 10 - 20 MeV. The gemstone that irradiated by an electron beam produced very high temperature in gems; therefore, the sample must cool it down and prevent gems breaking by using water flowed through the gemstone while irradiated. Electrons give higher energy to the gemstones; then, the irradiation time is shorter and clearer color changing than gamma ray.

จุฬาลงกรณ์มหาวิทยาลัย
Chulalongkorn University

Figure 2.11 Linear electron accelerators.

2.3.3 High energy neutron radiation is the radiation obtained from nuclear reactors with a high energy of 1 - 2 MeV (Figure 2.12), which provided neutrons from low energy to high energy. A low-energy neutron, called thermal neutron, which caused radioisotope emission in gems. The neutron irradiation in gemstones received consistent radiation throughout the stone like gamma rays. However, if the neutron radiation does not produce radioisotope in the gemstones, it will be the best radiation to improve the color of gems.

จุฬาลงกรณ์มหาวิทยาลัย
CHULALONGKORN UNIVERSITY

Electron-beam and neutron radiation have to requires a quarantine period for gemstones that were irradiated to allow the residual radioactivity to reach a safe level of less than 2 nanocuries per gram (nCi/g) or 74 becquerel per gram (Bq/g). Therefore, it could be used for industrial or academic benefits.

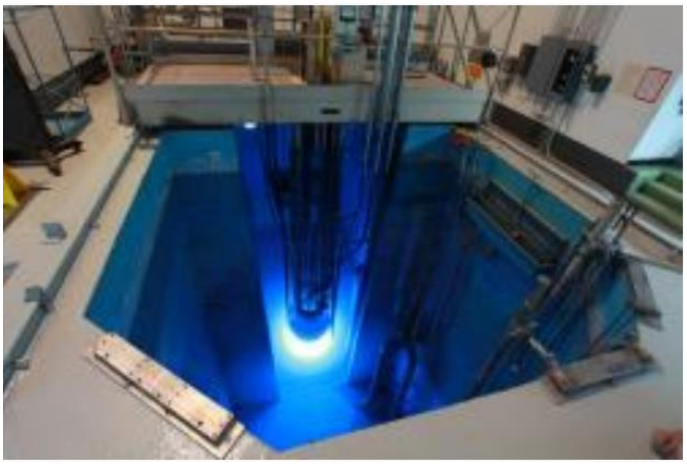

Figure 2.12 Thai research reactor 1 modification 1 (TRRM1/M1) [online: https://www.tint.or.th/home/index.php/th/2013-07-30-15-08-10?id=801]

จุฬาลงกรณ์มหาวิทยาลัย
CHULALONGKORN UNIVERSITY

CHAPTER III

MATERIAL AND METHODOLOGY

3.1 Material

Nigerian tourmaline samples were selected for this study (Figure 3.1) which can be grouped into two different color varieties including twenty pink tourmalines and five green tourmalines. First, two samples, one pink (Pk03) and one green (DG02), are principally samples in this study after that, another twenty-three samples were selected to investigate the correlation of color changing in tourmalines after irradiated with an electron beam and gamma radiation. Both varieties were prepared for electron beam irradiation and gamma irradiation.

Figure 3.1 Nigerian tourmaline samples.

3.2 Methodology

1. Twenty-five tourmaline samples were cut as square shape containing six polished facets (Table 3.1). Each sample was also cut into halves for two sample groups of experiments.

2. Two sample groups as shown in Tables 3.1 and 3.2 were taken for e-beam radiation (Group 1 in Table 3.1) and gamma radiation (Group 2 in Table 3.2).

Table 3.1 Nigerian tourmaline samples (Group 1) collected for an electron beam irradiation.

sample code	weight (carats)	Dichroism	
		parallel c-axis	perpendicular c-axis
Pk01	0.379	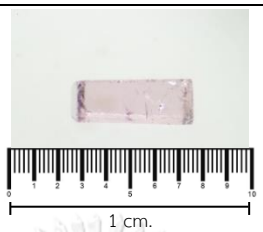	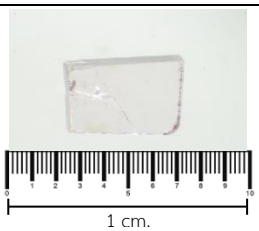
Pk02	0.430	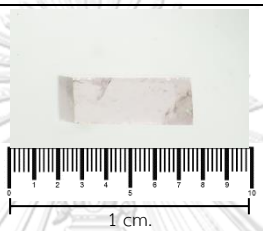	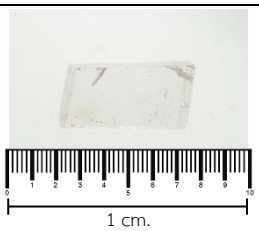
Pk03	0.182	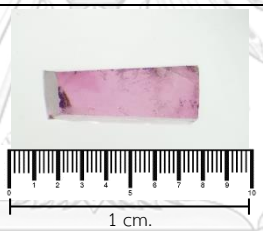	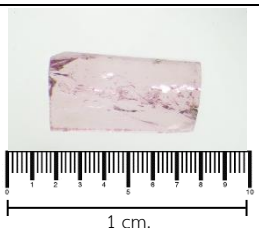
Pk04	0.614	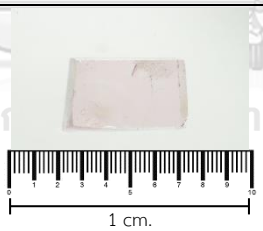	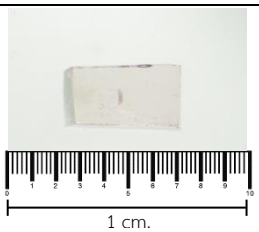
Pk05	0.955	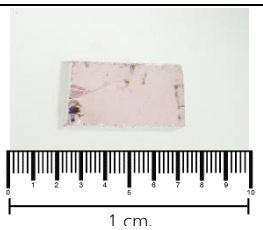	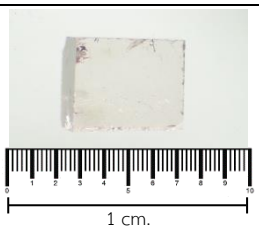
Pk06	1.000	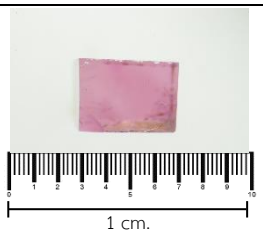	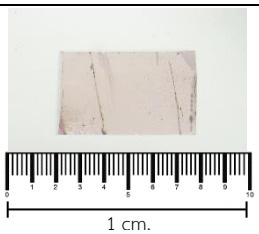

จุฬาลงกรณ์มหาวิทยาลัย
Chulalongkorn University

sample code	weight (carats)	Dichroism	
		parallel c-axis	perpendicular c-axis
Pk07	1.045	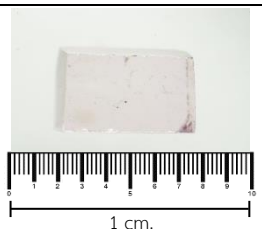	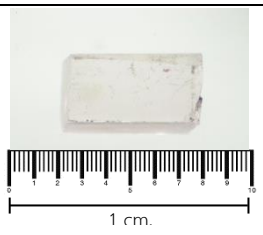
Pk08	0.608	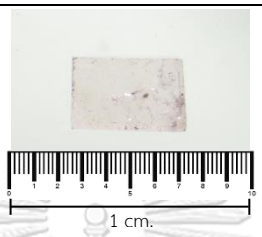	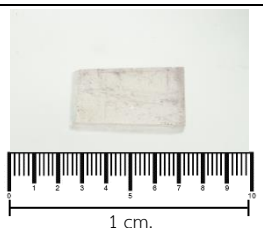
Pk09	0.950	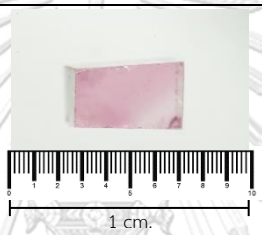	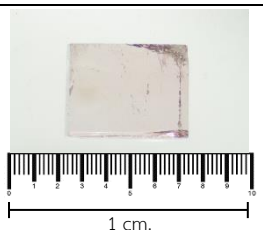
Pk10	0.820	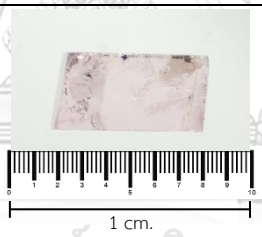	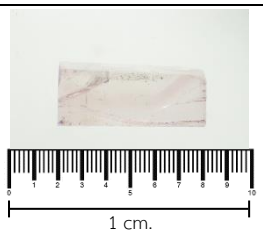
Pk11	0.218	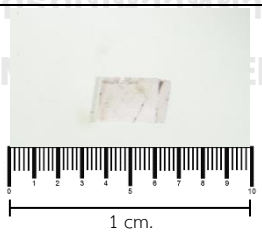	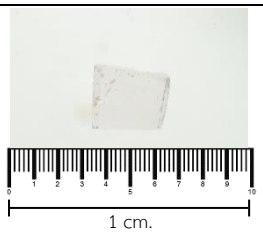
Pk12	1.152	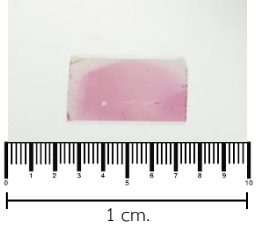	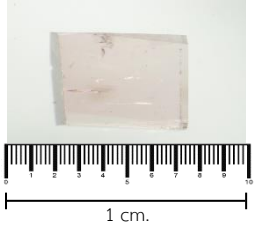

จุฬาลงกรณ์มหาวิทยาลัย
Chulalongkorn University

sample code	weight (carats)	Dichroism	
		parallel c-axis	perpendicular c-axis
Pk13	0.848	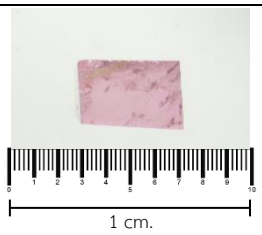	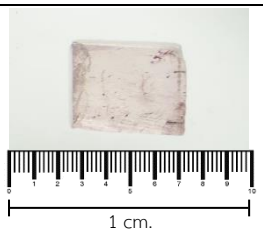
Pk14	0.595	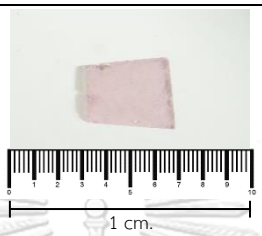	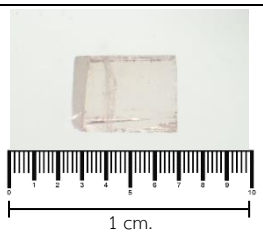
Pk15	0.338	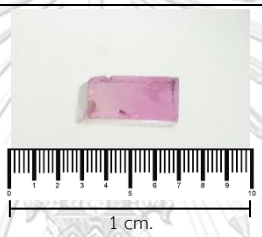	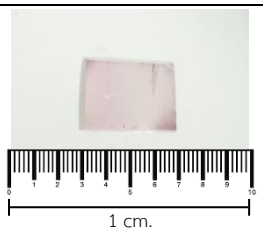
Pk16	0.517	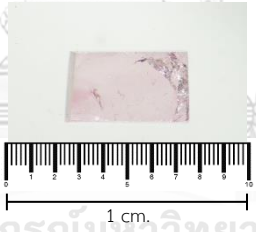	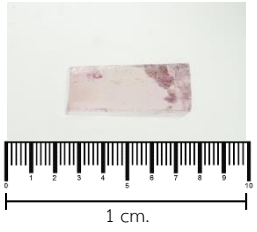
Pk17	0.513	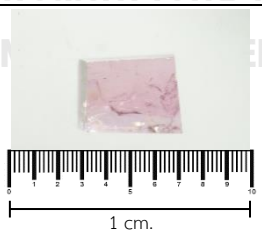	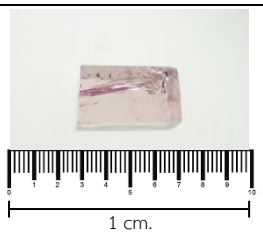
Pk18	0.340	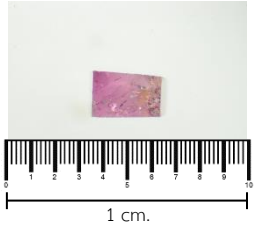	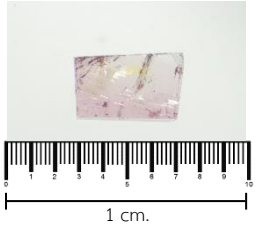

จุฬาลงกรณ์มหาวิทยาลัย
CHULALONGKORN UNIVERSITY

sample code	weight (carats)	Dichroism	
		parallel c-axis	perpendicular c-axis
Pk19	0.656	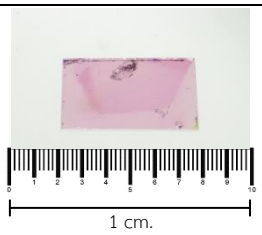	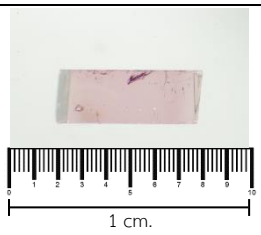
Pk20	0.615	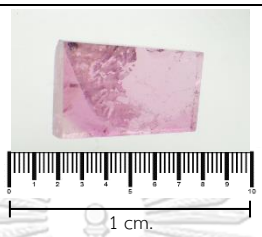	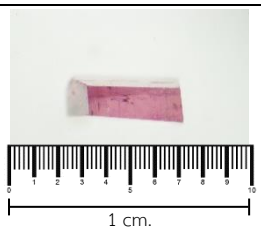
DG01	0.362	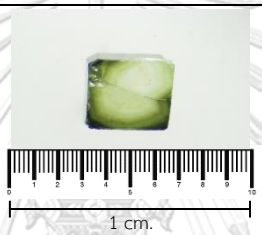	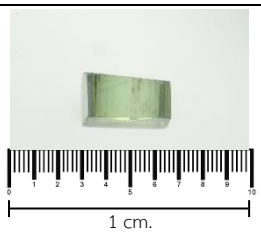
DG02	0.185	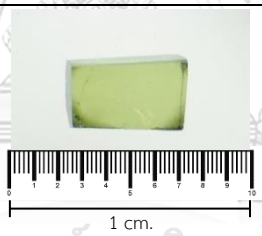	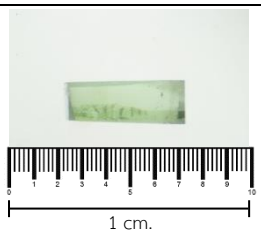
DG03	0.246	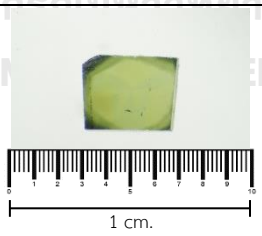	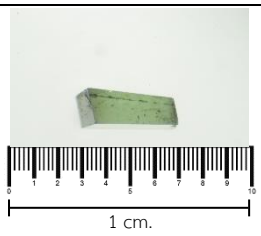
DG04	0.235	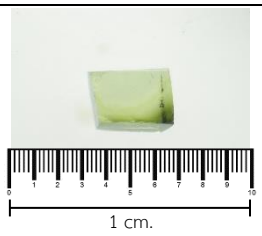	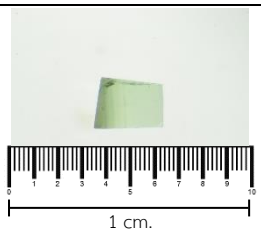

จุฬาลงกรณ์มหาวิทยาลัย
Chulalongkorn University

sample code	weight (carats)	Dichroism	
		parallel c-axis	perpendicular c-axis
DG05	0.663	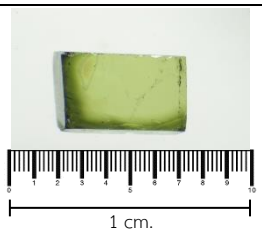	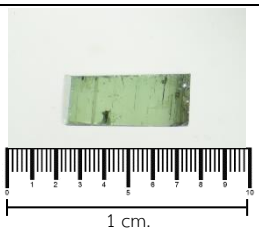

Table 3.2 Nigerien tourmaline samples (Group 2) for gamma irradiation.

sample code	weight (carats)	Dichroism	
		parallel c-axis	perpendicular c-axis
Pk01	0.340	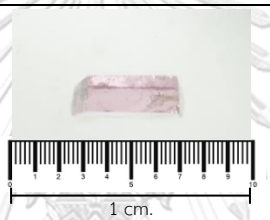	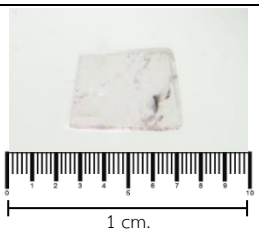
Pk02	0.360	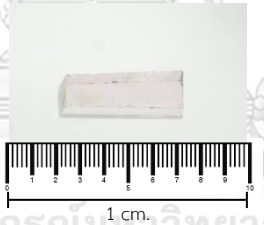	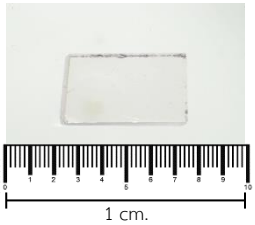
Pk03	0.135	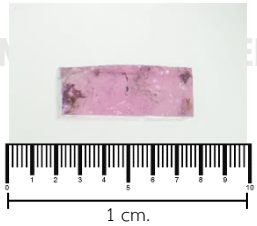	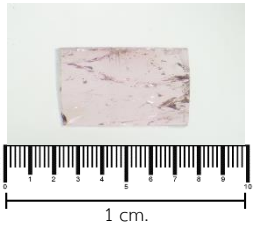
Pk04	0.461	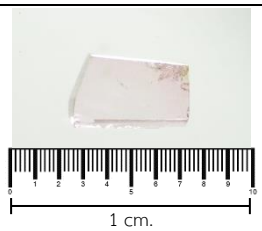	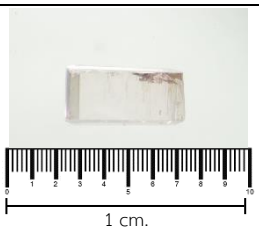

จุฬาลงกรณ์มหาวิทยาลัย
CHULALONGKORN UNIVERSITY

sample code	weight (carats)	Dichroism	
		parallel c-axis	perpendicular c-axis
Pk05	0.603	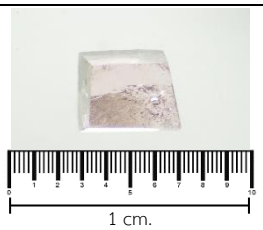	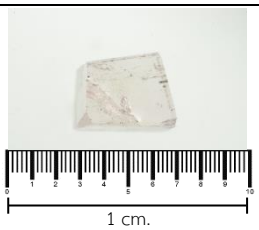
Pk06	0.855	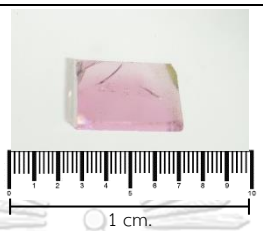	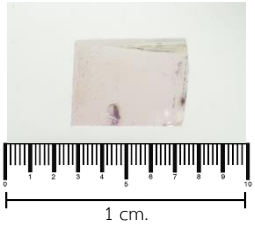
Pk07	0.731		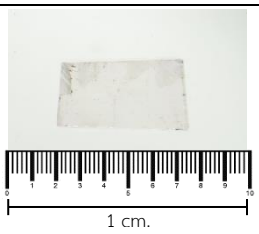
Pk08	0.567	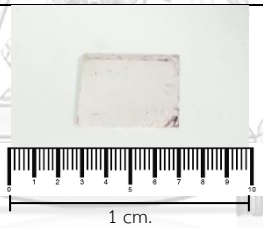	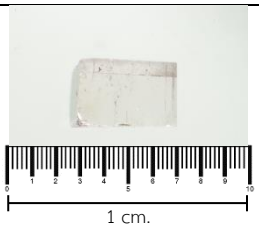
Pk09	0.816	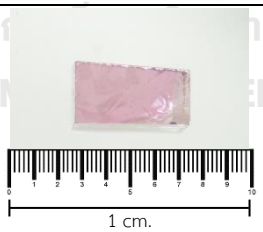	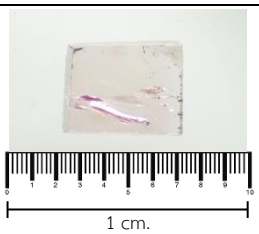
Pk10	0.562	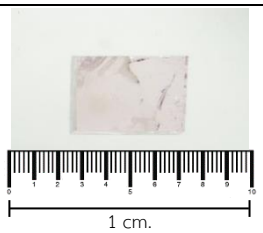	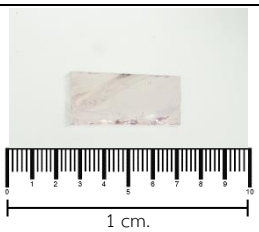

จุฬาลงกรณ์มหาวิทยาลัย
Chulalongkorn University

sample code	weight (carats)	Dichroism	
		parallel c-axis	perpendicular c-axis
Pk11	0.217	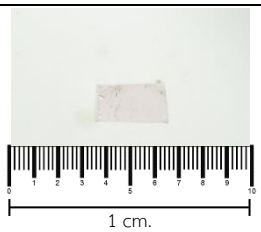	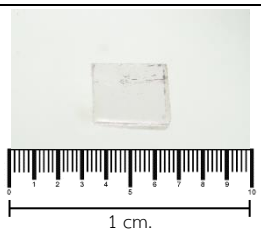
Pk12	0.850		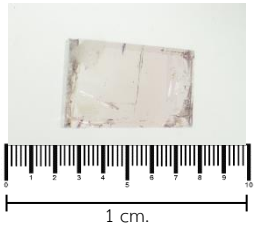
Pk13	0.746	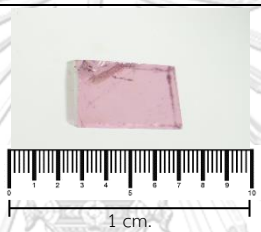	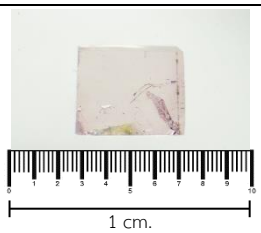
Pk14	0.422	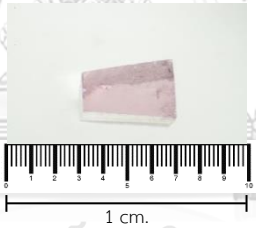	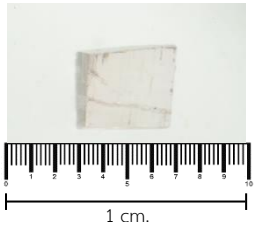
Pk15	0.323	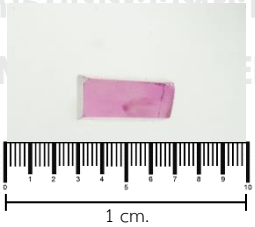	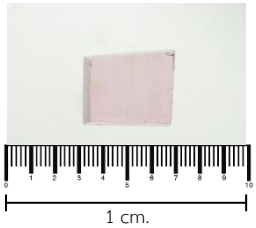
Pk16	0.445	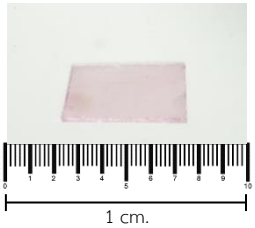	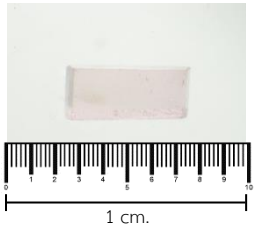

จุฬาลงกรณ์มหาวิทยาลัย
Chulalongkorn University

sample code	weight (carats)	Dichroism	
		parallel c-axis	perpendicular c-axis
Pk17	0.423	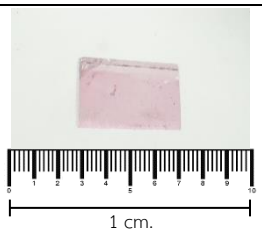	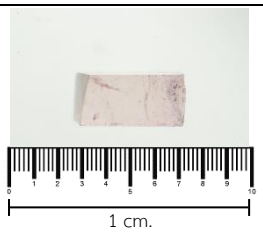
Pk18	0.315	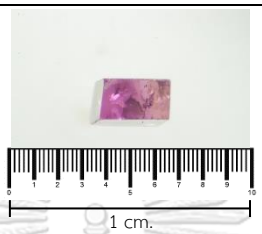	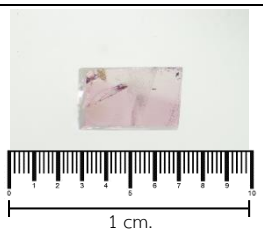
Pk19	0.652	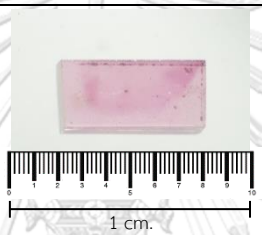	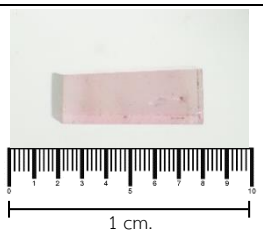
Pk20	0.419	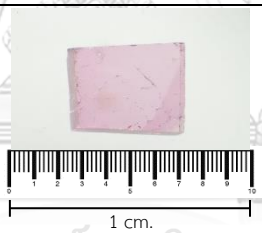	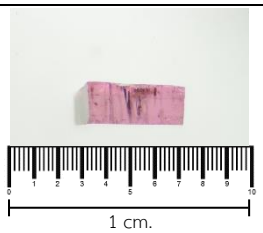
DG01	0.321	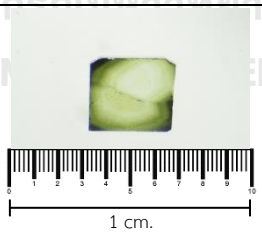	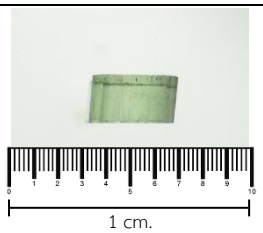
DG02	0.113	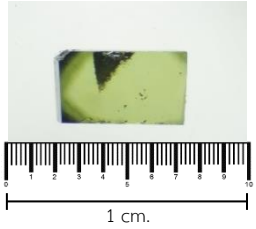	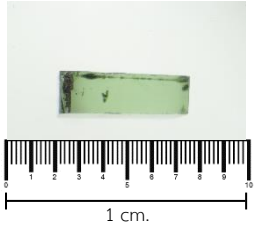

จุฬาลงกรณ์มหาวิทยาลัย
Chulalongkorn University

sample code	weight (carats)	Dichroism	
		parallel c-axis	perpendicular c-axis
DG03	0.235	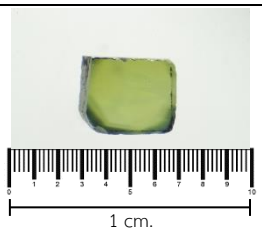	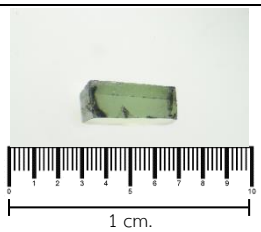
DG04	0.203	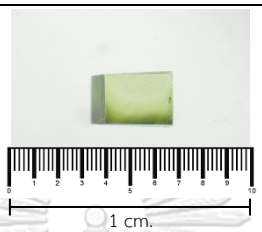	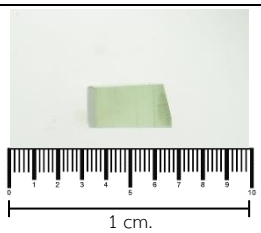
DG05	0.537	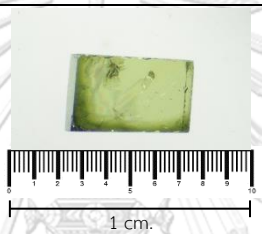	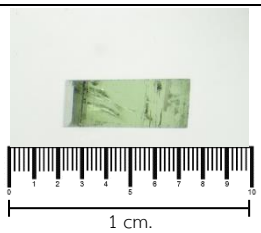

3. All tourmaline samples were investigated for physical properties using basic gem testing equipment which belong to the College of Creative Industries Srinakharinwirot University. Details of these equipment are as followed.

จุฬาลงกรณ์มหาวิทยาลัย
Chulalongkorn University

3.1 Polariscope was taken to analyze optic character and optic figure of samples as shown in Figures 3.2 and 3.3, respectively. The polariscope consists of two polarizing filters, one on the top called analyzer and the on the bottom called polarizer, and condensing sphere also called conoscope (glass sphere on rod). Both analyzer and polarizer were rotated in cross position to make dark field then it possible to identify the optic character of gemstone. Using conoscope can determined the optic figure that related to optic axes (uniaxial and biaxial).

Figure 3.2 Optic character of tourmaline samples under polariscope displaying alternate dark and bright during rotation of the sample every 45 degree.

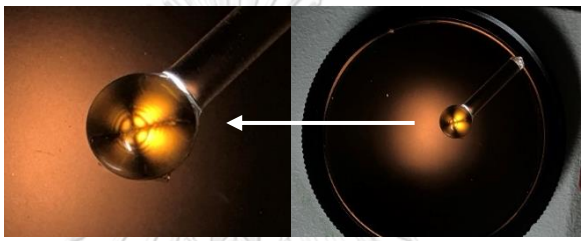

Figure 3.3 Uniaxial optic figure of samples, cross-shape, shown under polariscope with conoscope supplementary.

3.2 Refractometer was used to analyze refractive indices (R.I. of all samples which fall within the range of tourmaline (1.62 to 1.64), given in Figure 3.4. Refractometer is an equipment use with refraction liquid to identify the refractive index (R.I.) and birefringence in each gemstone. The refractive index value can use to classify species of gems and related to crystal system. Some gemstone will be single refraction that have refractive index of one value and the other will be double refraction that probably have refractive index of two or three values.

จุฬาลงกรณ์มหาวิทยาลัย
Chulalongkorn University

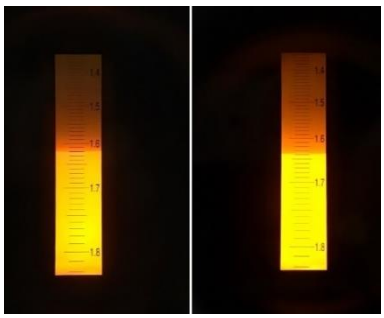

Figure 3.4 Refractive indices of tourmaline samples read under refractometer.

3.3 Hydrostatic weighing balance, METTLER TOLEDO, ML204 model, was applied to measured specific gravity (S.G.) of tourmaline samples. The specific gravity of gemstones can be calculated based on of Archimedes principle. It is difference between weight in air and weight in water as present in equation (3):

$$\text{Specific gravity} = \frac{\text{Gemstone's weight in air}}{\text{Gemstone's weight in air} - \text{Gemstone's weight in water}} \quad \text{Equation (3)}$$

3.4 Fluorescence of samples were observed under UV lamps with short wave (SWUV) and UV-long wave (LWUV).

4. Advanced analytical instruments were subsequently taken which details are reported below.

4.1 Absorption spectrum of tourmaline samples were analyzed using UV-Vis-NIR spectrophotometer within two oriented directions parallel and perpendicular to the c axis. All polished samples were measured in the ultraviolet visible (UV-Vis) spectral ranges between 250 nm to 850 nm. A PerkinElmer UV-Vis-NIR spectrophotometer, model LAMBDA 900 (Figure 3.5) at Department of Earth Sciences, Faculty of Science, Kasetsart University, was engaged for correlation between spectra for natural color and altered colors from e-beam radiation and gamma radiation in each sample. Parameters and conditions for analysis are listed in Table 3.3.

UV-Vis-NIR spectrophotometer contains light sources are probably deuterium and tungsten or halogen lamp, monochromator that is generally a selector of required wavelength from many wavelengths emitted from the source, and detectors used to measure the dispersed components of beam when it passes through sample. Absorption features in the UV-Vis region are probably caused by electron defects, trace element, or chromophore elements, which related to the cause of colour in a gemstone.

Figure 3.5 UV-Vis-NIR spectrophotometer, LAMBDA 900, based at Department of Earth Sciences, Faculty of Science, Kasetsart University.

Table 3.3 Measurement parameters and configurations of UV-Vis spectrophotometer applied for this study.

Settings	Data
Measurement Type	Wavelength Scan
Data Mode	Absorbance (Abs)
Start Wavelength	850.00 nm
End Wavelength	250.00 nm
Slit width	20 nm
Scan Speed	441.71nm/min

จุฬาลงกรณ์มหาวิทยาลัย
CHULALONGKORN UNIVERSITY

4.2 FTIR spectrometer, Nicolet iS50 version of Thermo Scientific (Figure 3.5), was used to analyze hydroxyl molecules (-OH group) and water (H_2O) which situate within the structure of two principally tourmalines, such pink sample (Pk03) and green sample (DG02), operated at the Gem and Jewelry Institute of Thailand (Public Organization). Two samples were analyzed only before irradiation because of broken tool. Analytical parameters and configurations of FTIR spectrometer are summarized in Table 3.3.

Figure 3.6 Nicolet iS50 FTIR spectrometer based at the Gemological Testing Laboratory, the Gem and Jewelry Institute of Thailand (Public Organization) engaged for this study project.

Table 3.4 Analytical parameters and configurations of FTIR spectrometer in this study.

Settings	Data
Detector	DTGS KBr
Beam Splitter	KBr
Measurement Type	Wavenumber (cm^{-1})
Data Mode	Absorbance (Abs)
Wavenumber (Max)	8000 cm^{-1}
Wavenumber (Min)	400 cm^{-1}
Scan Speed	441.71 nm/min
Number of scans	64 cans

4.3 Raman spectroscope, T64000 model of JOBIN YVON HORIBA based at Department of Physics and Materials Science, Faculty of Science, Chiang Mai University (Figure 3.7) was used to analyze the structural characteristic of tourmaline samples before irradiation by Mr. Aekapong Kuntaru who is scientist. Two principally samples (Pk03 and DG02) were measured within a range of 4000-400 cm^{-1} using 532 nm laser. Raman spectra of tourmalines were compared with RRUFF databases.

Figure 3.7 Raman spectrometer, model T64000 JOBIN YVON HORIBA based at Department of Physics and Materials Science, Chiangmai University.

4.4 An Electron Probe Micro-analyzer, equipped with a wavelength-dispersive x-ray spectrometer (EPMA-WDS), is the most ordinarily method used to measure quantitative chemical analysis that reported as oxides of elements. Quantitative EPMA analysis able to detect elements with atomic number equal five (boron) or above. Gemstones (as a solid materials) preparation have to mounted in epoxy resin, polish sections, and coated with carbon on polished surface of samples.

EPMA technique, using model of JEOL JXA-8100 (Figure 3.8) based at Department of Geology, Faculty of Science, Chulalongkorn University was used to analyzed chemical composition of all tourmaline samples. Analytical condition setting was determined with accelerating voltage at 15.0 kV and 2.50 x 10^{-8} A. The measurement time of all samples was set at 10 seconds and the detection limit of analysis is about 0.005%.

Figure 3.8 JEOL JXA-8100 model of EPMA spectrometer based at Department of Geology, Faculty of Science, Chulalongkorn University.

When samples obtained the result of chemical analysis in oxide components then calculated atomic proportions and mineral formula that followed stoichiometric rules. For tourmaline, calculation of the chemical formula must be considered the total amount of anions based on thirty-one anions, including oxygen (O^{2-}), hydroxyl group (OH^-) or fluorine (F^-) (Clark, 2007). According to this study, all samples can detect F^- and they were considered the number of twenty-eight anions, from which subtract three of OH^- (31-4 = 27 apfu). The first step of calculation, all oxide elements were divided by their molecular weight to acquire molecular proportion. The second step to calculate atomic proportion of oxygen by multiplying of molecular proportion with number of oxygens in each oxide element. Next, calculated oxygen factor (o-factor) by taken the expected number oxygen in mineral formula divided by the total atomic proportion of oxygen. Then multiplied each atomic proportion of oxygen with o-factor to obtain number of oxygens for each oxide element based on the total number oxygen. Finally, calculation of cation by multiplying of the number of oxygens with the cation to anion ratio (such as the ratio of B_2O_3 is 2/3) for each oxide element.

4.5 X-ray Absorption spectroscope (XAS) operated at beamline 1.1W station: Multiple X-ray Techniques at Synchrotron Light Research Institute (Public Organization), Nakhon Ratchasima facility (Figure 3.9). XAS technique was applied to study the oxidation state of manganese and iron in tourmalines before and after irradiation that

จุฬาลงกรณ์มหาวิทยาลัย
Chulalongkorn University

also probably related to the altering color of irradiated tourmaline. Not all samples were measured because a long collection time for low concentration, about two to four samples per day based on the amount of expected elements in the samples. Thus, two principally tourmalines, Pk03 and DG02, were selected in this technique and they were analyzed before irradiation and after irradiation at radiation dose at 400 and 800 kilogreys. Irradiated sample at 1,200 kilogreys dosage was not analyzed because of electron beam failure and electron irradiation process was stopped working in five months after samples were irradiated at 800 kilogreys.

Figure 3.9 Beam line 1.1W: Multiple X-ray Techniques (BL1.1W: MXT) at Synchrotron Light Research Institute (Public Organization).

จุฬาลงกรณ์มหาวิทยาลัย
Chulalongkorn University

The concentration of expected elements (manganese and iron) in two main samples (Pk03 and DG02) were analyzed by XRF technique to determine the scanning time for XAS measurement. Sample with extremely low concentration was measured about five scans to improve signal to noise ratio. Furthermore, the sample with relatively higher concentration was measured in the macro set up for automatic measurement (Figure 3.10) with two or three scans.

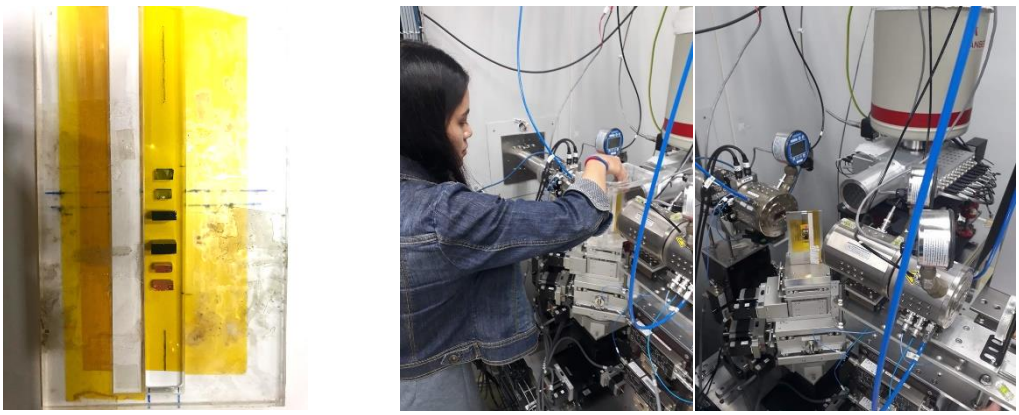

Figure 3.10 (left) samples in the holder used in macro set up for automatic XAS measurements, (right) placement sample holder in the sample stage.

4.6 Electron Paramagnetic Resonance (EPR) technique using a BRUKER EMXmicro model of EPR machine (Figure 3.11) at Scientific and Technological Research Equipment Centre, Chulalongkorn University was engaged to analyze signal of color center in tourmaline that may be caused by irradiation. Process of EPR analysis was operated by Miss Maneerat Limsuwatthanathamrong, provided in Figure 3.11 (right). Two principally tourmalines, Pk03 and DG02, were selected in this technique and they were analyzed before irradiation and after irradiation at radiation dose only at 400 kilogreys. Two principally samples were measured in temperature room with a range between 50 to 650 milliTesla. EPR technique was set parameters of measurement with frequency of microwave at 9.849 gigahertz (GHz), power of microwave at 1.051 milliwatts (mW), and sweep time of 150 seconds per scan. Two samples were measured one scan for each sample.

EPR is magnetic resonance spectroscopy technique that is based on the phenomenon when unpaired electrons in an atom or molecule when they were under an external magnetic field and received the appropriate energy from the magnetic wave in the microwave wave range. Then, unpaired electrons were stimulated also have the opportunity to absorb energy into the higher energy state (Zeeman effect). Then, they can produce the EPR signal that presented absorption spectrum as a function of first derivative.

จุฬาลงกรณ์มหาวิทยาลัย
Chulalongkorn University

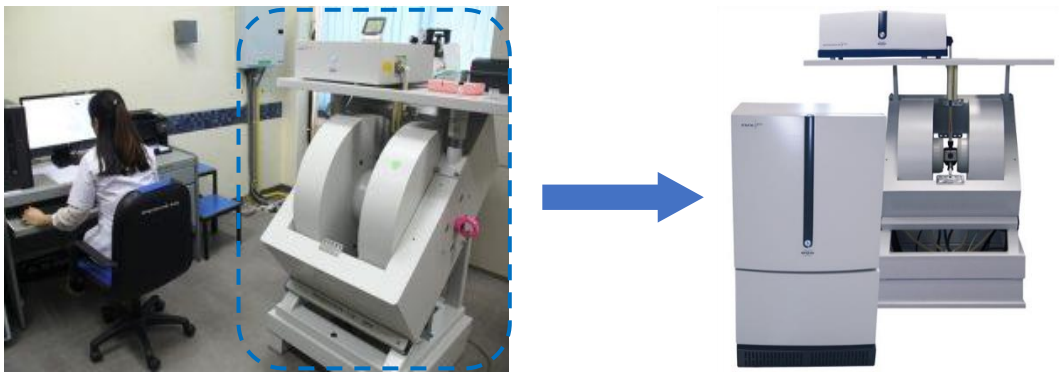

Figure 3.11 Electron Paramagnetic Resonance, Bruker EMX model at Scientific and Technological Research Equipment Centre, Chulalongkorn University.

When electrons placed in magnetic field (B_0), the spin state (S=1/2) split into two levels that defined by the magnetic spin quantum number (M_s = +1/2 and -1/2). As already described above, the energy difference is provided by

$$\Delta E = h\nu = g\mu_B B \qquad \text{Equation (4)}$$

Where h = Plank's constant (6.6262×10^{-34} J.s)

ν = frequency of microwave (Hz)

g = g-factor value is constant value that used to calculate the magnetic moment of electron spin.

μ_B = Bohr magneton (9.274×10^{-24} J/T)

B = magnetic resonance filed (Tesla, T)

จุฬาลงกรณ์มหาวิทยาลัย
Chulalongkorn University

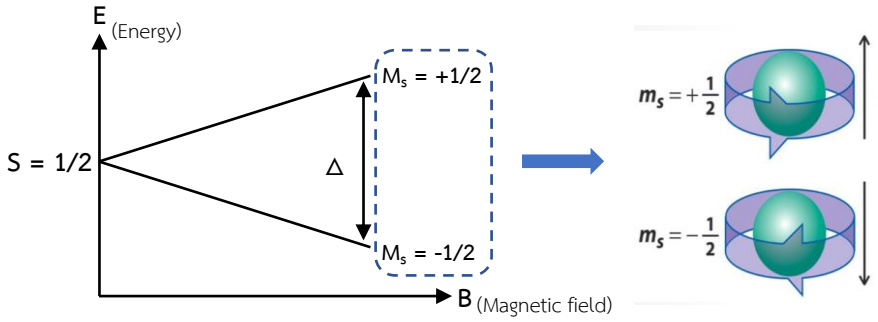

Figure 3.12 Schematic presentation of electron spin state splitting (S=1/2) resulted an applied magnetic field with two states that have different energies (Weil and Bolton, 2007).

5. Experimental treatments applied for all tourmaline samples were designed for three steps of dosage irradiation (400 kGy, 800 kGy, and 1200 kGy) using two radiation methods.

5.1 Electron beam irradiation was used in a high energy electron accelerator at an energy of 10 MeV with a power of 10 MW produced from electron gun. The electron gun, are provided in Figure 3.13 (left), was determined as source of focused and accelerated electron beam in linear direction. An electron radiation process was operated by Mr. Teerawat Utapong, a nuclear engineering, in control room are given in Figure 3.13 (right). A MB16-20 model of electron accelerator produced by Mevex Corporation Ltd, Canada located at the Gem Irradiation Center, Thailand Institute of Nuclear Technology (Public Organization), Nakhon Nayok facility, was used for this project.

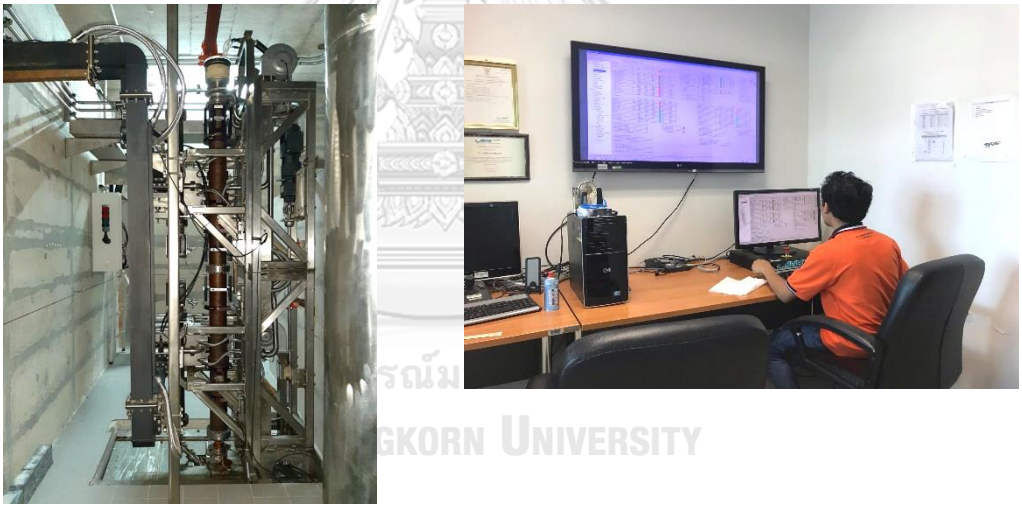

Figure 3.13 (left) electron gun was determined as source of electron beam (right) control room of electron beam irradiation operation system.

Polished samples were prepared in tray (Figure 3.14, left) and performed irradiation. Tray with samples containing was transported along the belt, presented in Figure 3.14 (right). When samples reached to belt that is position of No.1 (Figure 3.14, right), they will obtain electron radiation in this area, also called fraction.

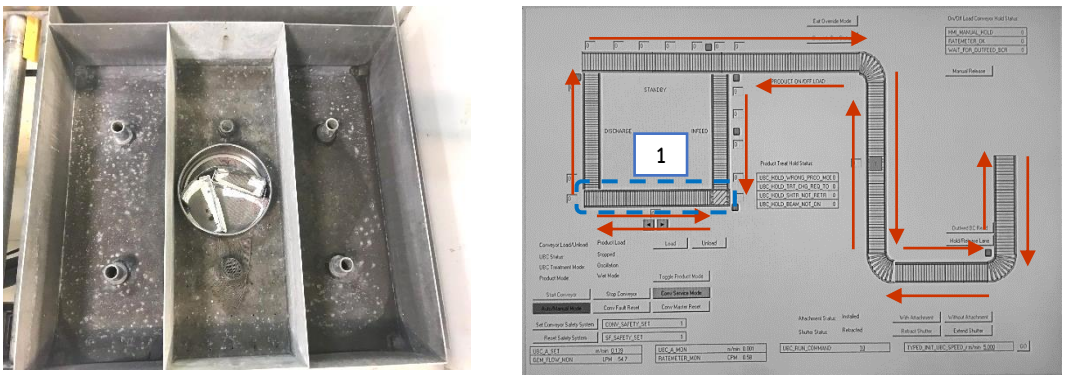

Figure 3.14 (left) sample preparation for electron beam irradiation (right) belt system for transportation of samples along red arrow direction.

5.2 Gamma irradiation operated by Mr. Teerawat Utapong, a nuclear engineering, was experimented using six columns of cobalt-60 sources produced by Paul Stephens Consultancy Ltd., England (Figures 3.15, left). Samples were prepared in container, as pot, and placed between six columns of cobalt-60. Control room of gamma irradiation is provided in Figure 3.16 used to command and perform for gamma irradiation.

Figure 3.15 (left) six pieces of cobalt-60 sources were used as gamma radiation source. (right) sample preparation for gamma irradiation *(Photo by T. Utapong).*

Figure 3.16 control room of gamma irradiation *(Photo by T. Utapong).*

6. Measurement of radioactivity produced in tourmaline samples after electron beam irradiated using survey meter. This facility belongs to the Gem Irradiation Center, Thailand Institute of Nuclear Technology (Public Organization).

7. Data analysis and discussion on aspects of trends in color changing of tourmaline after irradiation between electron beam radiation and gamma radiation, which are the final step of this research project prior to conclusion.

8. Report writing and manuscript preparation have been planned for thesis defense and publication.

จุฬาลงกรณ์มหาวิทยาลัย
CHULALONGKORN UNIVERSITY

CHAPTER IV

PHYSICAL AND GEMOLOGICAL PROPERTIES

4.1 Physical Properties

Physical and general gem properties of all tourmaline samples are summarized in Table 4.1. All details will be present in Appendix A (Table A.1). These properties indicate that all samples all samples fall within the characteristics of tourmaline.

All twenty-five tourmaline samples from Nigeria show optical characteristics as double refraction under the polariscope. Their physical properties are summarized in Table 4.1. which present refractive indices (R.I.) of 1.616 – 1.645, specific gravity (S.G.) of 3.034 – 3.079. Pleochroism, significantly revealing as dichroism, is moderately to strongly observed in all samples, particularly on the direction perpendicular to c-axis (Figure 4.1). Pink tourmaline samples usually present color tones of pale pink (Pk), orangy pink (oPk), orange (O) whereas green tourmaline samples show color tones of yellowish green (yG) to green (G). Fluorescence all samples disappear under ultra-violet light in both shortwave (SWUV) and longwave (LWUV).

Table 4.1 Summary of physical properties of tourmaline samples from Nigeria.

จุฬาลงกรณ์มหาวิทยาลัย
Chulalongkorn University

Sample	Optic character	Refractive index (R.I.)		Birefrin-gence	Specific gravity (S.G.)	Fluorescence		Pleochroism
		n_o	n_e			SWUV	LWUV	
Pink	DR (Uniaxial)	1.632 – 1.645	1.616 – 1.628	0.013 – 0.022	3.027 – 3.085	inert	inert	Dichroism (moderate to strong) - pink to orangey pink - pink to orange - orangey pink to orange
Green	DR (Uniaxial)	1.635 – 1.643	1.618 – 1.628	0.014 – 0.019	3.040 – 3.087	inert	inert	Dichroism (moderate) - yellowish green to green

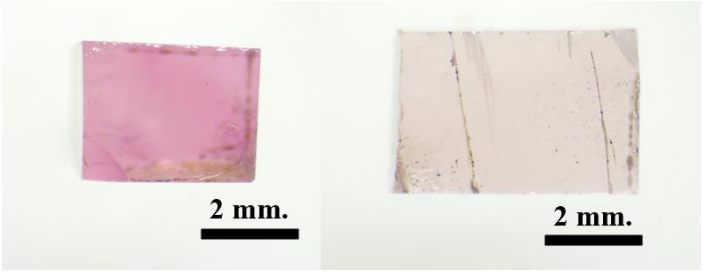

Figure 4.1 Orientated sample (Pk06) parallel and perpendicular to c-axis yielding clearly different shades of pink color.

4.2 Microscopic Internal Feature

Internal features in Nigerian tourmalines were investigated under a gemological microscope with high magnification. The most common features that found in tourmaline are liquid and two-phase inclusion. Additionally, tourmaline is also found growth tube and negative crystal inclusions. These inclusions are reported below:

- Two-phase inclusions include liquid and gas are shown in Figure 4.2 (A-B).
- Liquid inclusions are significant internal features for tourmaline, called “trichites”, which present as thread-like or fine hair features, shown in Figure 4.2 (C-F). Besides, liquid inclusions are also present as fingerprint features (Figure 4.2G) and liquid veil filled in cracks and spread along within gemstone (Figure 4.2H).
- Growth tube inclusions look hollow tube feature that arranged in parallel, shown in Figure 4.3 (A-B) and negative crystal inclusions that are provided in Figure 4.3 (C-D).

จุฬาลงกรณ์มหาวิทยาลัย
Chulalongkorn University

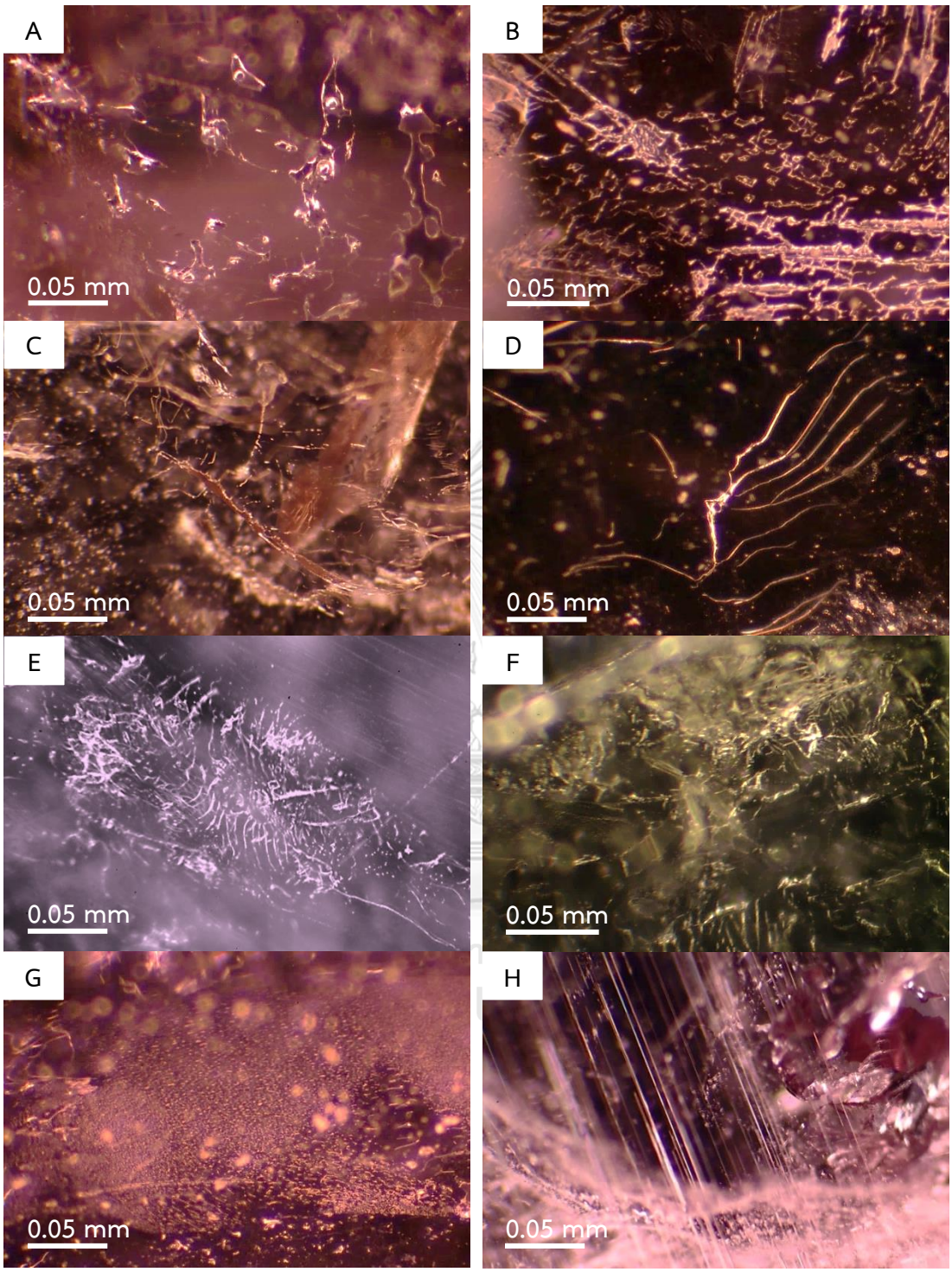

Figure 4.2 Significant inclusions are commonly found in tourmalines, such as two-phase inclusions include liquid and gas (A-B), trichites are liquid inclusions that present as thread-like or fine hair features (C-F), liquid inclusions present as fingerprint feature (G) and liquid veils that filled in cracks (H), magnified 62.50x.

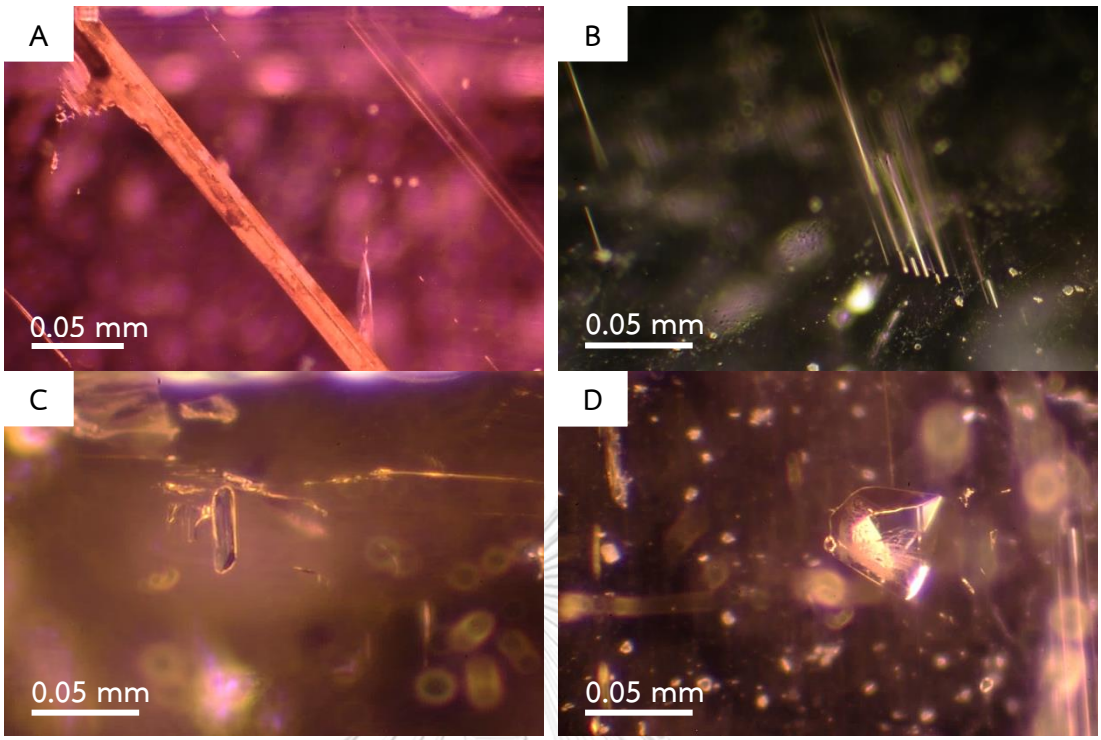

Figure 4.3 Growth tube inclusions that present as orange colored growth tubes (A) and needles-liked hollow tubes (B) and negative crystal (C-D), magnified 62.50x.

4.3 Chemical Compositions

Electron Probe Micro-Analyses (EPMA) was applied to all samples, presenting in oxide component (%wt), shown in Table 4.2. Recalculated atomic cations must be assumed on the basis of 31 anions (Clark, 2007) but Li^{+}, and OH^{-} could not be detected by EPMA technique because of the instrument limitation. Therefore, their recalculated will be carried out on the basis of 27. Both of Li^{+} and OH^{-} are estimated from the main atomic proportion. Li^{+} is assumed to be the main cations filling in the Y site apart from Al^{3+} and a few other cations, whereas OH^{-} is calculated using the formula as 3 + [1 - (F^{-} and Cl^{-})], suggested by Grice and Ercit (1993); Hawthorne and Dirlam (2011); Henry et al. (2011); and Okrusch et al. (2016).

Al_2O_3, SiO_2 and B_2O_3 appear to be the main composition of these tourmaline samples. Al_2O_3 ranges narrowly from 41.1 to 42.2 %wt, which are recalculated to about 7.13 to 7.96 Al^{3+} apfu. SiO_2 vary between 37.3 to 38.8 %wt equivalent to 5.53 to 5.79 Si^{4+} apfu, whereas B_2O_3 (10 to 11 %wt) is recalculated to 2.59 to 2.75 B^{3+} apfu. Al^{3+}

generally substitutes in Z-site and Y-site, but it can combine slightly with Si^{4+} in T-site and B^{3+}. Therefore, 6 apfu of Al^{3+} completely occupy the Z-site and it was allocated in a range of about 0.54 to 0.80 Al^{3+} apfu together with 2.59 - 2.75 B^{3+} apfu and 5.53 - 5.79 of Si^{4+} apfu, which they are completely filling up in T-site. The exceeding Al^{3+} (about 0.39 to 1.36 apfu) together with Li^{+} (estimated at about 1.60 to 2.38 apfu) should allocate in Y-site. Therefore, Y-site of these tourmaline samples are close to theoretical substitution (Al^{3+} + $2Li^{+}$) indicating elbaite end-member (Henry et al. 2011).

Moreover, all samples contain significant Na^{+} (0.60 to 0.85 apfu) allocated in the X-site which are recalculated from 2.5 to 2.9 %wt Na_2O. CaO contents appear to be subordinately allocated in this site, indicating in different component between pink and green samples. Green tourmalines consist of CaO (1.4 to 1.8 %wt) recalculated to 0.21 to 0.28 Ca^{2+} apfu, which are higher content than pink tourmalines (≤0.82 %wt) equivalent to ≤ 0.1 Ca^{2+} apfu. On the other hand, K_2O contents are negligible in all samples, apparently <0.01 K+ apfu. Therefore, Na+, Ca^{2+}, and K^{+} occupy the X-site which still remains ≤0.2 vacancy per formula unit. Plots of Na^{+}+K^{+}-Ca^{2+}-Vacancy of all samples fall within alkali tourmaline filed (Figure 4.4).

The other cations should mostly substitute in Y-site. Among these actions, Mn and Fe appear to be the major trace elements, relating to pink and green color (Table 4.2). In general, both elements significantly relate to pink and orange shading in pink tourmaline (Maneewong, 2009). However, all pink tourmalines in this study yield lower than 1% wt MnO (mostly <0.05 Mn apfu) which are relatively lower in near colorless and increasing towards pink color group. Moreover, less amount of FeO (≤0.1 %wt, equivalent to ≤0.02 Fe apfu) may cause slightly orangey shade in some pink tourmaline samples, e.g., Pk02, Pk04, Pk05, Pk10, Pk14 and Pk17 (Table 4.2). Whereas green tourmaline indicates dominantly Fe content that resulted about 1.6 to 2.1 %wt FeO (0.20 to 0.25 apfu) and also consist of Mn content is relatively high (1.0 to 1.5 %wt MnO, equivalent about 0.13 to 0.19 apfu). The remaining trace elements, such as Mg, Zn, Cu, Pb, Bi, Ga, V, Cr and Ti, are negligible components, mostly ≤0.1 %wt equivalent to ≤0.01 apfu

จุฬาลงกรณ์มหาวิทยาลัย
CHULALONGKORN UNIVERSITY

Table 4.2 EPMA analysis representing chemical compositions of all tourmalines.

Sample	Pk01	Pk02	Pk03	Pk04	Pk05	Pk06	Pk07	Pk08	Pk09	Pk10	Pk11	PK12	Pk13
Oxide (%wt)													
SiO_2	38.526	37.476	38.578	38.321	38.31	37.683	38.072	38.418	38.785	38.229	38.283	37.331	38.167
TiO_2	0.009	0.016	0.018	0.003	0.008	0.011	0.007	0.013	bdl	0.005	0.006	0.013	0.005
Al_2O_3	42.012	42.198	41.452	41.931	41.623	41.607	41.655	41.113	41.502	41.417	41.396	41.721	41.408
B_2O_3	10.512	10.349	10.738	10.535	10.571	10.34	10.663	10.369	10.261	10.301	10.171	10.214	10.137
Cr_2O_3	0.002	0.006	0.011	0.008	0.016	0.013	0.01	0.011	0.01	0.009	0.016	0.002	0.010
V_2O_3	0.005	0.004	0.005	0.009	0.002	0.019	0.017	0.007	0.005	0.012	0.008	0.004	0.026
Ga_2O_3	0.014	0.037	0.059	0.03	0.026	0.071	0.049	0.045	0.053	0.05	0.045	0.040	0.070
Bi_2O_3	0.045	bdl	0.019	0.045	0.023	0.023	0.018	0.024	0.021	0.027	0.025	0.007	0.023
MnO	0.142	0.026	0.268	0.023	0.036	0.141	0.295	0.344	0.031	0.068	0.146	0.011	0.167
FeO	0.014	0.006	0.014	0.013	0.023	0.155	0.019	0.048	0.014	0.009	0.006	0.010	0.002
PbO	0.063	0.117	0.047	0.096	0.009	0.005	0.001	0.017	0.006	0.016	0.019	0.023	0.025
CuO	0.033	0.025	0.013	0.011	0.007	0.011	0.004	0.02	0.006	0.024	0.001	0.021	0.018
ZnO	0.008	0.024	0.03	0.025	0.006	0.027	0.037	0.037	0.039	0.031	0.027	0.020	0.007
CaO	0.194	0.131	0.78	0.334	0.161	0.341	0.294	0.452	0.313	0.178	0.176	0.253	0.186
MgO	0.001	0.005	0.003	0.002	0.002	0.013	0.008	0.003	0.001	0.004	0.001	0.005	bdl
Na_2O	2.652	2.835	2.807	2.657	2.67	2.507	2.618	2.778	2.829	2.927	2.709	2.708	2.778
K_2O	0.018	0.011	0.012	0.016	0.013	0.026	0.02	0.018	0.021	0.016	0.008	0.013	0.008
F	0.814	0.781	0.705	0.751	0.685	0.65	0.641	0.665	0.656	0.627	0.717	0.704	0.739
Cl	0.012	0.009	0.002	0.006	0.004	0.003	0.013	0.009	0.005	0.006	0.011	0.006	0.004
The calculated atomic proportions (apfu.)													
T-site + B (= 9 apfu)													
Si	5.729	5.640	5.717	5.712	5.731	5.686	5.690	5.762	5.794	5.747	5.770	5.666	5.757
Al	0.573	0.672	0.537	0.578	0.539	0.621	0.560	0.554	0.561	0.580	0.584	0.659	0.603
B	2.698	2.688	2.747	2.710	2.730	2.693	2.751	2.684	2.646	2.673	2.646	2.676	2.640
Al in Z-site	**6.000**	**6.000**	**6.000**	**6.000**	**6.000**	**6.000**	**6.000**	**6.000**	**6.000**	**6.000**	**6.000**	**6.000**	**6.000**
Y-site (= 3 apfu)													
Ti	0.001	0.002	0.002	0.000	0.001	0.001	0.001	0.002	0.000	0.001	0.001	0.001	0.001
Al	0.790	0.812	0.703	0.788	0.800	0.778	0.777	0.713	0.746	0.759	0.768	0.804	0.759
Cr	0.000	0.001	0.001	0.001	0.002	0.002	0.001	0.001	0.001	0.001	0.002	0.000	0.001
V	0.001	0.000	0.000	0.001	0.000	0.002	0.002	0.001	0.000	0.001	0.001	0.000	0.003
Ga	0.001	0.004	0.006	0.003	0.002	0.007	0.005	0.004	0.005	0.005	0.004	0.004	0.007
Bi	0.002	0.000	0.001	0.002	0.001	0.001	0.001	0.001	0.001	0.001	0.001	0.000	0.001
Mn	0.018	0.003	0.034	0.003	0.004	0.018	0.037	0.044	0.004	0.009	0.019	0.001	0.021
Fe	0.002	0.001	0.002	0.002	0.003	0.020	0.002	0.006	0.002	0.001	0.001	0.001	0.000
Pb	0.003	0.005	0.002	0.004	0.000	0.000	0.000	0.001	0.000	0.001	0.001	0.001	0.001
Cu	0.004	0.003	0.001	0.001	0.001	0.001	0.000	0.002	0.001	0.003	0.000	0.002	0.002
Zn	0.001	0.003	0.003	0.003	0.001	0.003	0.004	0.004	0.004	0.003	0.003	0.002	0.001
Mg	0.000	0.001	0.001	0.000	0.000	0.003	0.002	0.001	0.000	0.001	0.000	0.001	0.000
*Li_{cal}	2.178	2.166	2.244	2.193	2.184	2.165	2.168	2.221	2.236	2.215	2.200	2.180	2.204
X-site (= 1 apfu)													
Ca	0.031	0.021	0.124	0.053	0.026	0.055	0.047	0.073	0.050	0.029	0.028	0.041	0.030
Na	0.765	0.827	0.806	0.768	0.774	0.733	0.758	0.808	0.819	0.853	0.792	0.797	0.813
K	0.003	0.002	0.002	0.003	0.003	0.005	0.004	0.004	0.004	0.003	0.002	0.003	0.002
*$vacancy_{cal}$	0.201	0.150	0.068	0.176	0.197	0.207	0.191	0.116	0.127	0.115	0.178	0.159	0.156
V+W site (= 4 apfu)													
F	0.043	0.041	0.037	0.040	0.036	0.034	0.034	0.035	0.035	0.033	0.038	0.037	0.039
OH, O	0.000	0.000	0.000	0.000	0.000	0.000	0.000	0.000	0.000	0.000	0.000	0.000	0.000
OH	3.957	3.959	3.963	3.960	3.964	3.966	3.966	3.965	3.965	3.967	3.962	3.963	3.961
Mn/Fe ratio	10.548	4.485	19.646	1.789	1.541	0.919	15.837	7.324	2.322	8.102	24.560	1.112	72.559

*Abbreviation: bdl = below detection limit. The values vacancy, Li, OH, O (apfu) were calculated (see in the main text).

จุฬาลงกรณ์มหาวิทยาลัย
Chulalongkorn University

Table 4.2 (continued).

Sample	Pk14	Pk15	Pk16	Pk17	Pk18	Pk19	Pk20	DG01	DG02	DG03	DG04	DG05
Oxide (%wt)												
SiO_2	38.026	38.007	38.344	38.242	38.688	38.353	38.610	38.222	37.495	38.667	38.307	38.140
TiO_2	0.012	0.003	0.003	0.007	0.012	0.003	0.008	0.008	0.006	0.016	0.015	0.020
Al_2O_3	42.155	41.896	41.560	41.461	41.374	41.427	41.785	41.644	41.500	41.361	41.668	41.665
B_2O_3	10.171	10.355	10.342	10.290	10.368	10.202	10.208	10.411	10.466	10.349	10.615	10.375
Cr_2O_3	0.005	0.006	0.015	0.013	0.015	0.008	0.009	0.005	0.012	0.020	0.002	0.018
V_2O_3	0.015	0.014	0.005	0.009	0.004	0.013	0.003	0.003	0.007	0.002	0.008	0.011
Ga_2O_3	0.081	0.073	0.036	0.093	0.043	0.060	0.028	0.019	0.103	0.035	0.079	0.032
Bi_2O_3	0.010	0.008	0.004	0.016	0.072	0.028	0.005	0.011	0.007	0.027	0.026	0.024
MnO	0.024	0.246	0.972	0.066	0.075	0.273	0.249	1.021	1.254	1.331	1.188	1.495
FeO	0.012	0.013	0.015	0.008	0.013	0.013	bdl	1.792	2.125	2.063	1.607	2.036
PbO	0.035	0.054	0.061	0.025	0.060	0.040	0.056	0.084	0.059	0.080	0.024	0.133
CuO	0.006	0.020	0.017	0.011	0.004	0.001	0.022	0.005	0.004	0.009	0.008	0.011
ZnO	0.015	0.029	0.020	0.042	0.024	0.014	0.026	0.021	0.030	0.013	0.040	0.057
CaO	0.015	0.451	0.818	0.570	2.575	0.656	0.129	1.424	1.460	1.768	1.364	1.426
MgO	0.006	0.008	0.002	bdl	0.003	0.003	bdl	0.014	0.017	0.024	0.007	0.019
Na_2O	2.730	2.646	2.707	2.735	2.614	2.804	2.813	2.314	2.948	2.643	2.656	2.379
K_2O	0.007	0.020	0.016	0.039	0.016	0.013	0.020	0.023	0.022	0.018	0.027	0.021
F	0.687	0.677	0.686	0.703	0.670	0.677	0.732	0.644	0.698	0.770	0.712	0.711
Cl	0.006	0.001	0.009	0.013	0.012	0.010	0.010	0.009	0.001	0.004	0.006	0.009
The calculated atomic proportions (apfu.)												
T-site + B (= 9 apfu)												
Si	5.711	5.690	5.707	5.738	5.742	5.748	5.769	5.631	5.534	5.651	5.611	5.602
Al	0.652	0.634	0.636	0.597	0.671	0.613	0.599	0.722	0.799	0.738	0.706	0.768
B	2.637	2.676	2.657	2.665	2.587	2.639	2.633	2.647	2.666	2.611	2.684	2.630
Al in Z-site	**6.000**	**6.000**	**6.000**	**6.000**	**6.000**	**6.000**	**6.000**	**6.000**	**6.000**	**6.000**	**6.000**	**6.000**
Y-site (= 3 apfu)												
Ti	0.001	0.000	0.000	0.001	0.000	0.000	0.001	0.001	0.001	0.002	0.002	0.002
Al	0.810	0.759	0.655	0.734	0.593	0.704	1.358	0.509	0.420	0.387	0.487	0.444
Cr	0.001	0.001	0.002	0.002	0.004	0.001	0.001	0.001	0.001	0.002	0.000	0.002
V	0.001	0.001	0.001	0.001	0.000	0.001	0.000	0.000	0.001	0.000	0.001	0.001
Ga	0.008	0.007	0.003	0.009	0.013	0.006	0.003	0.002	0.010	0.003	0.007	0.003
Bi	0.000	0.000	0.000	0.001	0.000	0.001	0.000	0.000	0.000	0.001	0.001	0.001
Mn	0.003	0.031	0.123	0.008	0.003	0.035	0.032	0.127	0.157	0.165	0.147	0.186
Fe	0.002	0.002	0.002	0.001	0.001	0.002	0.000	0.221	0.262	0.252	0.197	0.250
Pb	0.001	0.002	0.002	0.001	0.000	0.002	0.002	0.003	0.002	0.003	0.001	0.005
Cu	0.001	0.002	0.002	0.001	0.000	0.000	0.003	0.001	0.000	0.001	0.001	0.001
Zn	0.002	0.003	0.002	0.005	0.000	0.002	0.003	0.002	0.003	0.001	0.004	0.006
Mg	0.001	0.002	0.000	0.000	0.001	0.001	0.000	0.003	0.004	0.005	0.001	0.004
*Li_{cal}	2.169	2.189	2.208	2.237	2.385	2.246	1.598	2.130	2.139	2.177	2.150	2.094
X-site (= 1 apfu)												
Ca	0.002	0.072	0.130	0.092	0.406	0.105	0.021	0.225	0.231	0.277	0.214	0.224
Na	0.795	0.768	0.781	0.796	0.603	0.815	0.815	0.661	0.844	0.749	0.754	0.677
K	0.001	0.004	0.003	0.007	0.002	0.002	0.004	0.004	0.004	0.003	0.005	0.004
*$vacancy_{cal}$	0.202	0.156	0.085	0.105	0.000	0.078	0.161	0.110	0.000	0.000	0.027	0.094
V+W site (= 4 apfu)												
F	0.036	0.036	0.036	0.037	0.034	0.036	0.039	0.034	0.037	0.041	0.037	0.037
OH, O	0.000	0.000	0.000	0.000	0.000	0.000	0.000	0.000	0.000	0.000	0.000	0.000
OH	3.964	3.964	3.964	3.963	3.966	3.964	3.961	3.966	3.963	3.959	3.963	3.963
Mn/Fe ratio	1.957	19.696	67.109	8.490	2.486	21.802	utd	0.577	0.598	0.653	0.749	0.744

*Abbreviation: bdl = below detection limit; utd = uable to determine. The values vacancy, Li, OH, O (apfu) were calculated (see in the main text).

จุฬาลงกรณ์มหาวิทยาลัย
Chulalongkorn University

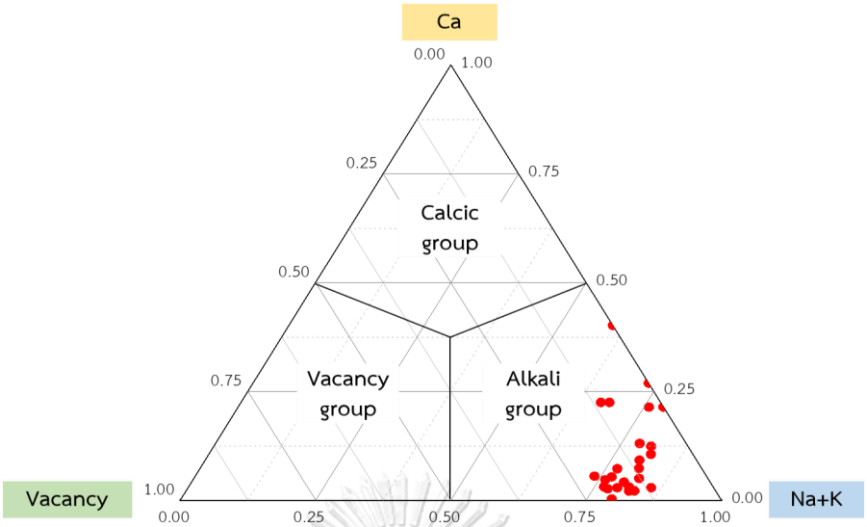

Figure 4.4 $Na^{+}+K^{+}$-Ca^{2+}-Vacancy ternary classification diagram (modified from Henry et al.,2011) indicating all tourmaline samples belong to alkali group.

4.4 Structural Analysis with Raman Shift

Representative samples, pink tourmaline (Pk03) and green tourmaline (DG0 2), were analyzed by Raman spectroscope in two directions, parallel and perpendicular to C-axis, covering the range of 3800-100 cm^{-1} (Figures 4.5 and 4.6). Two ranges of these Raman shifts are clearly distinguished as detailed below.

1. Raman shifts in the range of 1200-1500 cm^{-1} (Table 4.3) relate to B–O stretching within the BO_3 triangles. Pink tourmaline appears B-O stretching bands at 1456.61 cm^{-1} in parallel to C-axis and 1455.49 cm^{-1} in perpendicular to C-axis. Whereas the B-O stretching band of green sample indicates only in perpendicular to C-axis at 1380.38 cm^{-1}.

2. Raman shifts in the range of 1200-1500 cm^{-1} (Table 4.3) relate to B–O stretching within the BO_3 triangles. Pink tourmaline appears B-O stretching bands at 1456.61 cm^{-1} in parallel to C-axis and 1455.49 cm^{-1} in perpendicular to C-axis. Whereas the B-O stretching band of green sample indicates only in perpendicular to C-axis at 1380.38 cm^{-1}.

3. Raman shifts in the range of 400-1100 cm^{-1} (Table 4.3) present series of patterns including the Si-O stretching, the O-Si-O bending, B-O stretching deformation, and the symmetrical and asymmetrical stretching of Si-O bond in SiO_4 rings. These bands are explained below:

- The Si-O stretching bands for pink absorb at 975.15, 1060.33 cm^{-1} in parallel to C-axis and at 946.29, 976.24, 1064.08 cm^{-1} in perpendicular to C-axis. Si-O bands of green appear at 965.28, 1081.60 cm^{-1} in parallel to C-axis and at 972.43, 1059.26 cm^{-1} in perpendicular to C-axis.
- The Si-O bending bands for pink sample appear at range about 872 and 876 cm^{-1} in parallel and perpendicular to C-axis, respectively. Whereas green sample is only showing the Si-O bending band in perpendicular to C-axis about 832 cm^{-1}.
- Next band related to B-O stretching deformation absorb at about 745 cm^{-1} (parallel to C-axis) range and close to 900 cm^{-1} range (perpendicular to C-axis) in both pink and green samples. Moreover, the asymmetrical (Si-O) rings stretching bands of both samples show the main absorption band at 707.20 cm^{-1} (pink) and 702.57 cm^{-1} (green) in parallel to C-axis, whereas these bands appear at 726.50 cm-1 (pink) and 725.37 (green) in perpendicular to C-axis that are relatively intense peaks.
- The symmetrical (Si-O) rings stretching bands of pink sample show the absorbed bands (about 450, 515, 540 cm^{-1}) are not remarkably different in both parallel and perpendicular to C-axis. Whereas green sample appears the symmetrical (Si-O) rings stretching bands only at 510.91 cm^{-1} in parallel to C-axis and also appears four small peaks at 445.77, 473.15, 511.40, and 548.25 cm^{-1}, respectively.
- The Si-O bending bands of pink sample indicate at 406.52 cm^{-1} in parallel to C-axis and at 408.87 cm^{-1} in perpendicular to C-axis. Green sample show these absorbed bands at 408.36 cm^{-1} in parallel to C-axis and at 410.04 cm^{-1} perpendicular to C-axis.

4. The Raman spectra in the range of 120-380 cm^{-1} (Table 4.3) associated with the stretching deformation of Al-O bond, the bending vibration of O-Al-O bond that may substituted with M-O (M: Fe, Mn, Mg), and the FeO_5 (F,OH) bond. (Reddy et al., 2007). These bands are ascribed below:

จุฬาลงกรณ์มหาวิทยาลัย
Chulalongkorn University

- The Al-O stretching bands of pink sample appear main peak only at 375.37 cm^{-1} in parallel to C-axis and main peak at 377.84 cm^{-1} with one small peak at 329.61 cm^{-1} in perpendicular to C-axis. For green sample show main peaks close to 375 cm^{-1} (both parallel and perpendicular to C-axis) and small peaks appear at 317.18 cm^{-1} (parallel to C-axis) and at 333.18 cm^{-1} in perpendicular to C-axis.

- The Al-O bending absorption bands indicate main peaks at about 223 cm^{-1} (parallel and perpendicular to C-axis) in both samples. Besides, the minor bands of Al-O bending for pink sample appear at 245.09, 270.98 cm^{-1} (parallel to C-axis) and 242.07, 277.59 cm^{-1} (perpendicular to C-axis). Whereas green sample show minor bands at about 240 cm^{-1} (both parallel and perpendicular to C-axis) and also appear 276.39 cm^{-1} only in perpendicular to C-axis.

- The FeO5(F, OH) bands of pink sample absorb at 138.56 cm^{-1} (parallel to C-axis) and at 128.12 cm^{-1} (perpendicular to C-axis). For green sample appear the absorbed bands at 157.04 cm^{-1} (parallel to C-axis) and two bands at 133.03, 162.45cm^{-1} (perpendicular to C-axis).

5. Raman shifts in the range of 3200-3800 cm^{-1} are ascribed in Table 4.3, which assigned to the OH1 vibrations in W-site location at about 3615 cm^{-1} up. The OH1 group is connected with three cations located in Y-site, which is YYY octahedral sharing the O(1) atom with ^{W}OH group. The presence of OH3 at Raman frequency of 3420-3595 cm-1 range also connects with one cation occupied in Y-site location and two cations located in Z-site, are three YZZ octahedral with VOH group. The vibration of OH group in this range (3200-3800 cm^{-1}) can be classified to tourmaline specie and also assigned to both samples are elbaite tourmaline. Determination of tourmaline species by Raman depended on the chemistry in OH group (Gasharova et al., 1997; Reddy et al., 2007; Watenphul et al., 2016). Moreover pink and green tourmalines also can be classified with the OH absorption bands in the range between 3200-3800 cm^{-1}, that reported below:

- According to Raman shift of pink sample that associated with OH3 group, as $(OH3)_{v\text{-}site}{}^{Y}(Fe+Mn)^{Z}Al^{Z}Al\text{-}2^{Y}Al^{Z}Al^{Z}Al$, it will appear peak at 3439.39 cm^{-1} (parallel to C-axis) and 3446.04 cm^{-1} (perpendicular to C-axis), respectively. These OH3 bands show the concentration in parallel to C-axis more pronounce perpendicular to C-axis.

Table 4.3 Assignment of Raman shift (cm^{-1}) associated with the OH bands and environments in Nigerian tourmaline (Gasharova et al., 1997; Reddy et al., 2007; Watenphul et al., 2016).

Raman shift (cm^{-1})				Type of modes
Pink tourmaline		Green tourmaline		
//C	⊥C	//C	⊥C	
		3647.62	3647.62	$(OH1)_{W\text{-}site}\ ^{Y}Li^{Y}Al^{Y}Al$
3624.04	3625.10	3624.04	3622.98	
3558.17	3559.25	3561.40	3563.20	$(OH3)_{V\text{-}site}\ 2^{Y}(Fe+Mn)^{Z}Al^{Z}Al\text{-}\ ^{Y}Al^{Z}Al^{Z}Al$
		3535.49	3535.49	$(OH3)_{V\text{-}site}\ 2^{Y}Li^{Z}Al^{Z}Al\text{-}^{Y}Al^{Z}Al^{Z}Al$
3439.39	3446.04	3460.78	3467.76	$(OH3)_{V\text{-}site}\ ^{Y}(Fe+Mn)^{Z}Al^{Z}Al\text{-}2^{Y}Al^{Z}Al^{Z}Al$
1456.61	1455.49		1380.38	B-O stretching
1060.33	1064.08	1081.60	1059.26	Si-O_{br} stretching
975.15	976.24	965.28	972.43	Si-O stretching
	946.29			
872.11	875.98		832.15	O-Si-O bending
744.62	796.40	745.67	798.07	B-O stretching deformation
707.20	726.50	702.57	725.37	asymmetrical (Si-O) rings stretching
	675.42			
638.81	643.89	634.93	639.37	
538.49	540.79		548.25	symmetrical (Si-O) rings stretching
516.59	517.75	510.91	511.40	
			473.15	
446.94	453.36		445.77	
406.52	408.87	408.36	410.04	O-Si-O bending
375.27	377.84	373.59	377.64	Al-O stretching
	329.61	317.18	333.18	deformation
270.98	277.59		276.39	Fe-O, Mn-O, Mg-O
245.09	242.07	240.95	240.86	in O-Al-O bending
223.32	223.32	223.41	223.32	
		157.04	162.45	FeO_5(F, OH)
138.56	128.12		133.03	

* Abbreviation: O_{br} = bridging oxygens in the Si-O rings.

จุฬาลงกรณ์มหาวิทยาลัย
Chulalongkorn University

Additional $(OH3)_{v\text{-site}}$ bands of pink sample, coordinated with $2^{Y}(Fe+Mn)^{Z}Al^{Z}Al\text{-}^{Y}Al^{Z}Al^{Z}Al$, appear at 3558.17 cm^{-1} (parallel to C-axis) and 3559.25 cm^{-1} (perpendicular to C-axis). Moreover pink sample also appear the absorbed band of OH1 group, as $(OH1)_{w\text{-site}}$ $^{Y}Li^{Y}Al^{Y}Al$, at 3624. cm^{-1} (parallel to C-axis) and 3625.10 cm^{-1} (perpendicular to C-axis).

- Raman shift of green sample related to three OH3 groups, as $(OH3)_{v\text{-site}}$ $^{Y}(Fe+Mn)$ $^{Z}Al^{Z}Al\text{-}2^{Y}Al^{Z}Al^{Z}Al$, $(OH3)_{v\text{-site}}$ $2^{Y}Li^{Z}Al^{Z}Al\text{-}^{Y}Al^{Z}Al^{Z}Al$, and $(OH3)_{v\text{-site}}$ $2^{Y}(Fe+Mn)^{Z}Al^{Z}Al\text{-}^{Y}Al^{Z}Al^{Z}Al$. These bands are similarly appearing the absorbed band in both parallel and perpendicular to C-axis at range about 3460, 3535, and 3560 cm^{-1}, respectively.

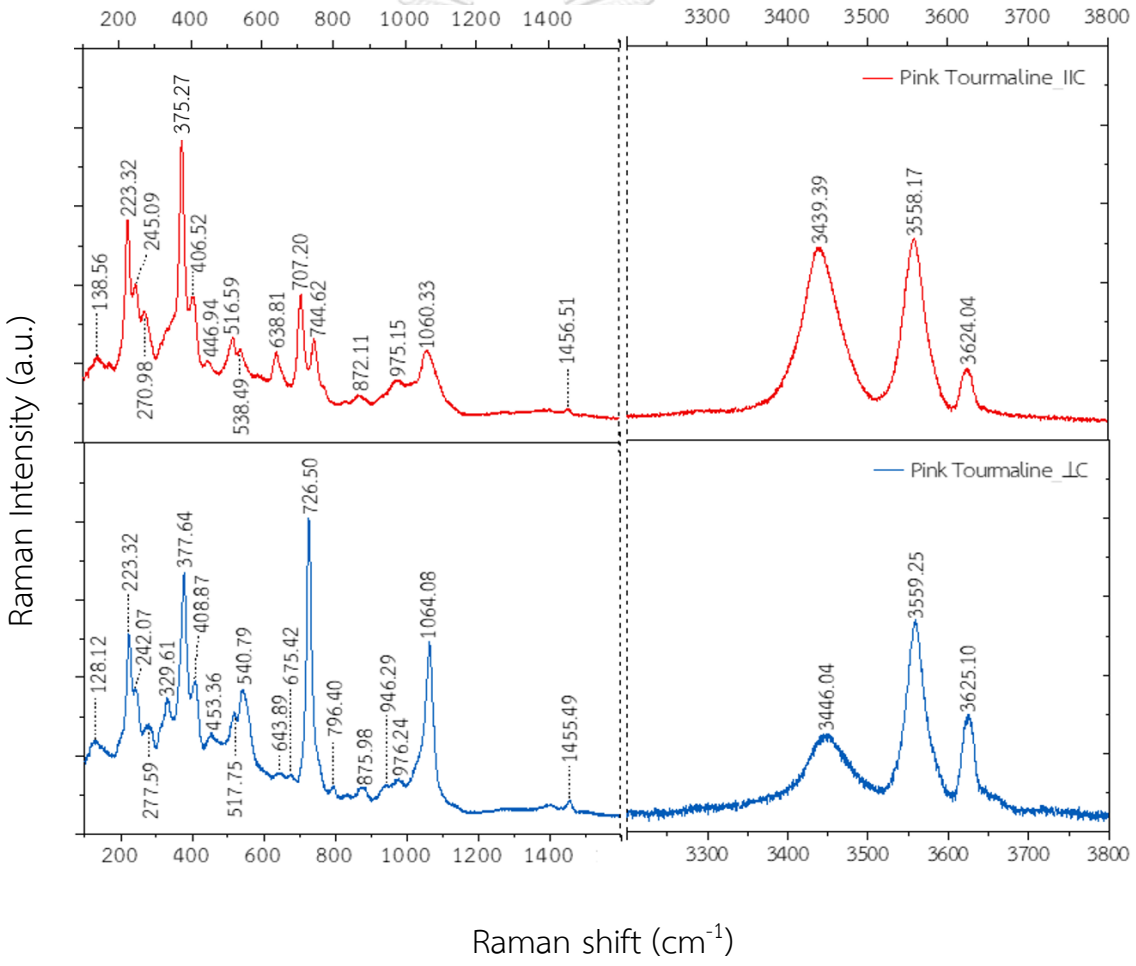

Figure 4.5 Absorption Raman spectra within range between 100-3800 cm^{-1} of pink tourmaline; upper red spectrum analyzed in parallel to C-axis and lower blue spectrum analyzed in perpendicular to C-axis.

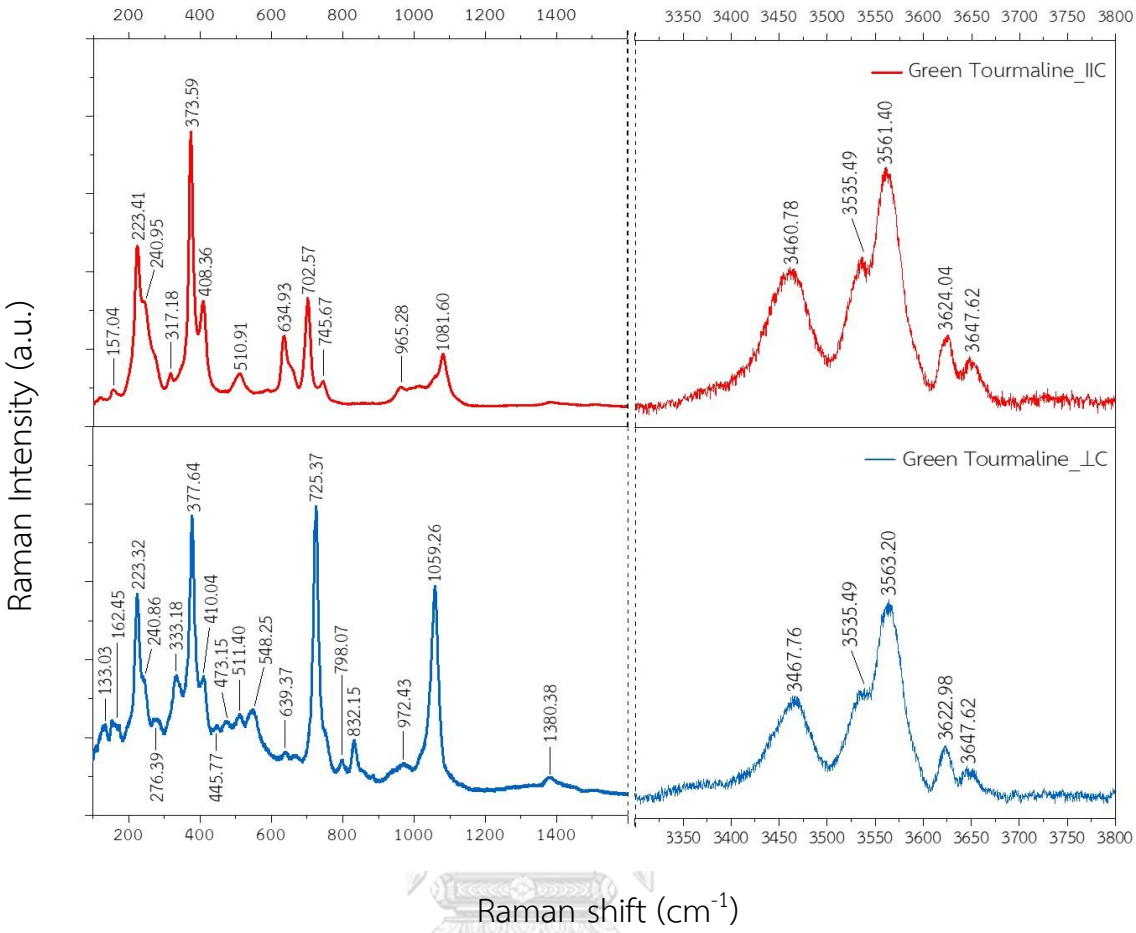

Figure 4.6 Absorption Raman spectra within range between 100-3800 cm^{-1} of green tourmaline; upper red spectrum analyzed in parallel to C-axis and lower blue spectrum analyzed in perpendicular to C-axis.

จุฬาลงกรณ์มหาวิทยาลัย
Chulalongkorn University

4.5 Hydroxyl Group

Functional -OH group in structure of representative samples were analyzed using Fourier Transform Infrared (FTIR) spectrometer. Two representative samples including pink tourmaline sample (Pk03) and green tourmaline sample (DG02) are reported here. IR spectra with wavenumber range between 8000 and 2500 cm^{-1} are shown in Figures 4.7 and 4.8. Two directions, parallel and perpendicular to C-axis, were measured for both samples which these IR spectra indicate absorption intensities and absorption characteristics differently in both directions. Four specific ranges (Table 4.4) can be described as followed.:

1. Range of 7600 to 6700 cm^{-1} was assigned to the first overtone of OH stretching mode (Oliveira et al., 2002). Pink tourmaline sample shows absorption bands at 7133.03, 6992.25, and 6790.24 cm^{-1} in direction parallel to C-axis. In direction perpendicular to C-axis, absorption bands at 7584.30, 7132.55, 6995.15, and 6740.58 cm^{-1} are present. Green tourmaline sample shows absorption bands at 7000.45 cm^{-1} in direction parallel to C-axis and 7578.99, 7133.03, 7012.50, and 6800.85 cm^{-1} in direction perpendicular to C-axis.

2. Range of 5400 to 5100 cm^{-1} relates to H_2O molecule combination between stretching and bending modes (Oliveira et al., 2002). H_2O absorption bands of pink tourmaline appear at 5195.38 cm^{-1} in parallel to C-axis, and at 5370.39 and 5198.75 cm^{-1} in perpendicular to C-axis. On the other hand, green tourmaline shows OH absorption bands at 5175.13 cm^{-1} in parallel to C-axis, and at 5360.26 and 5180.43 cm^{-1} in perpendicular to C-axis.

3. Range of 4600-3800 cm^{-1} associated with M-OH combination inducing OH bending mode where M can be occupied by Al, Mg, Mn, and Fe (Frost et al., 2007). Absorption bands located at 4600, 4500, and 4400 cm^{-1} are assigned for ^{Y}M-OH1, whereas band at 4300 cm^{-1} is associated with ^{Z}M-OH3. Moreover, additional OH3 for ^{Y}M-OH3 yields absorption bands at about 4100, 3900, and 3800 cm^{-1}. M-OH absorption band of both samples show the absorbed positions are not remarkably different. However, M-OH absorption band indicates concentration along to directional axis, differently

4. For the range of 3700-3100 cm^{-1}, assigned to the OH stretching modes (Castañeda et al., 2000; Oliveira et al., 2002) that consisted of two OH3 with ^{Y}(Fe+Mn)^{Z}Al^{Z}Al environment, which located at 3470-3400 cm^{-1}. Second position is OH1 connected with two YYY octahedral, ^{Y}(Fe+Mn)^{Y}Al^{Y}Al at 3625-3615 cm^{-1} and ^{Y}Li^{Y}Al^{Y}Al at 3660-3650 cm^{-1}. The last of IR band shows the absorption located at 3340-3320 and 3165-3160 cm^{-1}, which related to the H_2O stretching. OH1 and H_2O absorption bands for pink and green samples are not present different bands, obviously. OH3 bands of pink sample show 3622.20 - 3400.42 cm^{-1} in parallel to C-axis and at 3618.35 - 3436.10

จุฬาลงกรณ์มหาวิทยาลัย
CHULALONGKORN UNIVERSITY

cm^{-1} in perpendicular to C-axis. Whereas green sample presents OH3 bands about 3625- 3470 cm^{-1} in both parallel and perpendicular to C-axis.

Table 4.4 Assignment of infrared absorption band (cm^{-1}) related to hydroxyl group (OH group) for pink and green tourmalines from Nigeria source (Castañeda et al., 2000; Oliveira et al., 2002; Frost et al., 2007).

Wavenumber (cm^{-1})				Type of modes	
Pink tourmaline		Green tourmaline			
//C	⊥C	//C	⊥C		
	7584.30		7578.99	The first overtone of OH stretching mode	
7133.03	7132.55		7133.03		
6992.25	6995.15	7000.45	7012.50		
6790.24	6740.58		6800.85		
	5370.39		5360.26	H_2O combination: stretching & bending modes of molecular water	
5195.38	5198.75	5175.13	5180.43		
4598.02	4598.50	4598.02	4595.61	OH combination: M-OH bending modes	^{Y}M-OH1
4534.38	4532.45	4535.35	4540.65		
4432.17	4432.65	4444.23	4440.85		
4342.01	4340.09	4344.91	4345.39		^{Z}M-OH3
4144.34	4154.47	4170.38	4165.56		^{Y}M-OH3
	4024.29	4048.40	4033.94		
3901.35	3902.80	3900.39			
		3850.25	3850.25		
3650.65	3654.99	3660.77	3660.29	OH1 $^{Y}Al^{Y}Al^{Y}(Al,Li)$	
3622.20-	3618.35-	3625.65-	3625.58-	(OH3) $^{Y}(Fe,Mn,Mg,Al)^{Z}Al^{Z}Al$	
3400.42	3436.10	3470.33	3469.37	(OH3) $^{Z}Al^{Z}Al^{Y}(Al,Li)$	
3320.39	3330.04	3340.64	3340.16	H_2O stretching	
3160.33			3165.15		

จุฬาลงกรณ์มหาวิทยาลัย
Chulalongkorn University

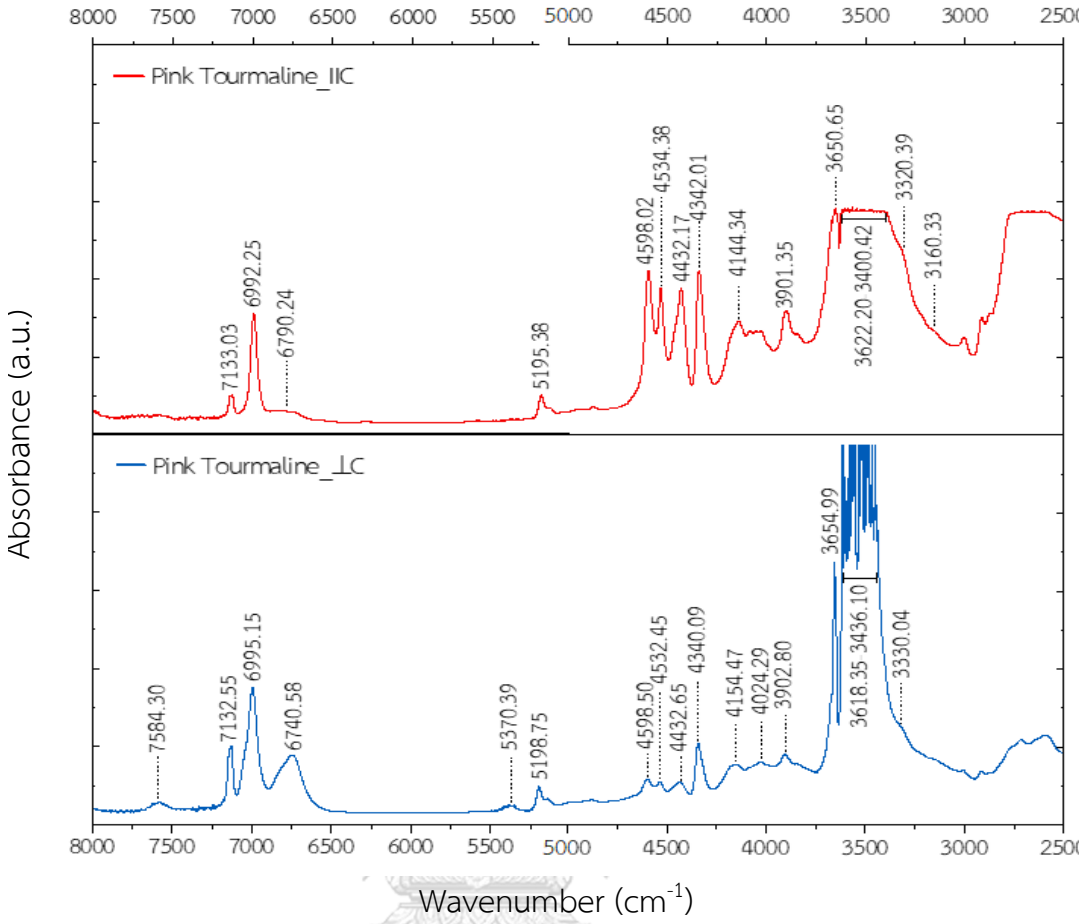

Figure 4.7 Absorption Infrared spectra within range of 8000-2500 cm^{-1} of pink tourmaline; upper red spectrum analyzed in parallel to C-axis and lower blue spectrum analyzed in perpendicular to C-axis.

จุฬาลงกรณ์มหาวิทยาลัย
Chulalongkorn University

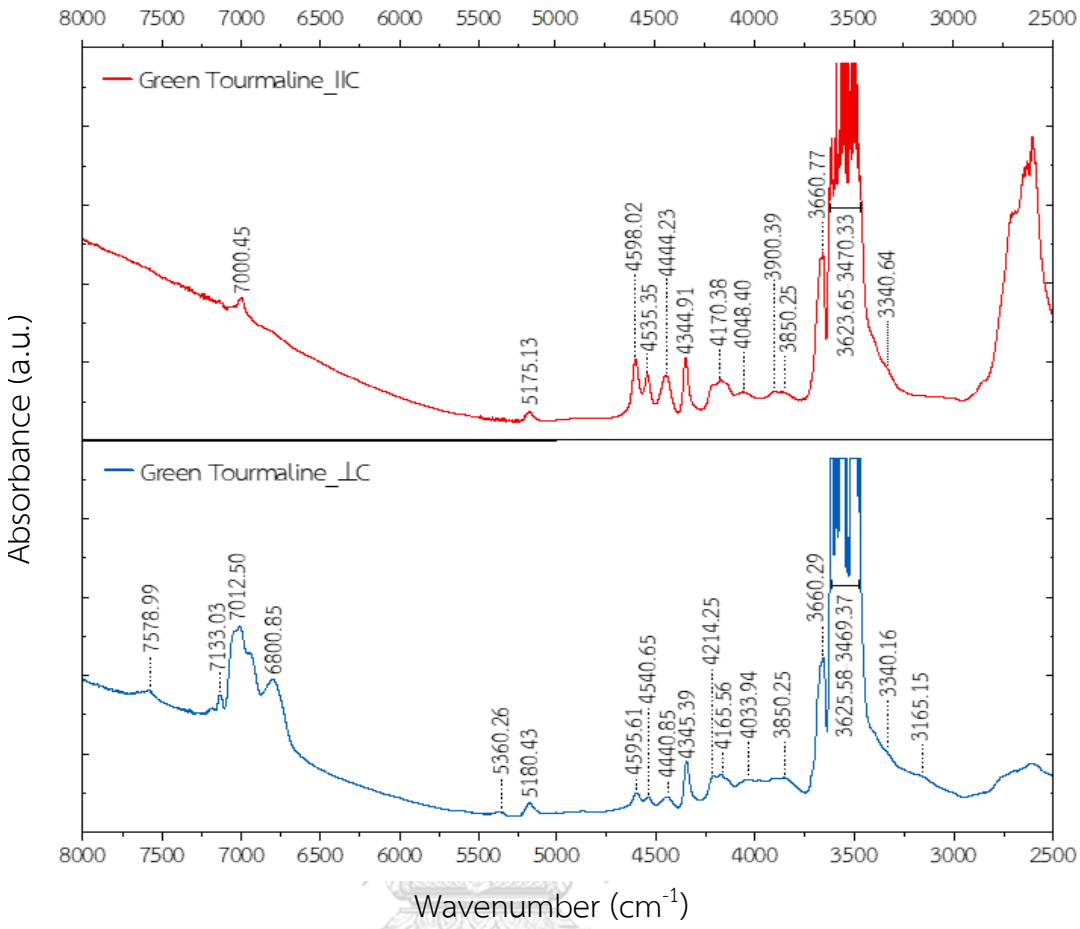

Figure 4.8 Absorption Infrared spectra within range of 8000-2500 cm^{-1} of green tourmaline; upper red spectrum analyzed in parallel to C-axis and lower blue spectrum analyzed in perpendicular to C-axis.

จุฬาลงกรณ์มหาวิทยาลัย
Chulalongkorn University

4.6 UV-Vis spectroscopy

The absorbance spectra of tourmaline samples were analyzed in visible range between 300 to 800 nanometers. The UV-Vis spectra of representative pink tourmalines measured in oriented directions, are shown in Figure 4.9 (A). Pink samples are usually appeared prominent absorbed band centered around 505-515 nm with maximum absorption and two small peaks at 450, 458, and 478 nm, which relate to Mn^{3+} ion (Taran et al., 1993). These absorptions influencing in the blue-green region and cause purple pink color of tourmaline. Next is minor band centered around 395 nm involved with Mn^{2+} ion (I.M. Reinitz & G.R. Rossman, 1988). This band absorbs in the purple region yields slightly yellow tonality in pink tourmalines. Additional band is

relatively weak broadband presents in a wavelength range between 675-700 nm, which related to Fe^{2+} ion (M.N. Taran et al., 1993). Comparing to the optical absorption spectra in oriented direction (parallel and perpendicular to C-axis) found that the absorption bands measure in parallel to C-axis are highly concentration than those measure in perpendicular to C-axis. Therefore, these absorption bands accord to body color of samples.

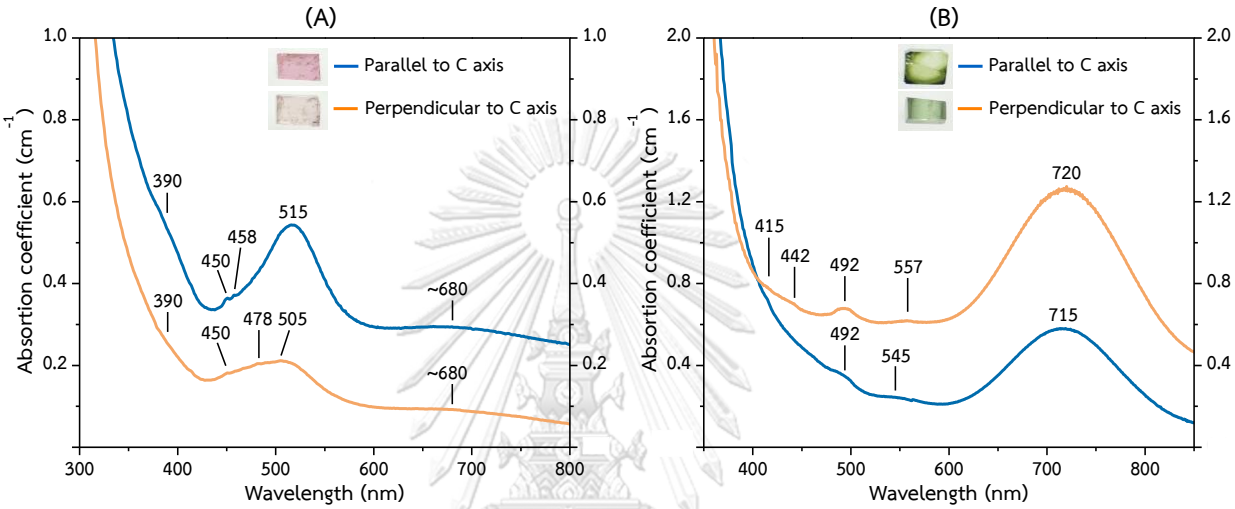

Figure 4.9 UV-Vis absorption spectra of representative pink and green tourmalines showing absorption coefficients in oriented directions compared between parallel and perpendicular to C-axis (A) natural Pk13 (B) natural DG01

จุฬาลงกรณ์มหาวิทยาลัย
Chulalongkorn University

Figure 4.9 (B) shows the optical absorption band of representative green tourmalines (DG01), were measured in oriented directions, wavelength of 350-850 nm. The UV-Vis absorption spectra present the distinct band centered around 715-720 nm with maximum absorption, assigned to the transition of Fe^{2+} ion (S.M. Mattson & G.R. Rossman, 1987; M.N. Taran et al., 1993). This band absorbs in red region cause green color in tourmaline. Two broadbands centered around 415 and 442 nm absorbed in purple-blue region, which yield slightly yellow shade in green tourmaline. These bands present as shoulder features and they would be assigned to transition of Mn^{2+} and Mn^{3+} ion (M.N. Taran et al., 1993; T. A. Carrino et al., 2019). Other bands are relatively weak band absorbed in blue-green region appear at 492 545, and 557 nm relate to Fe^{3+} (M.N. Taran et al., 1993).

4.7 Oxidation states of Manganese and Iron

The oxidation states of manganese and iron investigation are observed in four natural tourmaline samples, including two pink samples (Pk03) and two green samples (DG02). Regarding Mn, its *K*-edge XANES spectra in the energy range of 6520 – 6600 eV for pink and green tourmalines are shown in Figure 4.10 in comparison with two spectra of manganese oxide standard which are Mn (II) oxide as MnO (6544 eV), and Mn (III) oxide as Mn_2O_3 (6553 eV). Nigerian tourmaline samples clearly show the Mn *K*-edge spectra near 6546 eV which are between the MnO and Mn_2O_3 standards. Therefore, it may assume that Mn occupied in the structures of both pink and green tourmalines are enclosed with Mn^{2+} ion and Mn^{3+} ion.

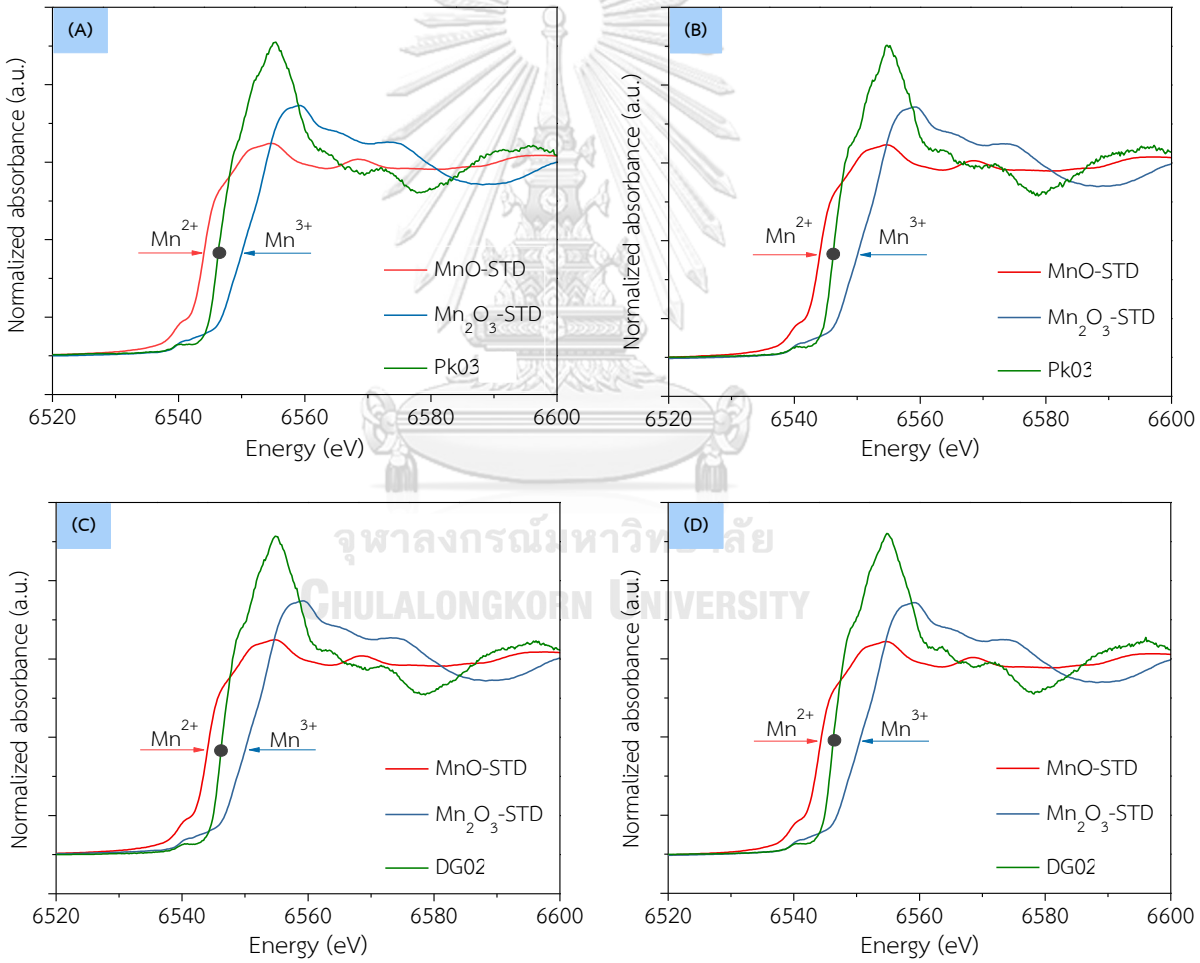

Figure 4.10 Normalized Mn *K*-edge XANES spectra of natural tourmalines: (A-B) Pk03 samples and (C-D) DG02 samples.

Fe *K*-edge XANES spectra of the natural tourmaline samples in the energy range of 7090 to 7200 eV are shown in Figure 4.11. The Fe *K*-edge spectra of the samples were compared with two iron compound standards, which are Fe (II) oxide (FeO) at 7119 eV, and Fe (III) oxide (Fe_2O_3) at 7123. The XANES analyses reveal that pink tourmaline samples are unclearly indicated because of low iron content (<0.1 wt.%) On the other hand, green tourmalines show Fe *K*-edge spectra at about 7119.57 and 7119.97 eV which are comparable to the FeO spectrum. Thus, it can be assumed that green tourmalines are composed of Fe^{2+} ion rather than Fe^{3+} ion.

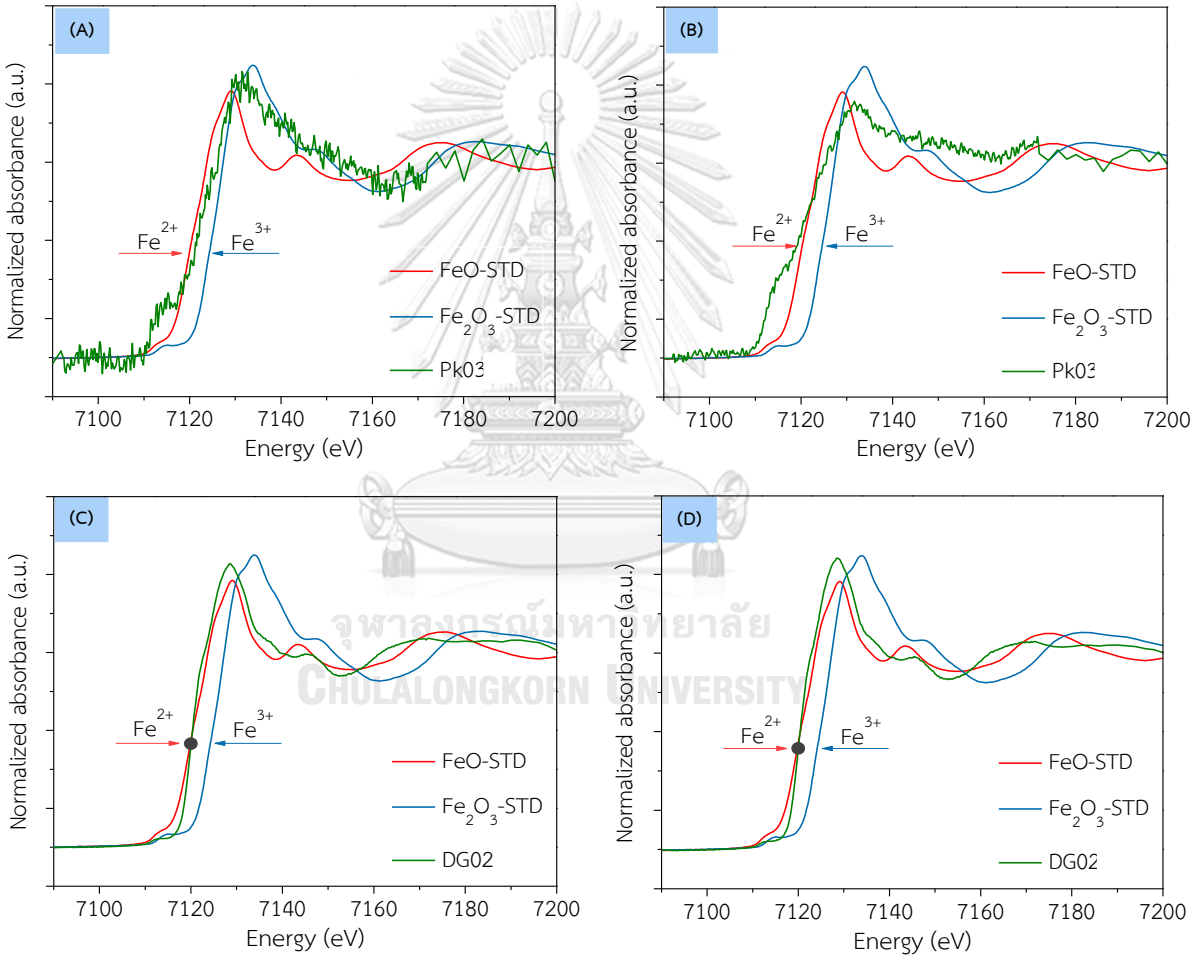

Figure 4.11 Normalized Fe *K*-edge XANES spectra of natural tourmalines: (A-B) Pk03 samples and (C-D) DG02 samples.

CHAPTER V

IRRADIATION EXPERIMENT

5.1 Color Modification

Color enhancement of tourmaline samples by using two irradiation processes, electron beam and gamma irradiation. The samples were irradiated with three doses, 400, 800, and 1,200 kilogreys, respectively. The natural color of representative samples (Pk03 and DG02) and their colors after irradiation processes are shown in Figure 5.1 and 5.2. The photograph of remaining samples will be presented in Appendix B1 and B2. These samples were investigated in two of directional along crystal axis, parallel and perpendicular to C-axis. The natural colors of pink tourmaline along to C-axis present near colorless, pale pink, pink, and orangey pink. For green tourmalines show natural color, which is mostly yellowish green. The natural colors of pink tourmaline in perpendicular to C-axis present pale orangey pink, orangey pink, and pinkish orange and also display green color in green tourmalines.

The result of improving color with irradiation processes found that most pink samples turn into intense pink color whereas some samples change to orange color after irradiation. In addition, some irradiated samples produce minor yellow shade together with intense pink color. Furthermore, electron beam irradiation potentially produces intense colors higher than those resulted from gamma ray irradiation, which the higher intense colors also yielded from higher dosage of irradiation, respectively. On the other hand, both electron beam and gamma ray produce slightly increasing yellow color in green tourmalines along to C-axis, whereas the irradiated color in perpendicular to C-axis are clearly unchanged.

จุฬาลงกรณ์มหาวิทยาลัย
Chulalongkorn University

Figure 5.1 Color modification after 3 steps of irradiation treatments, viewed in the direction parallel to c-axis.

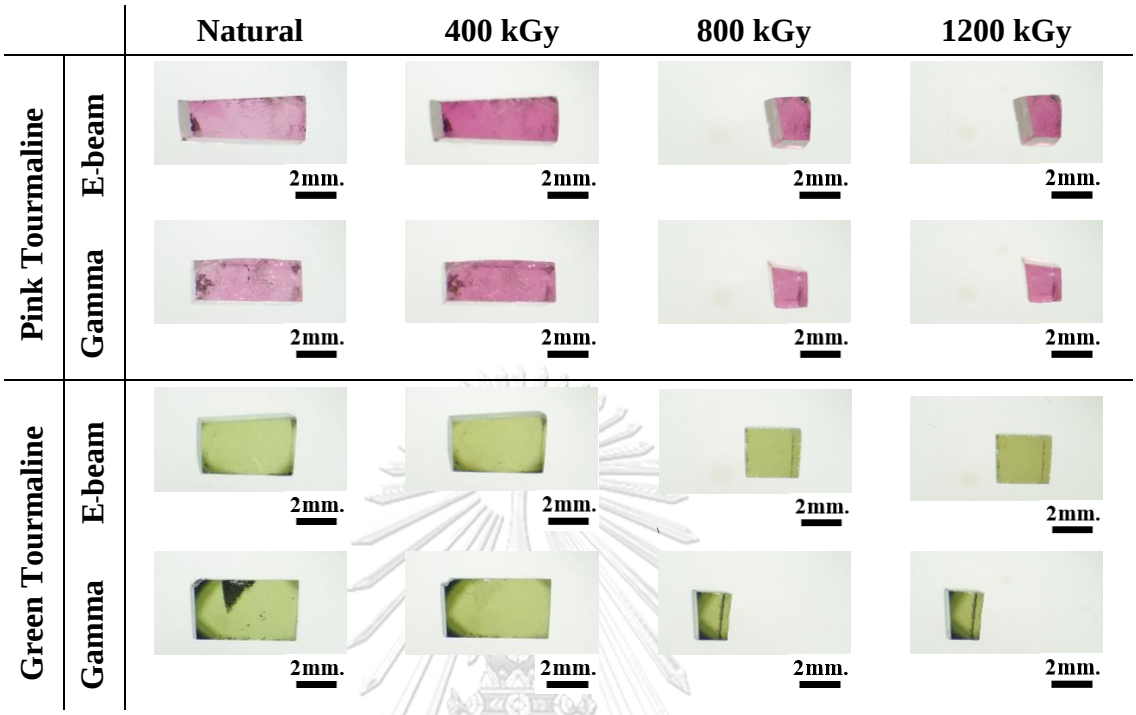

Figure 5.2 Color modification after 3 steps of irradiation treatments, viewed in the direction perpendicular to c-axis.

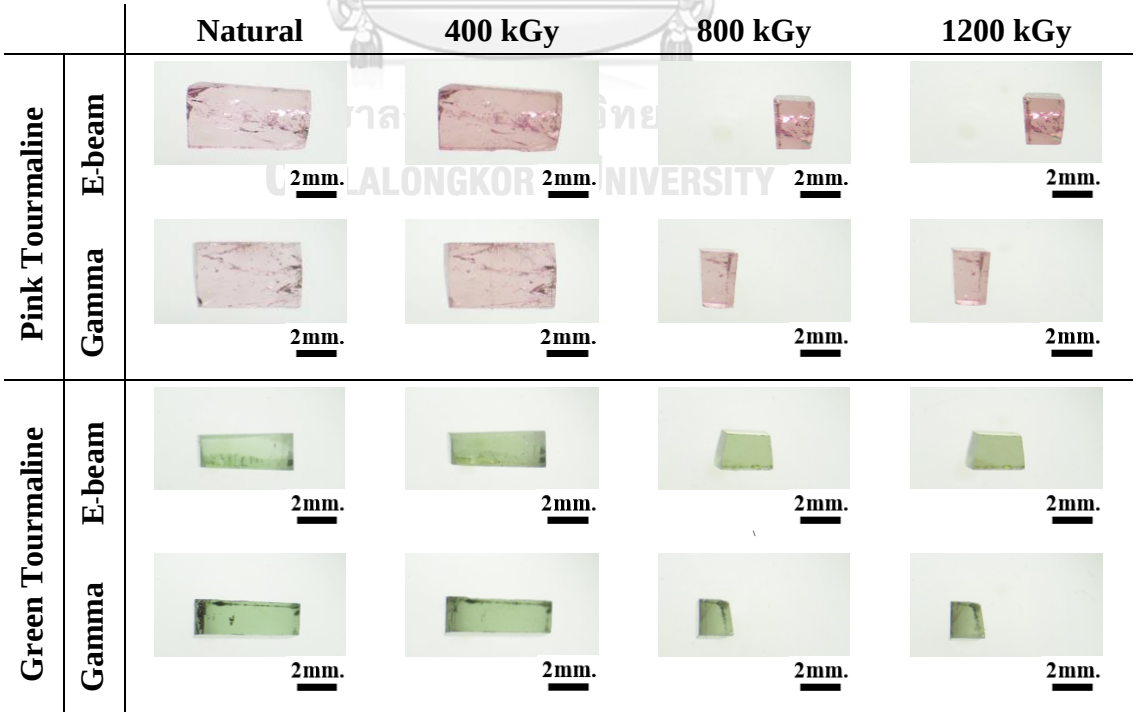

Pink tourmalines (Pk03) were measured color with the CIE L*a*b*, are shown in Figure 5.3 and 5.4. The irradiated pink sample with electron beam (Figure 5.3), the a* value has increased clearly (approached to a* positive value) and b* value has slightly increased. The irradiated pink sample with gamma ray yields a* value has increased obviously and b* value has slightly increased slightly. The color measurement in perpendicular to C-axis (Figure 5.4), the irradiated sample with electron beam and gamma ray have increasing of a* value and slightly increasing of b* value.

Considering the color difference values (ΔE) from of pink sample, these values will be increase according to the higher dosage of irradiation. The irradiated sample with electron beam indicates delta E values more increase than the irradiated sample with gamma ray. The results of color difference values illustrate that the irradiated tourmaline with electron beam produce intense pink color obviously than gamma ray.

The color measurement of green tourmalines is shown in Figure 5.5 and 5.6. Both irradiated tourmaline with electron beam, and irradiated sample with gamma ray present a* and b* values that are slightly increasing. The color measurement results of green tourmalines are according to the color modification (Figure 5.1 and 5.2). For the color difference values (ΔE) of green tourmalines are negligible increasing, which accord to the higher dosage irradiation.

จุฬาลงกรณ์มหาวิทยาลัย
Chulalongkorn University

5.2 UV-Vis spectroscopy

The absorbance spectra of pink tourmaline samples were analyzed in visible range between 300 to 800 nanometers. The UV-Vis spectra of representative pink tourmaline (Pk03) measured parallel to C-axis, are shown in Figure 5.7 (A-B) and measured in perpendicular to C-axis are shown in Figure 5.7 (C-D). UV-Vis absorption spectra of more samples were collected in Appendix C1. Both electron beam and gamma radiation can produce intense pink color and minor yellow tonality in natural samples. The intense pink is significantly associated with increasing absorptions centered around 515 nm (parallel to C-axis), 505 to 515 nm (perpendicular to C-axis). On the other hand, the yellow shade produced after irradiation relates to increasing absorption centered around 390-395 nm both parallel and perpendicular to C-axis. Absorptions yielded

after electron beam irradiation (Figure 5.7A and 5.7C) are slightly higher than those obtained by gamma ray irradiation (Figure 5.7B and 5.7D), which reflects more intense color in electron beam-treated samples (Figures 5.1)

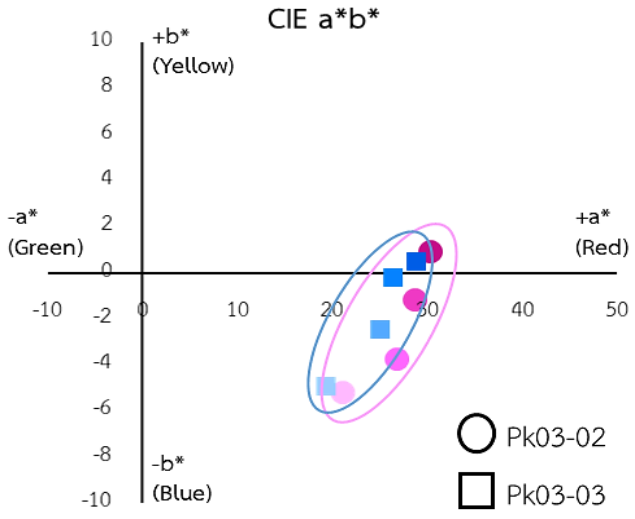

Figure 5.3 Correlation a* and b* diagram of pink tourmalines in parallel to C-axis, directionly.

Color measurement (IIC)

Pk03 irradiated with electron beam (Pk03-02)

	untreated	400 kGy	800 kGy	1200 kGy
L*	64.39	54.89	52.10	50.49
a*	20.96	26.75	28.59	30.29
b*	-5.16	-3.73	-1.12	0.94
ΔE		11.22	15.02	17.82

Pk03 irradiated with gamma (Pk03-03)

	untreated	400 kGy	800 kGy	1200 kGy
L*	66.93	59.45	57.86	55.45
a*	19.34	24.97	26.31	28.81
b*	-4.91	-2.43	-0.17	0.54
ΔE		9.68	12.38	15.85

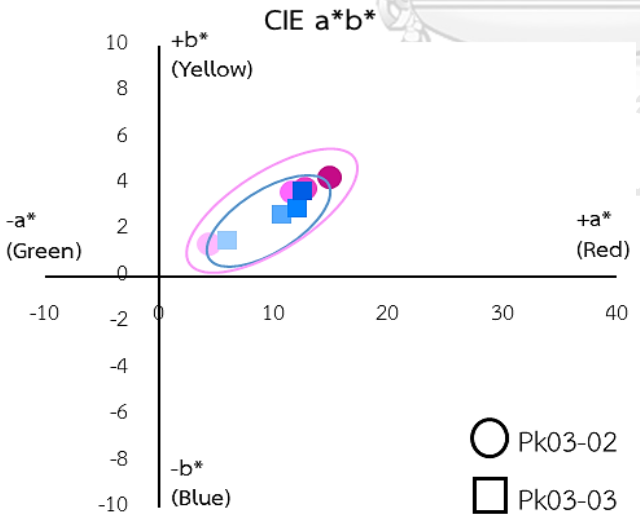

Figure 5.4 Correlation a* and b* diagram of pink tourmalines in perpendicular to C-axis, directionly.

Color measurement (⊥C)

Pk03 irradiated with electron beam (Pk03-02)

	untreated	400 kGy	800 kGy	1200 kGy
L*	77.03	70.80	67.15	65.39
a*	4.29	11.56	13.66	15.84
b*	1.43	3.67	3.85	4.35
ΔE		9.83	13.83	16.66

Pk03 irradiated with gamma (Pk03-03)

	untreated	400 kGy	800 kGy	1200 kGy
L*	78.83	71.85	68.42	66.18
a*	5.90	10.67	11.97	13.43
b*	1.60	2.71	2.99	3.74
ΔE		8.53	12.13	14.88

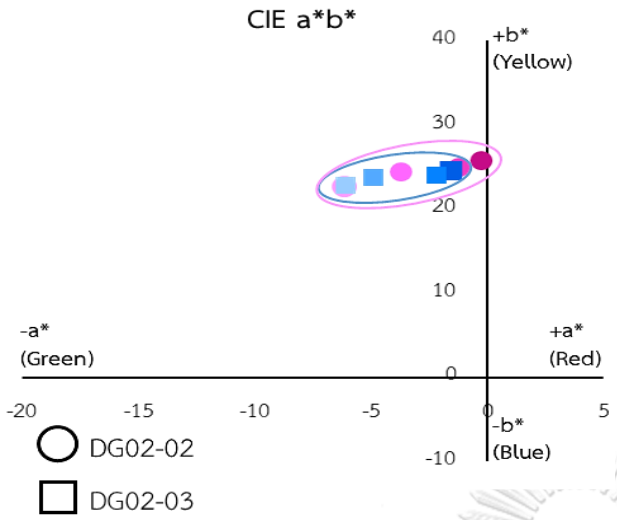

Figure 5.5 Correlation a* and b* diagram of green tourmalines in parallel to C-axis, directionly.

Color measurement (IIC)

DG02 irradiated with electron beam (DG02-02)

	untreated	400 kGy	800 kGy	1200 kGy
L*	49.73	46.83	44.43	43.71
a*	-6.17	-3.75	-1.25	-0.31
b*	22.71	24.44	25.08	25.84
ΔE		4.15	7.61	8.97

DG02 irradiated with gamma (DG02-03)

	untreated	400 kGy	800 kGy	1200 kGy
L*	50.41	47.92	46.75	45.06
a*	-6.11	-4.93	-2.19	-1.59
b*	22.84	23.79	24.11	24.57
ΔE		2.91	5.51	7.21

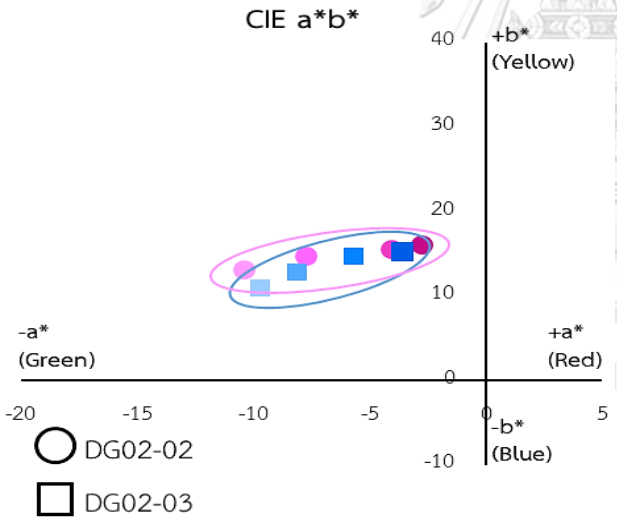

Figure 5.6 Correlation a* and b* diagram of green tourmalines in perpendicular to C-axis, directionly.

Color measurement (⊥C)

DG02 irradiated with electron beam (DG02-02)

	untreated	400 kGy	800 kGy	1200 kGy
L*	54.99	53.55	52.80	51.75
a*	-10.43	-7.79	-4.09	-2.78
b*	13.12	14.75	15.58	16.12
ΔE		6.90	7.14	8.83

DG02 irradiated with gamma (DG02-03)

	untreated	400 kGy	800 kGy	1200 kGy
L*	54.60	53.88	53.15	52.82
a*	-9.74	-8.16	-5.75	-3.64
b*	10.98	12.93	14.69	15.34
ΔE		2.61	5.64	7.71

The optical spectra of green tourmalines were analyzed in wavelength between 350 to 850 nanometers range. The UV-Vis spectra of representative green tourmaline (DG02) measured along to C-axis present in Figure 5.8 (A-B) and those measured in perpendicular to C-axis observe in Figure 5.8 (C-D). The optical absorption spectra of

more samples were collected in Appendix C1. Both electron beam and gamma produce negligible yellow shade in green tourmalines that relate to the increasing broad absorption band in the range between 400-500 nm (415, 442, 445, and 495 nm). Whereas the main absorption band centered around 715-720 nm are slightly decrease.

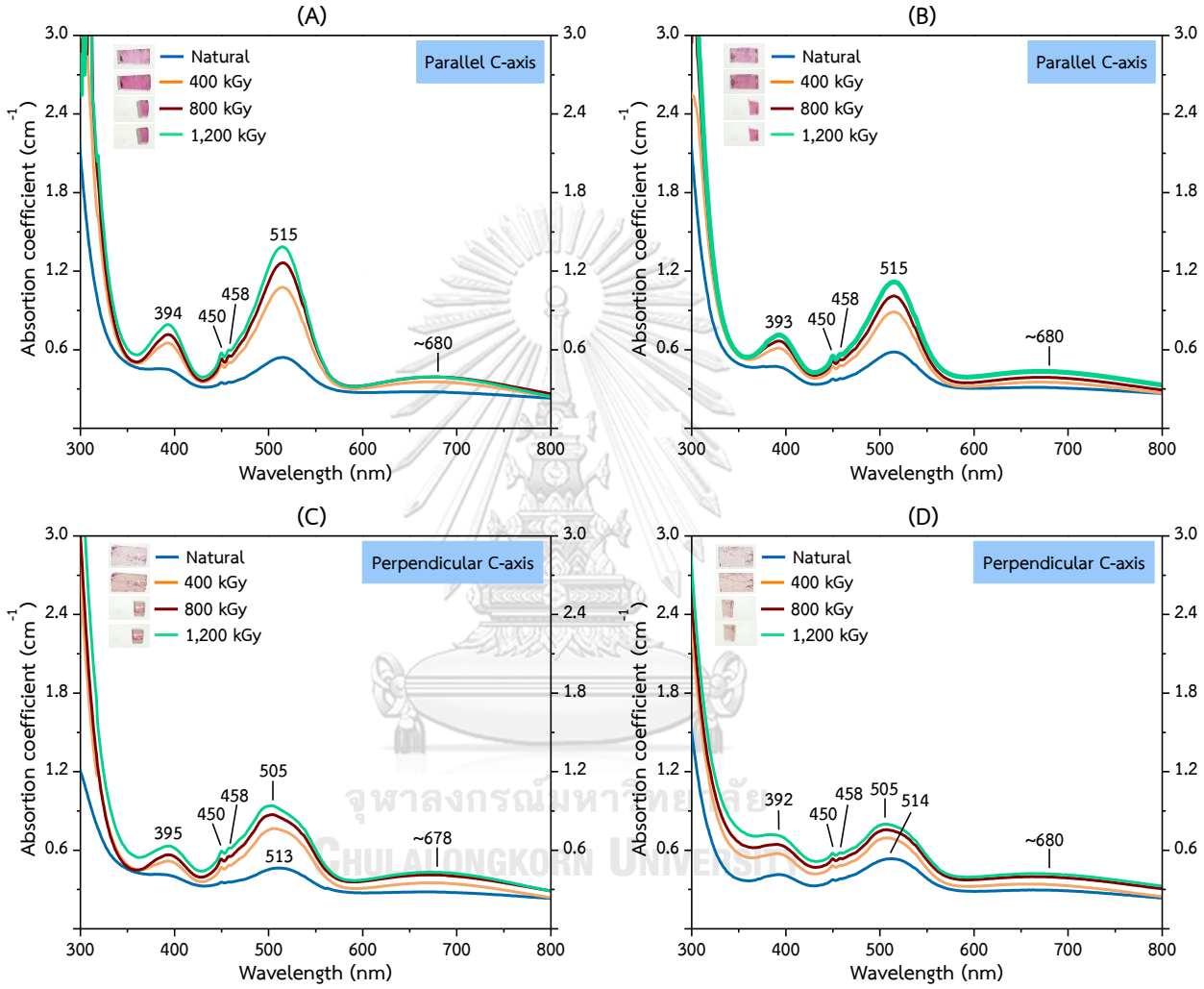

Figure 5.7 UV-Vis absorption spectra of Pk03 sample showing increasing absorption coefficients in oriented directions compared between natural and irradiated colors with different dosages: (A) e-beam irradiated color in //C-axis; (B) gamma irradiated color in //C-axis; (C) e-beam irradiated color in ⊥C-axis; (D) gamma irradiated color in ⊥C-axis.

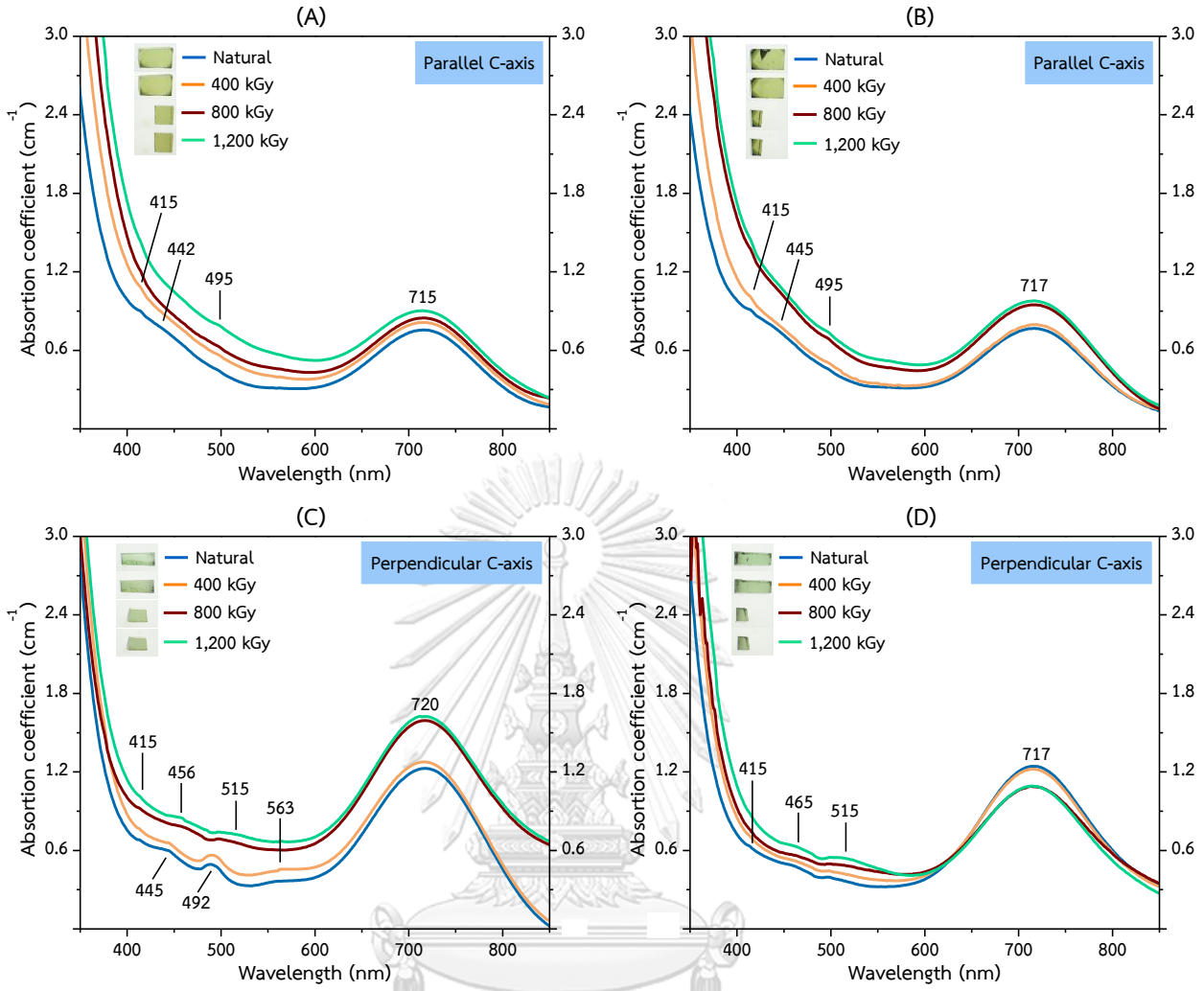

Figure 5.8 UV-Vis absorption spectra of DG02 sample showing increasing absorption coefficients in oriented directions compared between natural and irradiated colors with different dosages: (A) e-beam irradiated color in //C-axis; (B) gamma irradiated color in //C-axis; (C) e-beam irradiated color in ⊥C-axis; (D) gamma irradiated color in ⊥C-axis.

จุฬาลงกรณ์มหาวิทยาลัย
Chulalongkorn University

5.3 XAS spectroscopy

Figure 5.9 indicates the XANES absorption spectra of pink and green tourmalines comparing with natural and after irradiated with electron beam and gamma ray. The Mn *K*-edge spectra of representative natural samples appear near 6546 eV, which are located between Mn^{2+} (~6544 eV) and Mn^{3+} (~6553 eV). After irradiated with both electron beam and gamma-ray (400 and 800 kGy), these Mn *K*-edge spectra are clearly unchanged in both pink and green samples.

Fe *K*-edge spectra of pink samples show their spectra contain very noise signal shown in Figure 5.10 (A-B). The Fe *K*-edge energy of the natural sample appear near 7120 eV close to Fe^{2+} (7119 eV). When samples were irradiated at 400 kGy and 800 kGy, they shifted slightly to 7121 eV. However, this result could not assume that the radiation treatment induced the transformation of Fe oxidation state. Due to Fe K-edge spectra of pink samples show a lot of noise signal because pink sample contains Fe content less than 0.1 %wt and they could not analyze completely. Additionally, XANES spectra of green tourmalines are shown in Figure 5.10 (C-D). The Fe *K*-edge of natural green tourmalines are also close to Fe^{2+} (7119 eV). The Fe *K*-edge of irradiated samples with both electron beam and gamma ray are significantly unchanged.

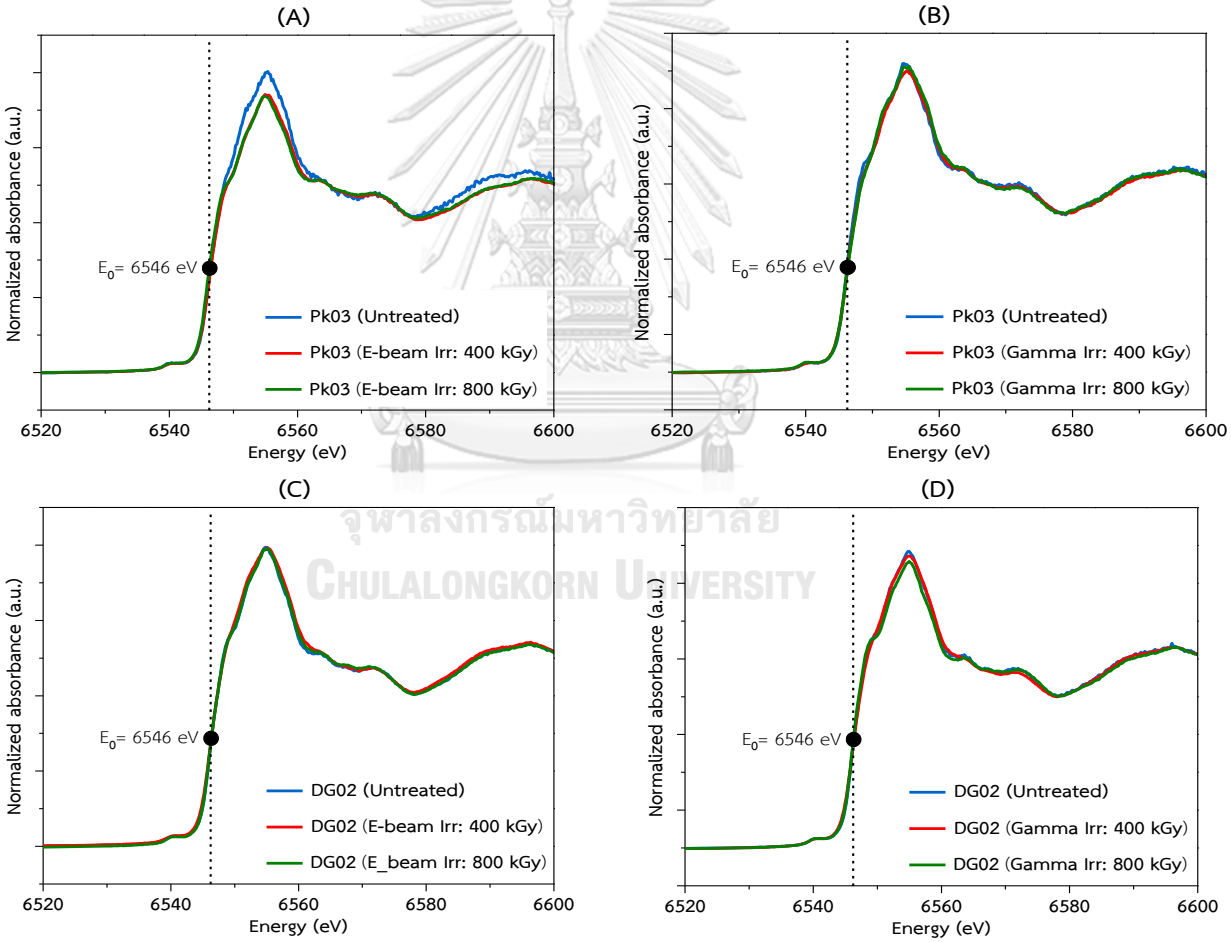

Figure 5.9 Normalized XANES spectra of Mn *K*-edge for Nigerian tourmalines before and after irradiation: (A) Pk03 irradiated with e-beam; (B) Pk03 irradiated with gamma; (C) DG02 irradiated with e-beam; (D) DG02 irradiated with gamma;

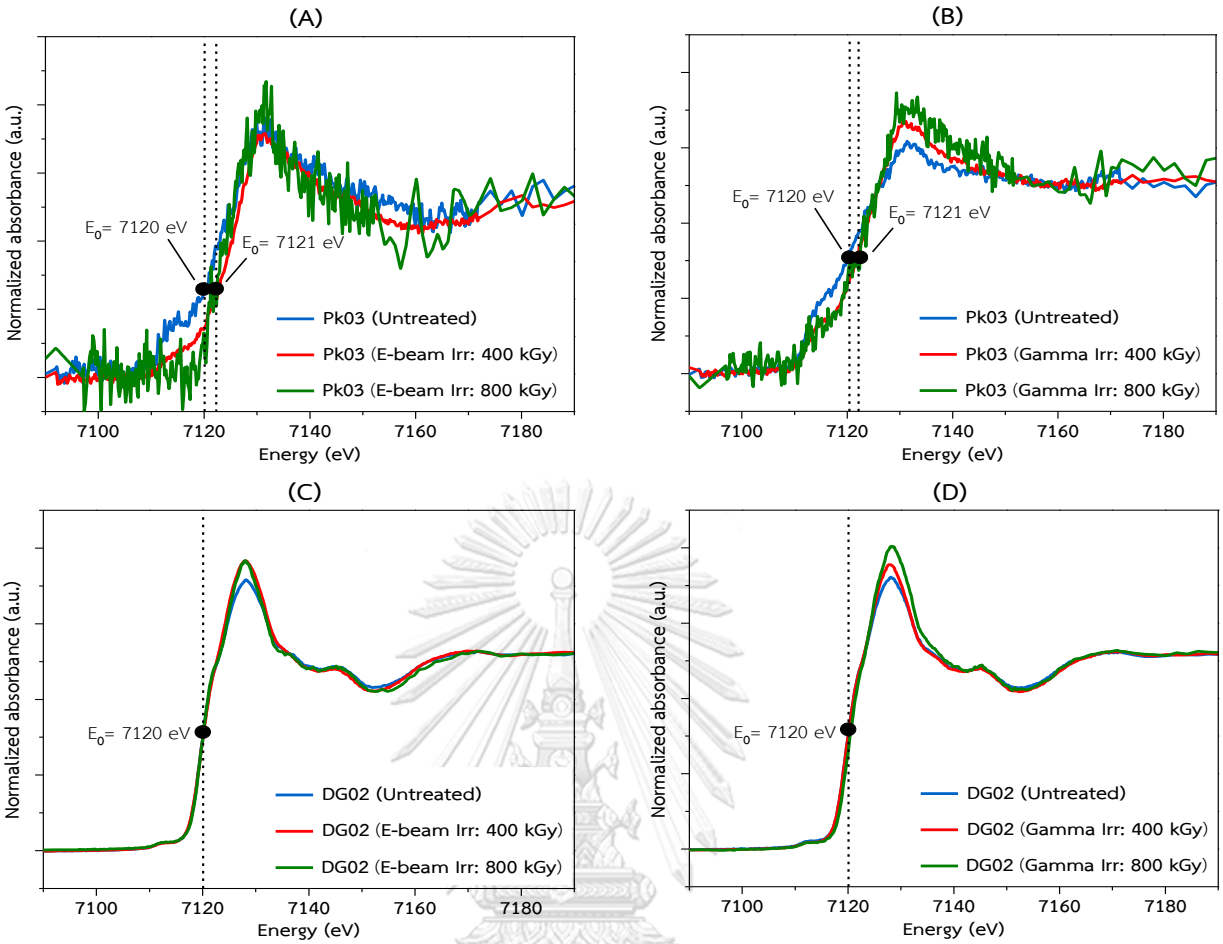

Figure 5.10 Normalized XANES spectra of Fe *K*-edge for Nigerian tourmalines before and after irradiation: (A) Pk03 irradiated with e-beam; (B) Pk03 irradiated with gamma; (C) DG02 irradiated with e-beam; (D) DG02 irradiated with gamma;

จุฬาลงกรณ์มหาวิทยาลัย
Chulalongkorn University

5.4 EPR spectroscopy

The most important parameter of EPR signal is g-factor which is a constant of proportionality used to calculate the magnetic moment of electron spin. The g-factor, present in Table IV, can be calculated using the equation:

$$h\nu = g\mu_B B$$

where h is Plank's constant equals 6.6262 x 10-34 J.s and μ_B is the Bohr magneton constant (9.274 x 10-24 J/T). Another factor is microwave frequency (ν) controlled by people whereas B is magnetic field.

Table 5.1. Calculated g-factor values from EPR signals.

Environments	g-factor	Magnetic field (mT)
Mn ions	2.66	264
	2.48	283
	2.33	302
Fe ions	1.97	357
H^0 center	2.17	324
	1.88	375
O^- center	2.07	339
	2.05	343
	2.00	351

EPR spectra of representative pink tourmalines (Pk03) are shown in Figure 4.12. In the natural sample, EPR spectrum recorded three resonance signals at 264 mT, 283 mT, and 302 mT (Figure 4.12A). These signals appear to be caused by Mn ion as suggested by Babinska et al. (2008).

After irradiation at 400 kGy by both techniques, the EPR spectra presented a set of paramagnetic signals, particularly in the range of 320 – 380 mT (Figures 4.12B and 4.12C) which these signal lines were ascribed as defects (Krambrock et al., 2002). Two kinds of color center including O^- center (hole center) and H^0 center (electron center) are the results of these defects. The H^0 center is indicated by two signals which are relatively sharp signals, at 324 mT and 375 mT whereas the O^- center is characterized by a broad signal at approximately 339-343 mT. However, electron beam irradiation produced more significant signals of color centers, which yielded more intense color in the samples.

จุฬาลงกรณ์มหาวิทยาลัย
Chulalongkorn University

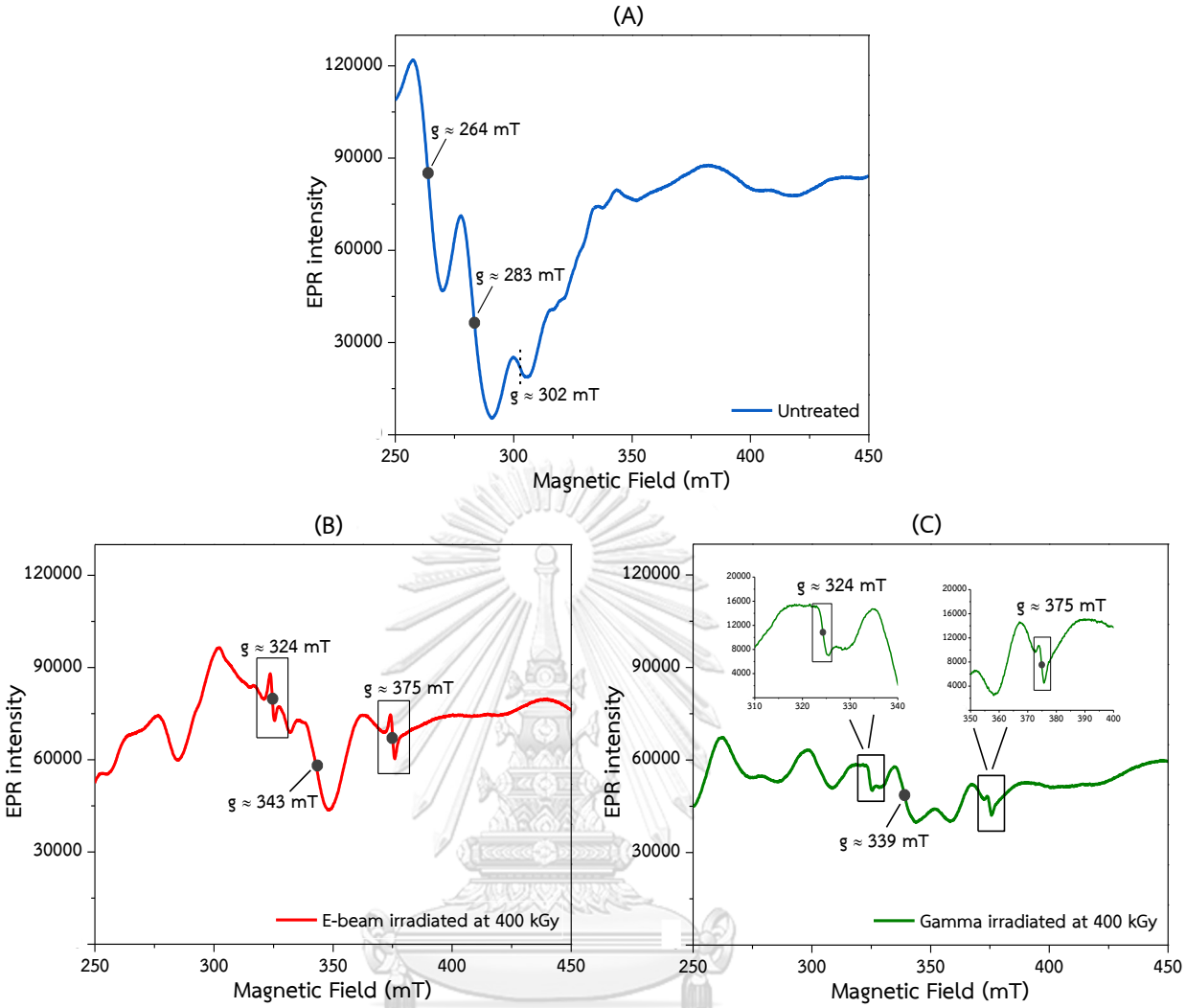

Figure 5.11 Room temperature EPR spectra of representative pink tourmaline sample (Pk03) for comparison between natural stone (A). EPR spectra the same sample after 400 kGy irradiations by e-beam technique (B) and gamma ray (C).

จุฬาลงกรณ์มหาวิทยาลัย
Chulalongkorn University

The EPR spectra of representative green tourmaline are present in Figure 4.13 (A-C). In the natural green samples appear two signals are signal at 283 mT, due to Mn content, and signal of Fe content at 357 mT (Cano et al., 2019), are shown in Figure 4.13 (A). When green samples were irradiated at 400 kGy with both techniques (Figure 4.13A and 4.13B), the irradiated samples present broad signals which related to O^- center at 343 mT and 351 mT. For the signal line of H0 center was not appear in irradiated green tourmaline in both techniques.

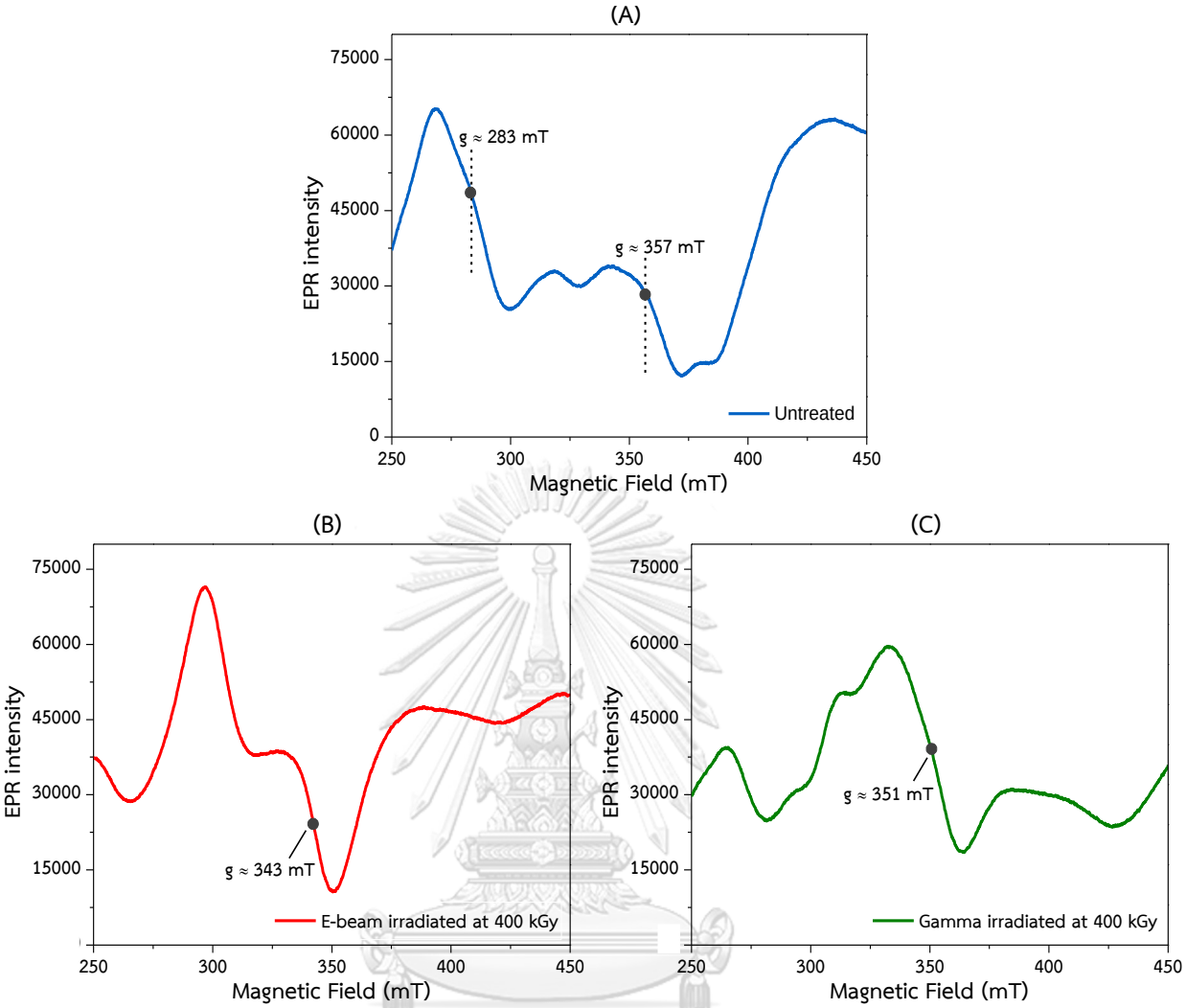

Figure 5.12 Room temperature EPR spectra of representative green tourmaline sample (DG02) for comparison between natural stone (A). EPR spectra the same sample after 400 kGy irradiations by e-beam technique (B) and gamma ray (C).

จุฬาลงกรณ์มหาวิทยาลัย
Chulalongkorn University

CHAPTER VI

DISCUSSIONS AND CONCLUSIONS

6.1 Discussions

Tourmaline samples in this study are from Nigerian sources, which are occurred in magmatic rocks associated with pegmatites rock. In general, a group of tourmalines depended on the chemistry in X-site. All samples have been classified into the alkali group because they contain sodium as the main component in X-site, which yielded about 0.685 to 0.885 apfu (Table 4.4) that was calculated from EPMA results. Moreover, assignment of tourmaline species depended on the chemistry in Y-site location. For elbaite specie, the general structural composition is $^{Y}(Al^{3+}_{1.5}Li^{+}_{1.5})$ or $^{Y}(Al^{3+}_{1}Li^{+}_{2})$. From calculation of EPMA results, all tourmalines consist of aluminium (about 0.39 to 1.36 apfu) together with Li^{+} (estimated at about 1.60 to 2.38 apfu) are allocated in Y-site. Therefore, all tourmaline samples are classified to elbaite end-member. The significant internal features of Nigerian tourmalines present characteristics of liquid inclusions or two-phase inclusions included liquid and gas, so-called “trichites”. Besides, it can be found colored growth tubes or hollow tubes, which are usually arranged in parallel to C-axis direction.

จุฬาลงกรณ์มหาวิทยาลัย
CHULALONGKORN UNIVERSITY

The significant internal features of Nigerian tourmalines present characteristic of liquid inclusions or two-phase inclusions included liquid and gas, so-called “trichites”. Besides, it can be found colored growth tubes or hollow tube, which usually arranged in parallel to C-axis direction.

Raman spectra of tourmalines in the range 3200-3800 cm^{-1}, can be apply to tourmaline species classifying. The Raman shift of 3200-3800 cm^{-1} associated with the hydroxy (OH) group in the W-site (OH1) and V-site (OH3), presented in Table 6.1. All tourmalines indicate the OH(1) bands connected with $^{Y}Li^{Y}Al^{Y}Al$ at 3647-3622 cm^{-1}. The absorption band of OH(3) sharing three O atoms with three YZZ octahedral, such as

$2^{Y}(Fe+Mn)^{Z}Al^{Z}Al$- $^{Y}Al^{Z}Al^{Z}Al$ at 3563-3558 cm^{-1}, $2^{Y}Li^{Z}Al^{Z}Al$-$^{Y}Al^{Z}Al^{Z}Al$ at 3535 cm^{-1}, and $^{Y}(Fe+Mn)^{Z}Al^{Z}Al$-$2^{Y}Al^{Z}Al^{Z}Al$ at 3467-3439 cm^{-1}. These OH bands are assigned to elbaite tourmaline.

Table 6.1 Raman frequency (cm^{-1}) of ^{V}OH and ^{W}OH stretching modes assignment.

Samples	**OH(3) in V-site**			**OH(1) in W-site**	
	$^{Y}(Fe+Mn)^{Z}Al^{Z}Al$-$2^{Y}Al^{Z}Al^{Z}Al$	$2^{Y}Li^{Z}Al^{Z}Al$-$^{Y}Al^{Z}Al^{Z}Al$	$2^{Y}(Fe+Mn)^{Z}Al^{Z}Al$-$^{Y}Al^{Z}Al^{Z}Al$	$^{Y}Li^{Y}Al^{Y}Al$	
Pink (IIC)	3439.39		3558.17	3624.04	
Pink (⊥C)	3446.04		3559.25	3625.10	
Green (IIC)	3460.78	3535.49	3561.40	3624.04	3647.62
Green (⊥C)	3467.76	3535.49	3563.20	3622.98	3647.62

FTIR spectroscopic results of Hydroxyl group analysis shows the absorption peaks at the wavenumber about 3600-3400 cm^{-1} that associated with OH stretching modes in W-site and V-site (Castañeda et al., 2000; Oliveira et al., 2002). These spectra are unable to determine tourmaline species obviously, because of the over absorbed band. In range of 4600-3850 cm^{-1} assigned to OH bending modes, which occupied by cations in octahedral site, such as Al, Mg, Mn, and Fe (Frost et al., 2007). Another IR band presented at wavenumber between 5200-5180 cm^{-1} and 7600-6700 cm^{-1}, which are related to water molecules (H_2O) (Oliveira et al., 2002). IR spectra of all tourmalines appear intensity and characteristic absorption bands, differently, based on the measurement in oriented directions (Figure 6.1).

Identification of manganese oxidation state for pink and green tourmalines present the Mn *K*-edge spectra at the energy of 6546 eV. When comparable the result of Mn *K*-edge spectra of the investigation samples to standard of manganese (II) oxide (MnO, Mn^{2+}) and manganese (III) oxide (Mn_2O_3, Mn^{3+}), it can be concluded that tourmalines

are contained both Mn^{2+} ion and Mn^{3+} ion mutual component in their structure. Figure 6.2 shows E_0-value of Mn *K*-edge for tourmaline samples (~6546 eV), which approach to E_0-value of MnO standard. Also, both pink and green

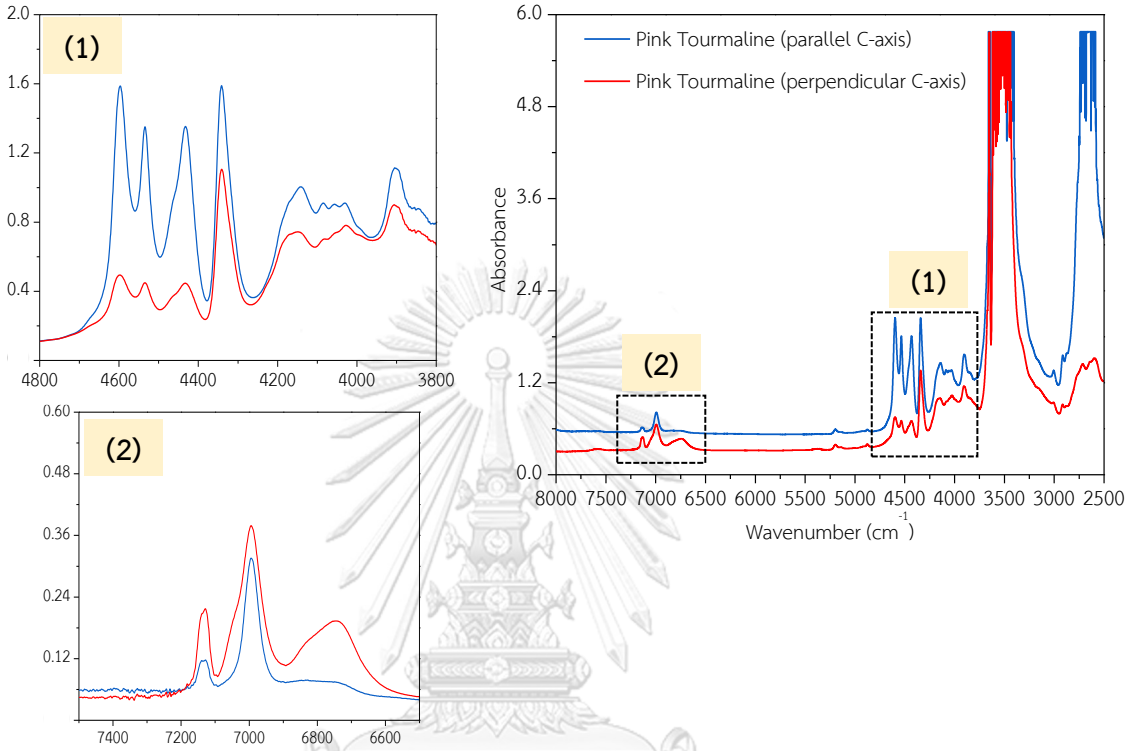

Figure 6.1 Comparison IR spectra of pink tourmaline along to different crystal direction: (blue line) parallel C-axis, (red line) perpendicular C-axis.

จุฬาลงกรณ์มหาวิทยาลัย
Chulalongkorn University

tourmalines have Mn^{2+} ion components more than Mn^{3+} ion components. The Fe *K*-edge spectra of pink tourmaline samples are unable to indicate the oxidation state clearly because they have the iron component below 0.1 %wt. The spectra contain a lot of noise signals then it could not be measured completely. XANES analysis of green tourmalines presents the Fe *K*-edge spectra in the range between 7119.5 to 7120 eV, which approach to the energy spectrum of FeO standard (~7119.3 eV). Therefore, green tourmalines are composed of Fe^{2+} ion rather than Fe^{3+} ion (Figure 6.3).

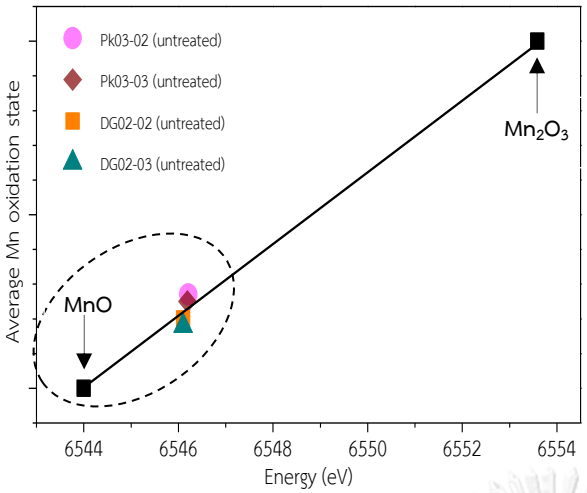

Figure 6.2 Comparison the oxidation state of Mn between MnO (Mn^{2+}) and Mn_2O_3 (Mn^{3+}) for tourmaline samples derived from the *K*-edge energy.

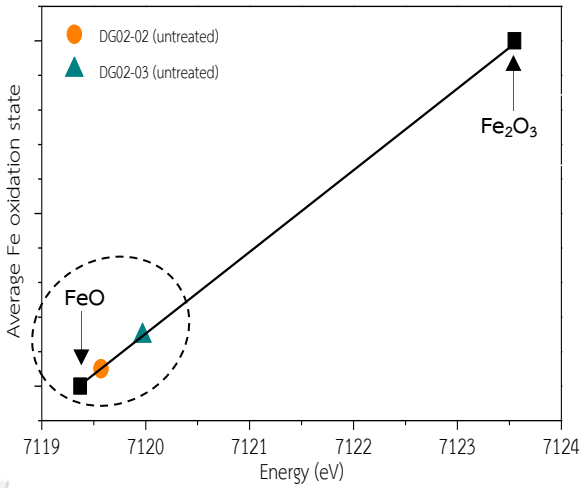

Figure 6.3 Comparison the oxidation state of Fe between FeO (Fe^{2+}) and Fe_2O_3 (Fe^{3+}) for green tourmalines derived from the *K*-edge energy.

The samples of pink tourmalines in natural elbaite are light pink to near colorless. The color along the parallel to C-axis is a shade of pink rather perpendicular to C-axis is a shade of orang. Considering the trace elements from EPMA results of pink tourmaline, manganese and iron were detected in these samples. The iron concentration is rather low, so the pink color is probably due to manganese. According to UV-Vis absorption spectra of pink tourmalines (parallel to C-axis) generally appear mainly band of Mn^{3+} ion (Taran et al., 1993) center around 515 nm (maximum intensity) with two small peaks at 450 and 458 nm due to the absorption of light in blue-green region of spectrum, so the crystal color resulting in a purple-pink. The minor band at around 395 nm is Mn^{2+} ion (Reinitz and Rossman, 1988) that absorbed light in purple region, so this absorption band also yields slightly yellow tonality in pink tourmalines. Besides, the small band around 680 nm could be related to Fe^{2+} ion (Mattson and Rossman, 1987; Taran et al., 1993). Nassau (1987) suggested that Mn^{2+} is the cause of yellow color whereas Mn^{3+} is the cause of pink color, thus pink elbaites are probably due to the interaction between Mn^{2+}-Mn^{3+} ion yielding pink as the main color with minor yellow together in samples. Then, these results are conformed to the measurable absorption spectrum.

จุฬาลงกรณ์มหาวิทยาลัย
Chulalongkorn University

Pink tourmaline irradiation causes the intense pink color in natural samples, which present the increasing bands at 395 nm and 515 nm. These bands present more absorbed intensity in electron beam-irradiated spectrum than gamma-irradiated spectrum (Figure 6.4). Considering XANES spectra of Mn K-edge, these samples were not obviously shifted in the samples undertaken both irradiation techniques. In addition, EPR results of irradiated pink tourmalines (perpendicular to C-axis) show the signal of O^- center (hole center) at 343 mT ($g \approx 2.05$) and two signals of H^0 center (electron trapped) at 375 mT ($g \approx 1.88$) and 324 mT ($g \approx 2.17$). An electron beam-irradiated pink tourmalines present defect signals with more intensity than the gamma-irradiated samples. Moreover, higher Mn/Fe ratio in pink sample yielded significantly intense pink after both irradiation techniques.

The irradiated green tourmalines yielded slightly yellow tonality in both parallel and perpendicular to C-axis. UV-Vis spectra and XANES spectra of green samples are clearly unchanged. For the EPR spectra of green tourmalines after irradiated, they appeared only the signal of O^- center (hole center) at 343 mT ($g \approx 2.05$) and 351 mT ($g \approx 2.00$) in parallel C-axis.

The observation of EPR result for the irradiated pink tourmalines indicates that both radiations produce electron centers (H^0 center) and hole trapped center (O^- center). Krambrock et al. (2004) suggested that O^- center caused yellow color, so these investigations conclude that intense pink cause by radiation is probably associate with manganese impurity with electron centers (H^0 center).

In the gem market, color improvement of pink tourmaline can increase the market value to twice or even three times over the original cost of raw material. However, their enhancing costs should also be taken into account. According to the service charge of irradiation (Table 6.2), electron beam is the most suitable technique for irradiation of tourmaline at 1,200 kilogreys which its service cost (5,000 THB/kg

tourmaline) is over two times cheaper than gamma ray radiation (11,900 THB/kg tourmaline). Moreover, the electron beam also takes shorter time of radiation.

Table 6.2 Rate of service charge for tourmaline irradiation (data from Thailand Institute of Nuclear Technology, 2020).

	Radiation dosages	Service fees / kg.
E-beam	0 – 10,000 kGy	5,000 THB
	10,000 – 20,000 kGy	10,000 THB
Gamma	0 – 150 kGy	1,400 THB
	150 kGy up	extra charge 10 THB / 1 kGy

6.2 Conclusions

1. Nigerian tourmalines in this study are classified to elbaite, based on EPMA analyses. Furthermore, Raman spectra of OH stretching mode in V-site and W-site structure (around 3,200 to 3,800 cm^{-1}) also indicate elbaite structure.

2. Natural pink tourmalines contain high manganese to iron ratio (Mn/Fe) (Table 4.2) resulting in intense pink after irradiation. For green tourmalines, they are significantly unchanged in color after undertaking both radiations. Electron beam is more suitable for color enhancement of pink tourmalines because it can produce more intense pink than those undertaken gamma ray irradiation at the same radiation dosage. Moreover, electron beam-irradiated tourmaline does not produce residual radioactive. In addition, e-beam irradiation costs much cheaper at high dosage irradiation.

3. Both electron beam and gamma irradiations can enhance pink elbaites tourmaline yielding intense pink color with slightly yellow to orange tonality. which related to color centers. Yellow color is due to O^- -center whereas intense pink color is caused by H^0 center in association with high manganese content.

จุฬาลงกรณ์มหาวิทยาลัย
Chulalongkorn University

REFERENCES

Babinska, J., Dyrek, K., Pieczka, A. and Sojka, Z (2008). "X and Q band EPR studies of paramagnetic centres in natural and heated tourmaline." European Journal of Mineralogy. **20**(2): 233-240.

Bosi, F. (2018). "Tourmaline crystal chemistry." American Mineralogist **103**(2): 298-306.

Bunnag, N. a. S., T. (2019). "Gamma irradiation on rubellite tourmaline." Chiang Mai Journal of Science. **46**(6): 1249-1255.

Cano, N. F., Rao, T.K.G., Ayala-Arenas, J.S., Gonzales-Lorenzo, C.D., Oliveira, L.M. and Watanabe, S. (2019). "TL in green tourmaline: Study of the centers responsible for the TL emission by EPR analysis." Journal of Luminescence. **205**: 324-328.

Castañeda, C., Eeckhout, S.G., da Costa, G.M. and Botelho, N.F., De Grave, E. (2006). "Effect of heat treatment on tourmaline from Brazil." Physics and Chemistry of Minerals. **33**(3): 207-216.

Castañeda, C., Oliveira, E.F., Gomes, N. and Pedrosa-Soares, A.C. (2000). "Infrared study of OH sites in tourmaline from the elbaite-schorl series." American Mineralogist. **85**(10): 1503-1507.

De Camargo, M. B. a. I., S. (1988). "Optical absorption spectroscopy of natural and irradiated pink tourmaline." American Mineralogist. **73**(1-2): 172-180.

De Oliveira, E.F., Castañeda, C., Eeckhout, S.G., Gilmar, M.M., Kwitko, R.R., De Grave, E., and Botelho, N.F. (2002). "Infrared and Mössbauer study of Brazilian tourmalines from different geological environments." American Mineralogist. **87**(8): 1154-1163.

Fantini, C., Tavares, M.C., Krambrock., K., Moreira, R.L. and Righi, A. (2014). "Raman and infrared study of hydroxyl sites in natural uvite, fluor-uvite, magnesio-foitite, dravite and elbaite tourmalines." Physics and Chemistry of Minerals. **41**(4): 247-254.

Frost, R.L., Wain, D.L., Reddy, B.J., Martens, W., and Kloprogge, T. (2007). "Spectroscopic characterization of Mn-rich tourmalines." Vibrational Spectroscopy. **44**(1); 42-49.

Gasharova, B., Mihailova, B., and Konstantinov, L. (1997). "Raman spectra of various types of tourmaline." European Journal of Mineralogy. **9**(5): 935-940.

Gonzalez-Carreño, T., Fernández, M. and Sanz, J. (1988). "Infrared and electron microprobe analysis of tourmalines." Physics and Chemistry of Minerals. **15**(5): 452-460.

จุฬาลงกรณ์มหาวิทยาลัย
CHULALONGKORN UNIVERSITY

Grice, J.D. and Ercit, T.S. (1993). "Ordering of Fe and Mg in the tourmaline crystal structure: the correct formula." Neues Jahrbuch für Mineralogie - Abhandlungen. **165**(3): 245-266.

Hawthorne, F.C. and Dirlam, D.M. (2011). "Tourmaline the indicator mineral: from atomic arrangement to viking navigation." Elements Magazine. **7**(5): 307-312

Hawthorne, F.C. and Henry, D.J. (1999). "Classification of the minerals of the tourmaline group." European Journal of Mineralogy. **11**(2): 201-215.

Hawthorne, F.C., Macdonald, D.J., and Burns, P.C. (1993). "Reassignment of cation site occupancies in tourmaline: Al-Mg disorder in the crystal structure of dravite." American Mineralogist. **78**(3): 265-270.

Henry, D.J., Novák, M., Hawthorne, F.C., Ertl, A., Dutrow, B., Uher, P., Pezzotta, F. (2011). "Nomenclature of the tourmaline-supergroup minerals." American Mineralogist. **96**(5-6): 895-913.

Hoang, L. H., Nguyen, H.T.M., Chen, X-B., Nguyen, V.M. and Yang, I-S. (2011). "Raman spectroscopic study of various types of tourmalines." Journal of Raman Spectroscopy. **42**(6): 1442-1446.

Krambrock, K., Pinheiro, M.V.B., Guedes, K.J., Medeiros, S.M., Schweizer, S. and Spaeth, J.-M. (2004). "Correlation of irradiation-induced yellow color with the O- hole center in tourmaline." Physics and Chemistry of Minerals. **31**(3): 168-175.

Krambrock, K., Pinheiro, M.V.B., Guedes, K.J., Medeiros, S.M., Schweizer, S. and Spaeth, J.-M. (2002). "Investigation of radiation-induced yellow color in tourmaline by magnetic resonance." Nuclear Instruments and Methods in Physics Research Section B. **191**(1-4): 241-245.

Laurs, B. M., Simmons, W.B., Rossman, G.R., Fritz, E.A., Koivula, J.I., Anckar, B. and Falster, A.U. (2007). "Yellow Mn-rich tourmaline from the canary mining area, Zambia." Gems and Gemology. **43**(4): 314-331.

Maneewong, A. (2009). "Correlation of manganese and iron ratio in gamma irradiated tourmaline and color alteration." Master Dissertation. Department of Nuclear Technology, Faculty of Engineering, Chulalongkorn University. 126 pp.

Maneewong, A., Seong, B.S., Shin, E.J., Kim, J.S. and Kajornrith, V. (2016). "Color change of tourmaline by heat treatment and electron beam irradiation: UV-Visible, EPR, and Mid-IR Spectroscopic Analyses." Journal of the Korean Physical Society. **68**(1): 83-92.

จุฬาลงกรณ์มหาวิทยาลัย
Chulalongkorn University

Mattson, S. M., and Rossman, G.R. (1987). "Fe^{2+}-Fe^{3+} interactions in tourmaline." Physics and Chemistry of Minerals. **14**(2): 163-171.

Okrusch, M., Ertl, A., Schüssler, U., Tillmanns, E., Brätz, H., and Bank, H. (2016). Major- and Trace-element Composition of Paraíba-type Tourmaline from Brazil, Mozambique and Nigeria. The Journal of Gemmology. **35**(2): 120-139.

Pezzo, F., and Laurs, B.M. (2011). "Tourmaline: The Kaleidoscopic Gemstone." Elements Magazine **7**(5): 333-338.

Preoteasa, E.A., Preoteasa, E., and Suciu, I. (2012). "Atomic and Nuclear Surface Analysis Methods: A Novel Perspective for The Characterization of ental Composites." Dental Science, Materials and Technology. Nova Scientific Publisher, Inc. 206 pp.

Reddy, B. J., Frost, R.L., Martens, W.N., Wain, D.L. and Kloprogge, J.T. (2007). "Spectroscopic characterization of Mn-rich tourmalines." Vibrational Spectroscopy. **44**(1): 42-49.

Reinitz, I.M. and Rossman, G.R. (1988). "Role of natural radiation in tourmaline coloration." American Mineralogist. **73**(7-8): 822-825.

Rossman, G.R., Fritsch, E., and Shigley, J.E. (1991). "Origin of color in cuprian elbaite from São José de Batalha, Paraíba, Brazil." American Mineralogist. **76**(9-10): 1479-1484.

Synchroton Light Research Institute (Public Organization). (2020). Priciples of XAS technique (in Thai) [online]. from https://www.slri.or.th/th/beamline/sut-nanotec-slri.html?view=article&id=4564:%202016-08-03-07-54-27&catid=282:sut-nanotec-slri.

จุฬาลงกรณ์มหาวิทยาลัย
Chulalongkorn University

Taran, M. N., Lebedev, A.S. and Platonov, A (1993). "Optical absorption spectroscopy of synthetic tourmalines." Physics and Chemistry of Minerals. **20**: 209-220.

Thailand Institute of Nuclear Technology (Public Organization). (2020). Price of service fees for tourmaline irradiation (in Thai) [online]. from http://www0.tint.or.th/gems/gems5103.html

Thai research reactor 1 modification 1 (TRRM1/M1). (2020). Office of Atoms for Peace, Kasetsart University. [online]. from https://www.tint.or.th/home/index.php/th/2013-07-30-15-08-10?id=801]

Van Hinsberg, V. J., Henry, D.J. and Dutrow, B.L. (2011). "Tourmaline as a petrologic forensic mineral: a unique recorder of its geologic past." Elements Magazine. **7**(5): 327-332.

Watenphul, A., Burgdorf, M., Schlüter, J., Horn, I., Malcherek, T. and Mihailova, B. (2016). "Exploring the potential of Raman spectroscopy for crystallochemical analyses of complex hydrous silicates: II. Tourmalines." American Mineralogist. **101**(4): 970-985.

Weil, J.A., and Bolton, J.R. (2007). "Electron Paramagnetic Resonance: Elementary Theory and Practical Applications." Wiley Publisher, 688 pp.

Zang, J., and da Fonseca-Zang, W. (2002). "Is there really black tourmaline?" extraLapis English. **3:** 30-33.

จุฬาลงกรณ์มหาวิทยาลัย
CHULALONGKORN UNIVERSITY

APPENDICES

จุฬาลงกรณ์มหาวิทยาลัย
Chulalongkorn University

APPENDIX A

Table A.1 The basic properties analysis results of all tourmaline samples before irradiated.

Sample code	Optic character	Refractive index (R.I.)		Birefrin-gence	Specific gravity (S.G.)	Pleochro-ism	Fluorescence
		n_o	n_e				
Pk01	DR, Uniaxial	1.636	1.619	0.017	3.030	Pk-oPk	inert
Pk02	DR, Uniaxial	1.640	1.622	0.018	3.035	oPk-O	Inert
Pk03	DR, Uniaxial	1.639	1.620	0.020	3.045	Pk-oPk	Inert
Pk04	DR, Uniaxial	1.639	1.619	0.020	3.075	oPk-O	Inert
Pk05	DR, Uniaxial	1.640	1.622	0.018	3.055	oPk-O	inert
Pk06	DR, Uniaxial	1.640	1.627	0.013	3.062	Pk-O	inert
Pk07	DR, Uniaxial	1.634	1.619	0.015	3.059	Pk-oPk	Inert
Pk08	DR, Uniaxial	1.632	1.617	0.015	3.052	Pk-O	Inert
Pk09	DR, Uniaxial	1.640	1.622	0.019	3.050	Pk-O	inert
Pk10	DR, Uniaxial	1.639	1.620	0.019	3.054	Pk-O	inert
Pk11	DR, Uniaxial	1.637	1.620	0.017	3.063	Pk-O	inert
Pk12	DR, Uniaxial	1.637	1.618	0.019	3.046	Pk-O	inert
Pk13	DR, Uniaxial	1.636	1.619	0.018	3.048	Pk-O	inert
Pk14	DR, Uniaxial	1.640	1.620	0.020	3.074	oPk-O	inert
Pk15	DR, Uniaxial	1.635	1.619	0.016	3.046	Pk-oPk	inert
Pk16	DR, Uniaxial	1.639	1.622	0.017	3.043	Pk-oPk	inert
Pk17	DR, Uniaxial	1.640	1.622	0.019	3.040	Pk-oPk	Inert
Pk18	DR, Uniaxial	1.641	1.627	0.014	3.033	Pk-oPk	Inert
Pk19	DR, Uniaxial	1.644	1.626	0.018	3.039	Pk-oPk	inert
Pk20	DR, Uniaxial	1.644	1.627	0.017	3.044	Pk-oPk	Inert
DG01	DR, Uniaxial	1.643	1.628	0.015	3.078	yG-G	inert
DG02	DR, Uniaxial	1.639	1.621	0.019	3.069	yG-G	inert
DG03	DR, Uniaxial	1.639	1.621	0.019	3.064	yG-G	inert
DG04	DR, Uniaxial	1.642	1.625	0.017	3.060	yG-G	inert
DG05	DR, Uniaxial	1.636	1.618	0.018	3.055	yG-G	inert

จุฬาลงกรณ์มหาวิทยาลัย
Chulalongkorn University

APPENDIX B

Figure B1. Color modification after 3 steps of irradiation treatments; all samples are viewed in the direction parallel to c-axis.

Sample code	Electron beam irradiation				Gamma ray irradiation			
	Natural	400 kGy	800 kGy	1200 kGy	Natural	400 kGy	800 kGy	1200 kGy
Pk01								
Pk02								
Pk04								
Pk05								
Pk06								
Pk07								
Pk08								
Pk09								
Pk10								
Pk11								
Pk12								
Pk13								
Pk14								
Pk15								
Pk16								
Pk17								

Sample code	Electron beam irradiation				Gamma ray irradiation			
	Natural	400 kGy	800 kGy	1200 kGy	Natural	400 kGy	800 kGy	1200 kGy
Pk18								
Pk19	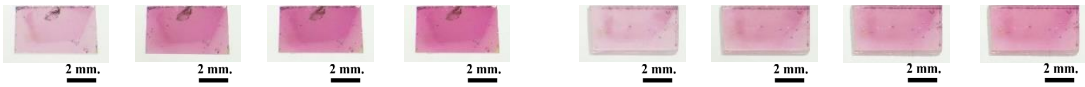							
Pk20								
DG01								
DG03								
DG04								
DG05								

จุฬาลงกรณ์มหาวิทยาลัย
Chulalongkorn University

Figure B2. Color modification after 3 steps of irradiation treatments; all samples are viewed in the direction perpendicular to c-axis.

Sample code	Electron beam irradiation				Gamma ray irradiation			
	Natural	400 kGy	800 kGy	1200 kGy	Natural	400 kGy	800 kGy	1200 kGy
Pk01								
Pk02								
Pk04								
Pk05								
Pk06								
Pk07								
Pk08								
Pk09								
Pk10	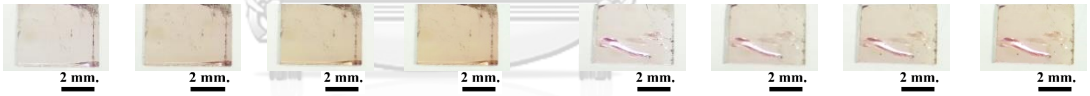							
Pk11	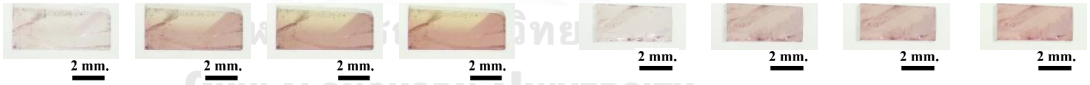							
Pk12								
Pk13								
Pk14	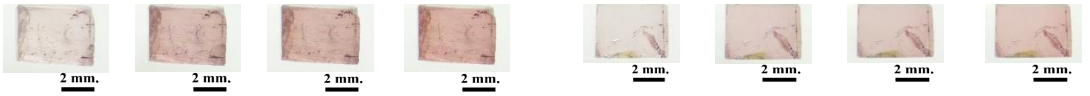							
Pk15								
Pk16								
Pk17								
Pk18								

Sample code	Electron beam irradiation				Gamma ray irradiation			
	Natural	400 kGy	800 kGy	1200 kGy	Natural	400 kGy	800 kGy	1200 kGy
Pk19	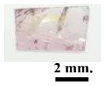	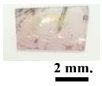		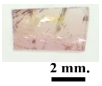	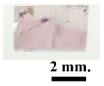	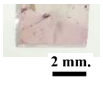		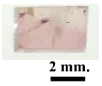
Pk20	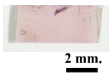	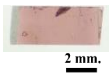	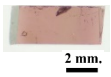	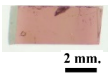	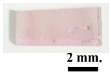	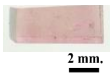	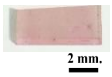	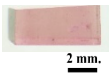
DG01	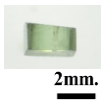	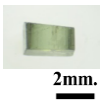	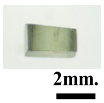	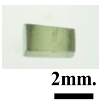	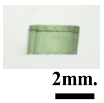	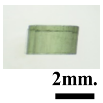	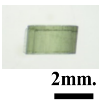	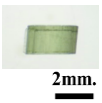
DG03	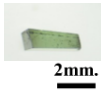	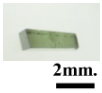	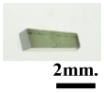	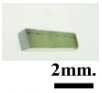	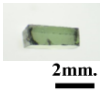	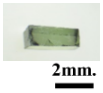	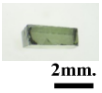	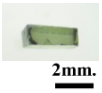
DG04								
DG05								

จุฬาลงกรณ์มหาวิทยาลัย
Chulalongkorn University

APPENDIX C

Figure C.1 UV-Vis spectra of natural tourmalines and after irradiation

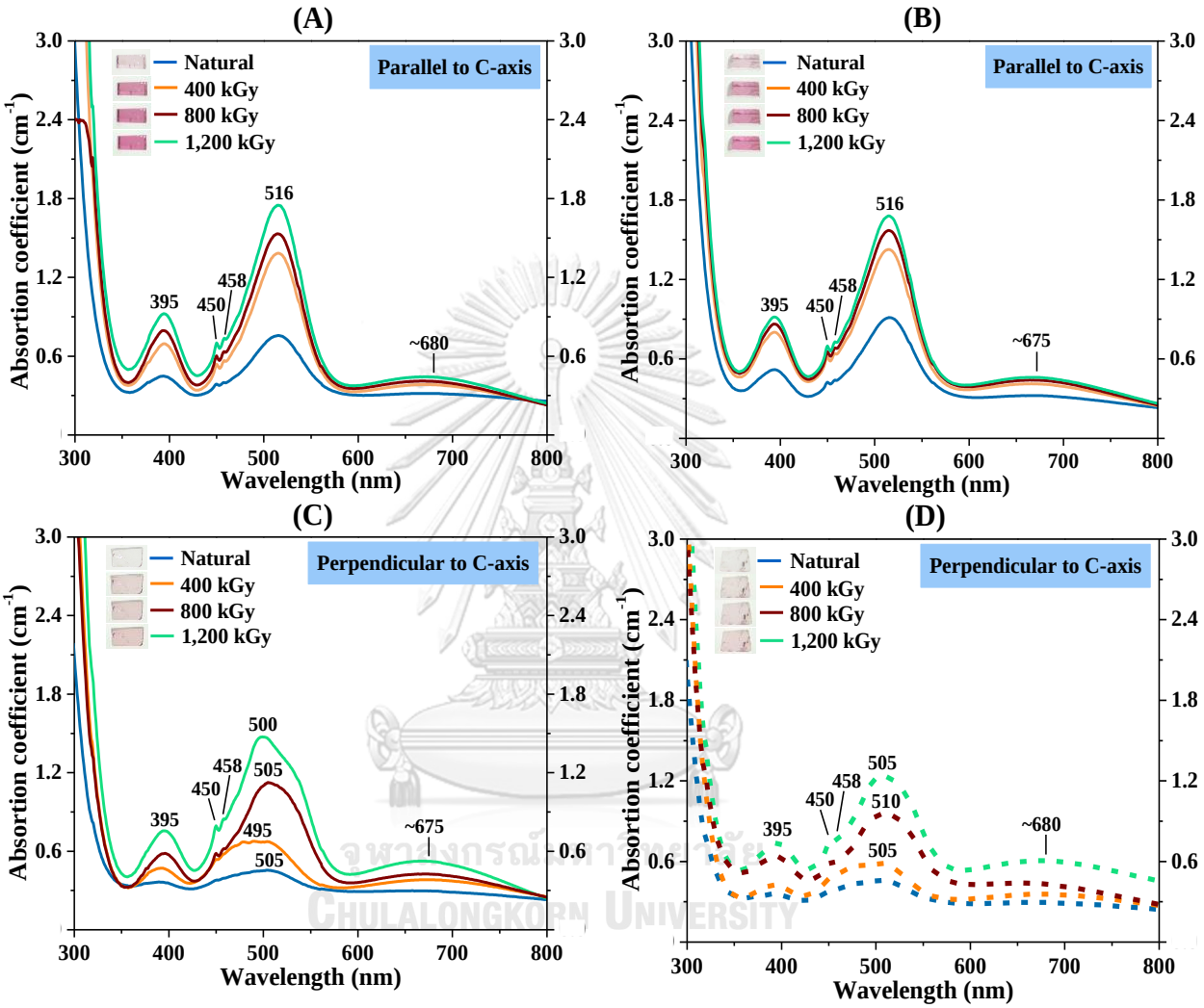

UV-Vis absorption spectra of Pk01 sample showing increasing absorption coefficients in oriented directions compared between natural and irradiated colors with different dosages: (A) e-beam irradiated color in //C-axis; (B) gamma irradiated color in //C-axis; (C) e-beam irradiated color in ⊥C-axis; (D) gamma irradiated color in ⊥C-axis.

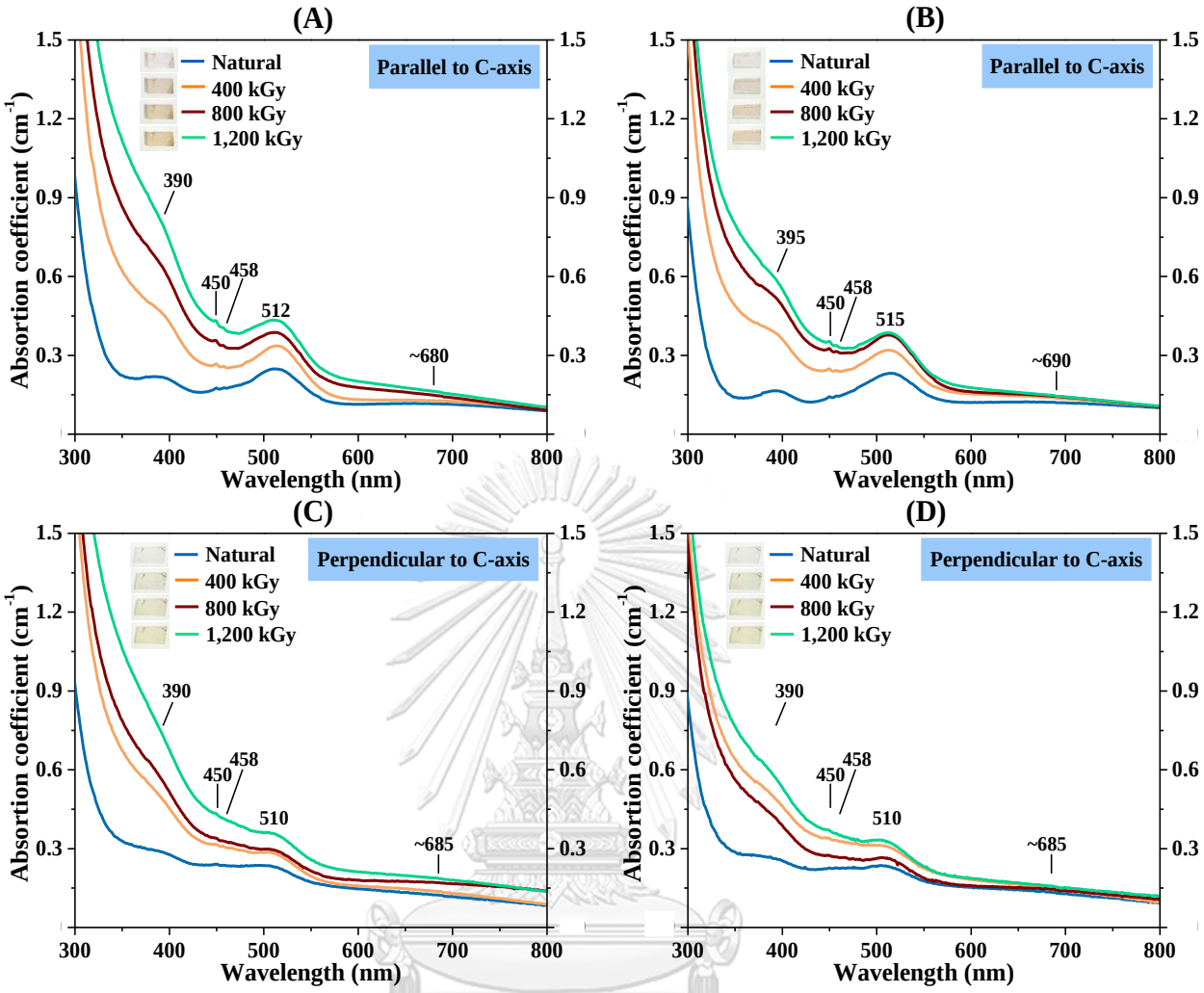

UV-Vis absorption spectra of Pk02 sample showing increasing absorption coefficients in oriented directions compared between natural and irradiated colors with different dosages: (A) e-beam irradiated color in //C-axis; (B) gamma irradiated color in //C-axis; (C) e-beam irradiated color in ⊥C-axis; (D) gamma irradiated color in ⊥C-axis.

จุฬาลงกรณ์มหาวิทยาลัย
CHULALONGKORN UNIVERSITY

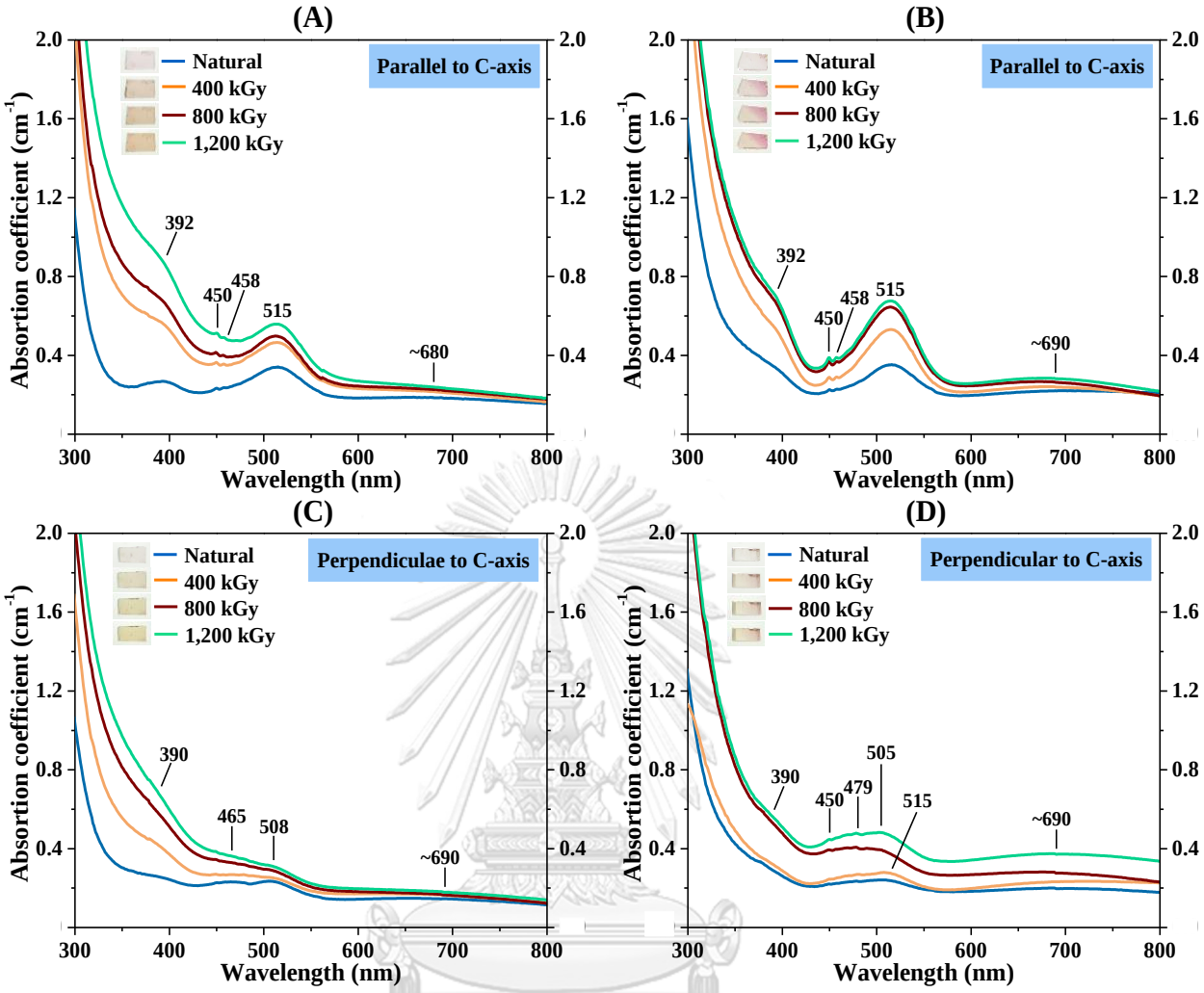

UV-Vis absorption spectra of Pk04 sample showing increasing absorption coefficients in oriented directions compared between natural and irradiated colors with different dosages: (A) e-beam irradiated color in //C-axis; (B) gamma irradiated color in //C-axis; (C) e-beam irradiated color in ⊥C-axis; (D) gamma irradiated color in ⊥C-axis.

จุฬาลงกรณ์มหาวิทยาลัย
Chulalongkorn University

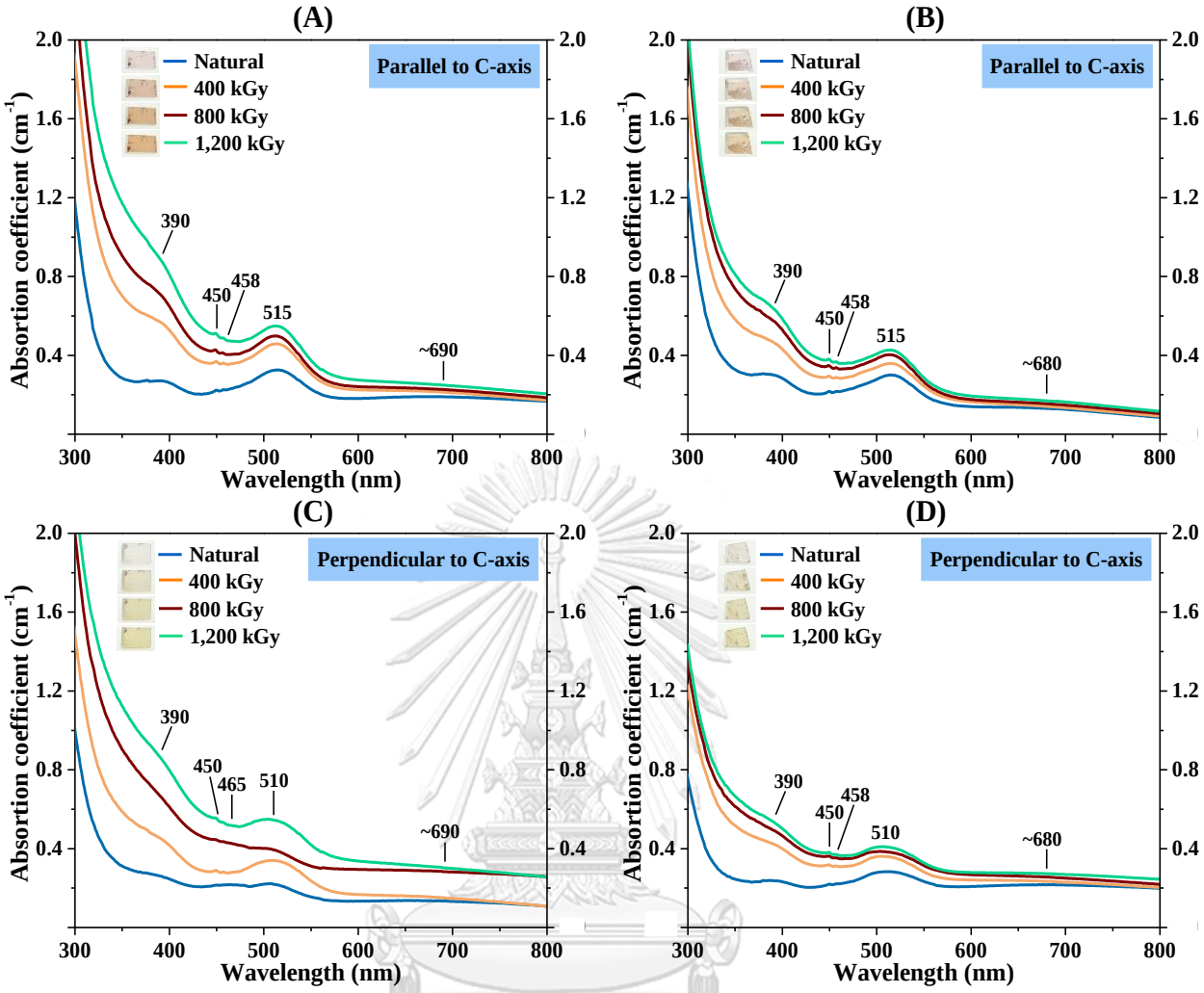

UV-Vis absorption spectra of Pk05 sample showing increasing absorption coefficients in oriented directions compared between natural and irradiated colors with different dosages: (A) e-beam irradiated color in //C-axis; (B) gamma irradiated color in //C-axis; (C) e-beam irradiated color in ⊥C-axis; (D) gamma irradiated color in ⊥C-axis.

จุฬาลงกรณ์มหาวิทยาลัย
Chulalongkorn University

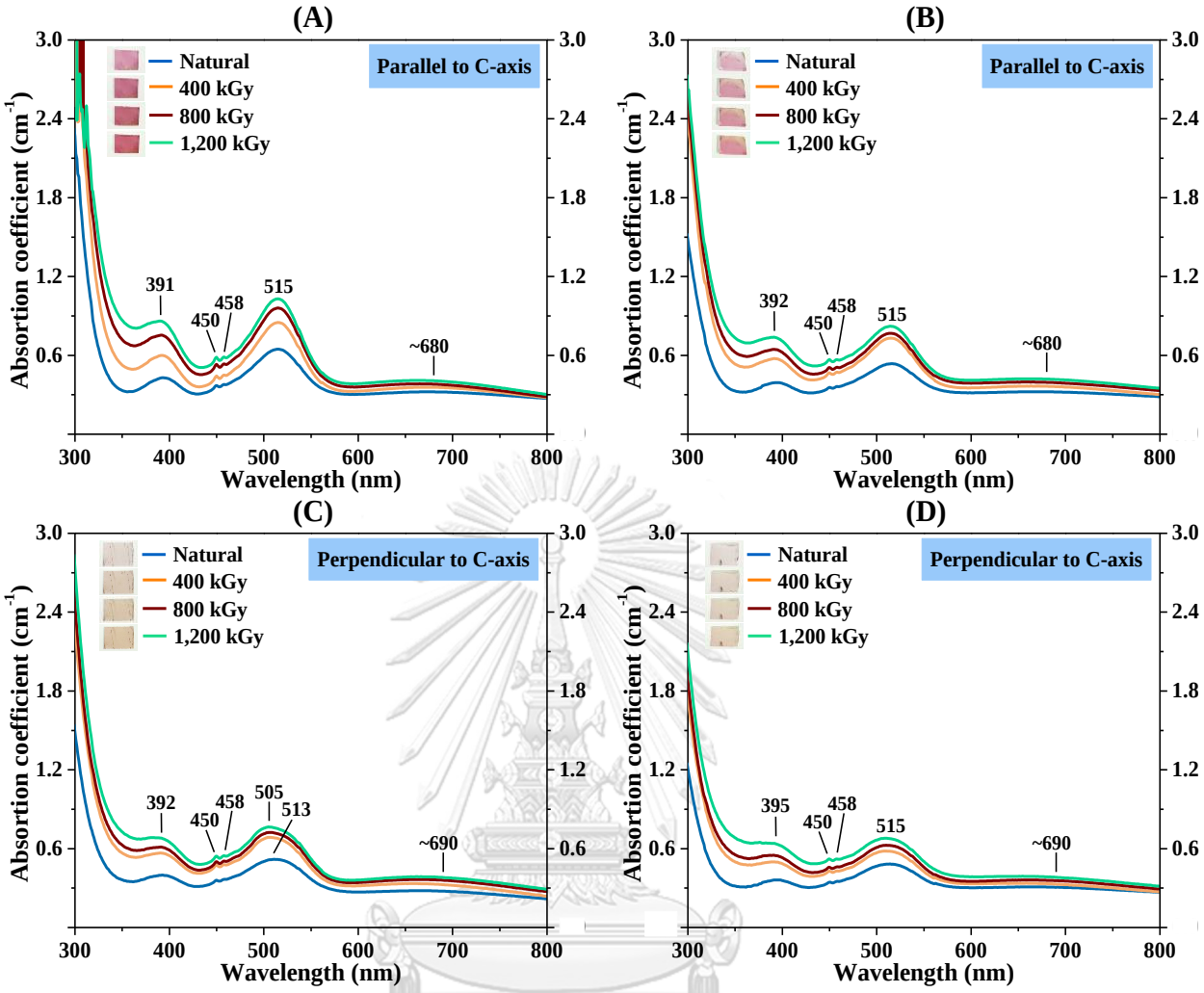

UV-Vis absorption spectra of Pk06 sample showing increasing absorption coefficients in oriented directions compared between natural and irradiated colors with different dosages: (A) e-beam irradiated color in //C-axis; (B) gamma irradiated color in //C-axis; (C) e-beam irradiated color in ⊥C-axis; (D) gamma irradiated color in ⊥C-axis.

จุฬาลงกรณ์มหาวิทยาลัย
Chulalongkorn University

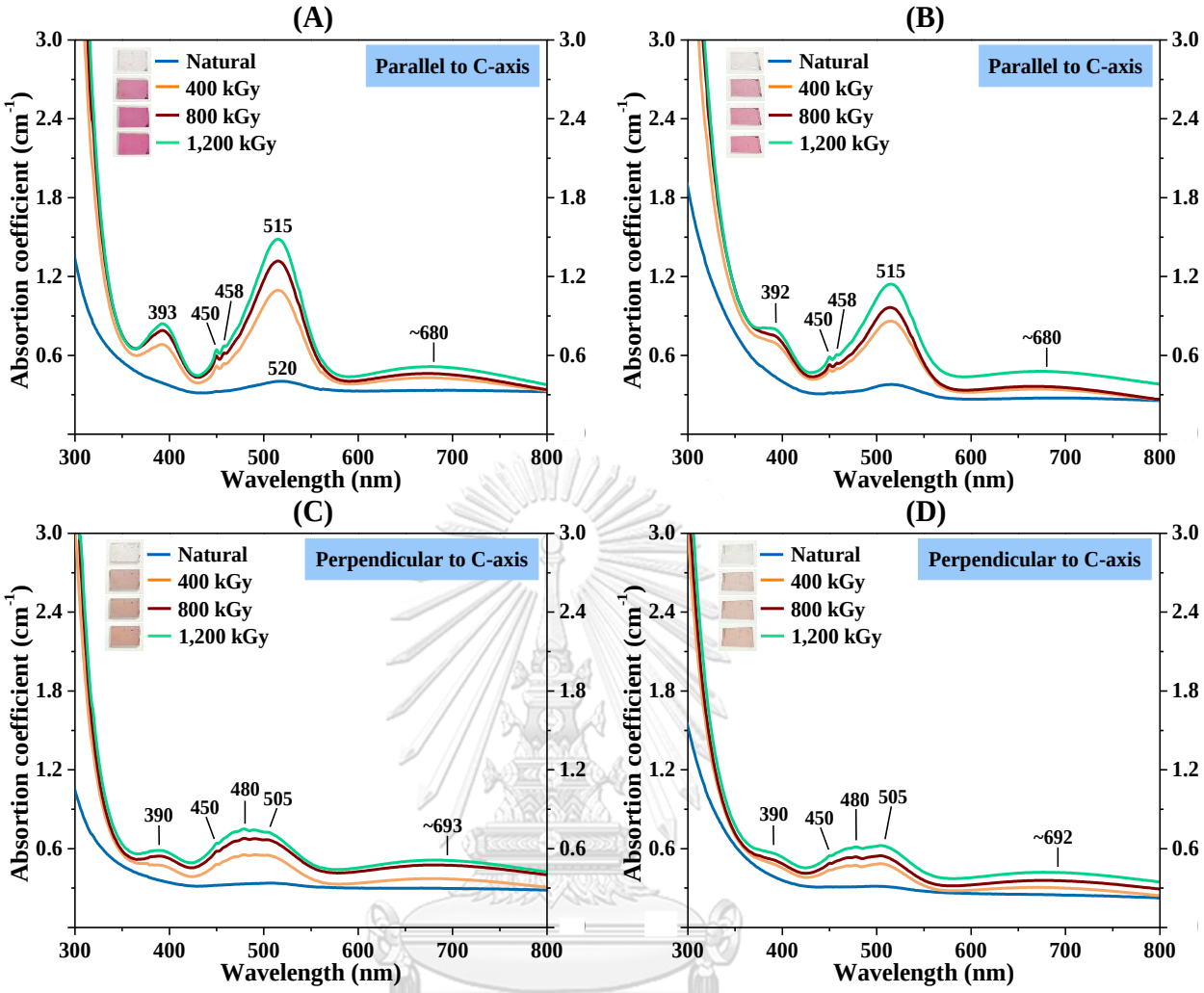

UV-Vis absorption spectra of Pk07 sample showing increasing absorption coefficients in oriented directions compared between natural and irradiated colors with different dosages: (A) e-beam irradiated color in //C-axis; (B) gamma irradiated color in //C-axis; (C) e-beam irradiated color in ⊥C-axis; (D) gamma irradiated color in ⊥C-axis.

จุฬาลงกรณ์มหาวิทยาลัย
Chulalongkorn University

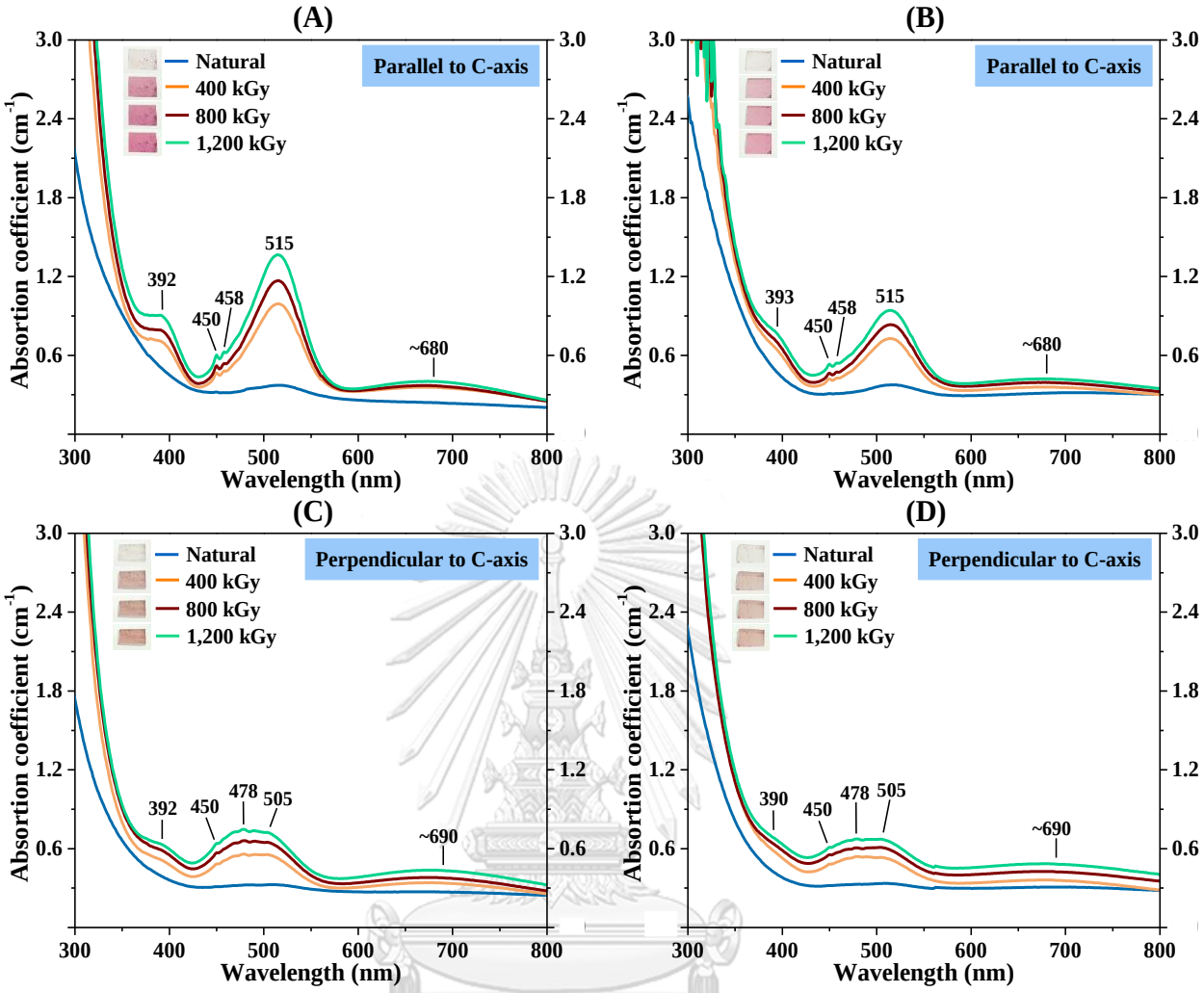

UV-Vis absorption spectra of Pk08 sample showing increasing absorption coefficients in oriented directions compared between natural and irradiated colors with different dosages: (A) e-beam irradiated color in //C-axis; (B) gamma irradiated color in //C-axis; (C) e-beam irradiated color in ⊥C-axis; (D) gamma irradiated color in ⊥C-axis.

จุฬาลงกรณ์มหาวิทยาลัย
Chulalongkorn University

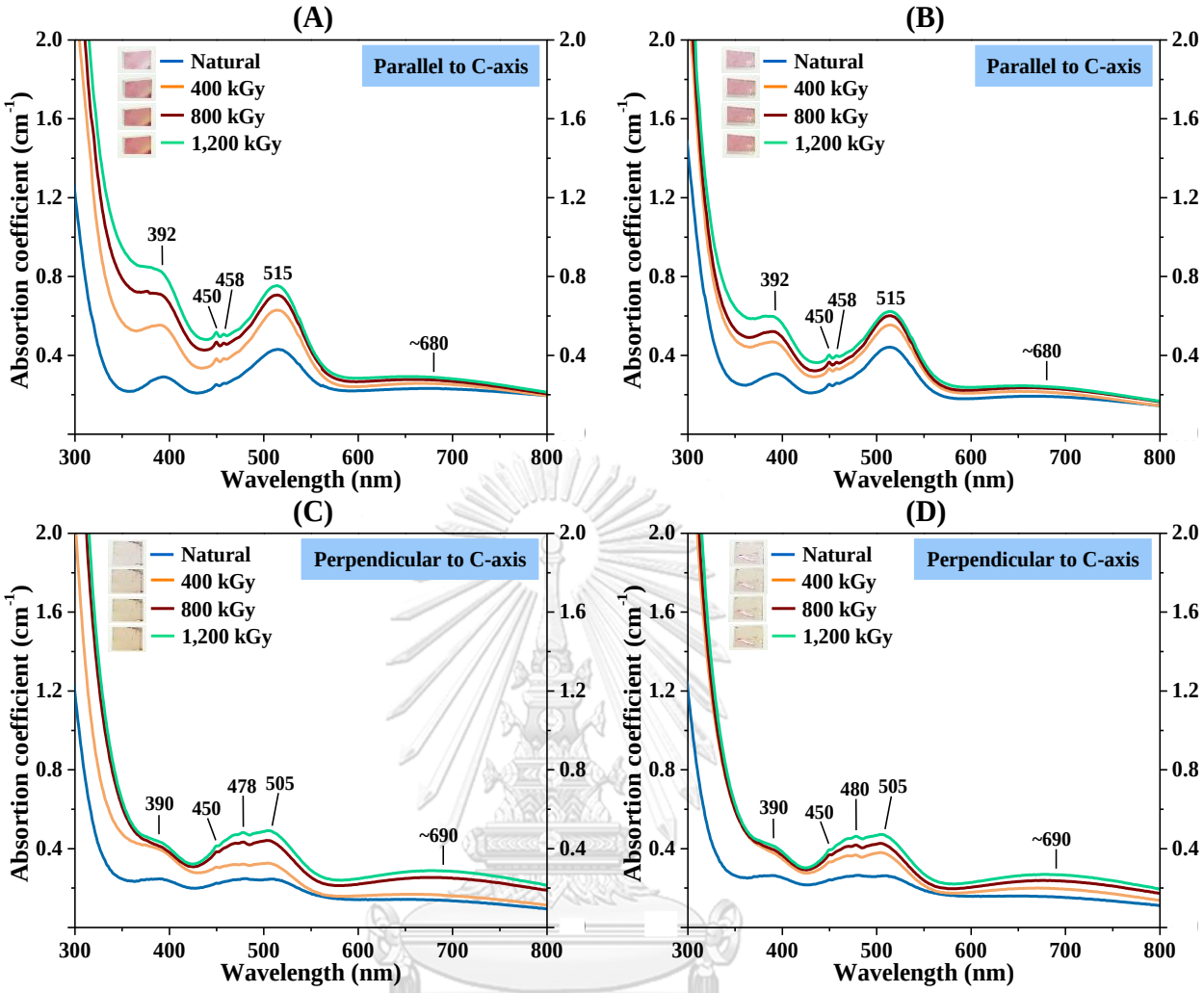

UV-Vis absorption spectra of Pk09 sample showing increasing absorption coefficients in oriented directions compared between natural and irradiated colors with different dosages: (A) e-beam irradiated color in //C-axis; (B) gamma irradiated color in //C-axis; (C) e-beam irradiated color in ⊥C-axis; (D) gamma irradiated color in ⊥C-axis.

จุฬาลงกรณ์มหาวิทยาลัย
Chulalongkorn University

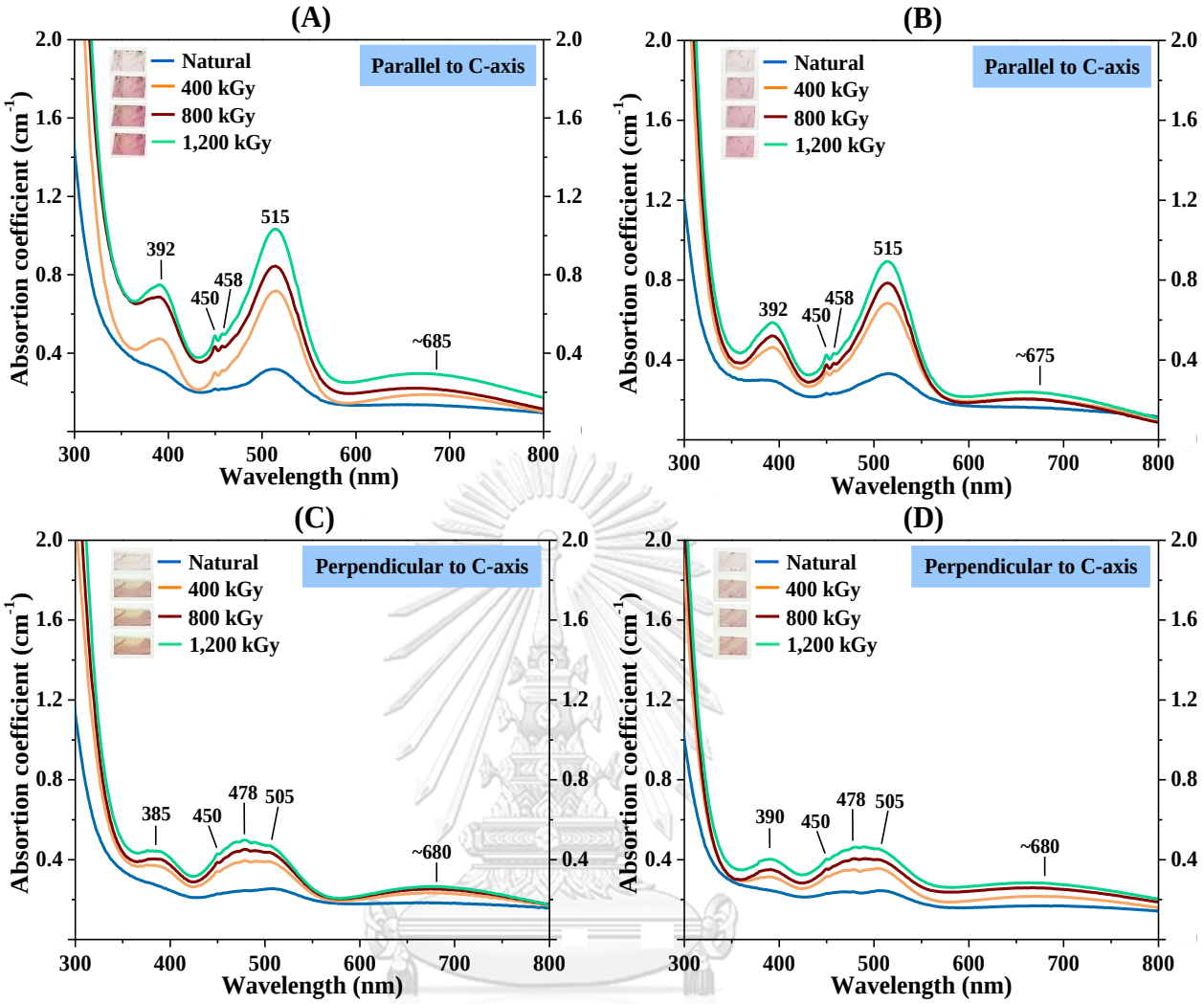

UV-Vis absorption spectra of Pk10 sample showing increasing absorption coefficients in oriented directions compared between natural and irradiated colors with different dosages: (A) e-beam irradiated color in //C-axis; (B) gamma irradiated color in //C-axis; (C) e-beam irradiated color in ⊥C-axis; (D) gamma irradiated color in ⊥C-axis.

จุฬาลงกรณ์มหาวิทยาลัย
CHULALONGKORN UNIVERSITY

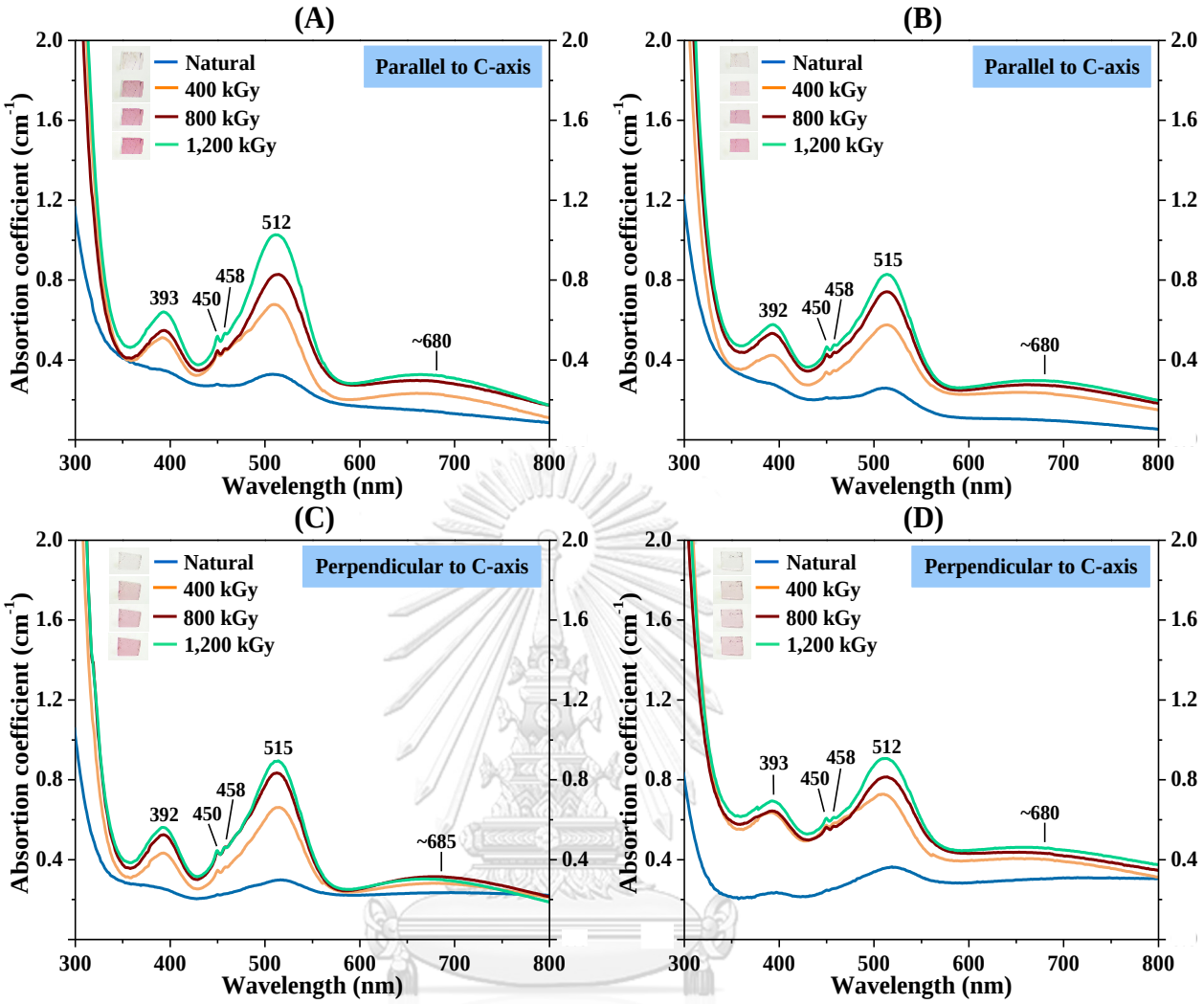

UV-Vis absorption spectra of Pk11 sample showing increasing absorption coefficients in oriented directions compared between natural and irradiated colors with different dosages: (A) e-beam irradiated color in //C-axis; (B) gamma irradiated color in //C-axis; (C) e-beam irradiated color in ⊥C-axis; (D) gamma irradiated color in ⊥C-axis.

จุฬาลงกรณ์มหาวิทยาลัย
CHULALONGKORN UNIVERSITY

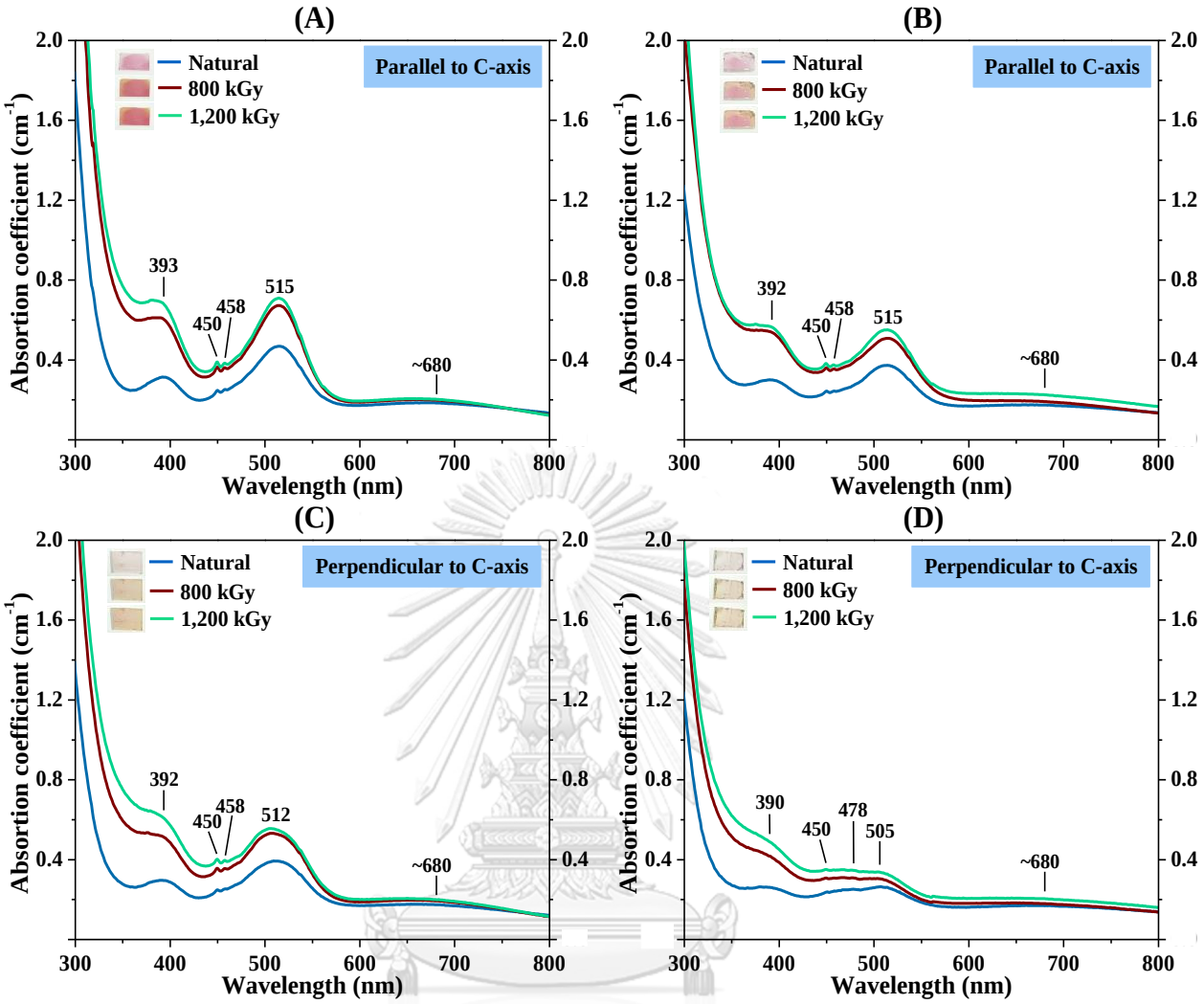

UV-Vis absorption spectra of Pk12 sample showing increasing absorption coefficients in oriented directions compared between natural and irradiated colors with different dosages: (A) e-beam irradiated color in //C-axis; (B) gamma irradiated color in //C-axis; (C) e-beam irradiated color in ⊥C-axis; (D) gamma irradiated color in ⊥C-axis.

จุฬาลงกรณ์มหาวิทยาลัย
CHULALONGKORN UNIVERSITY

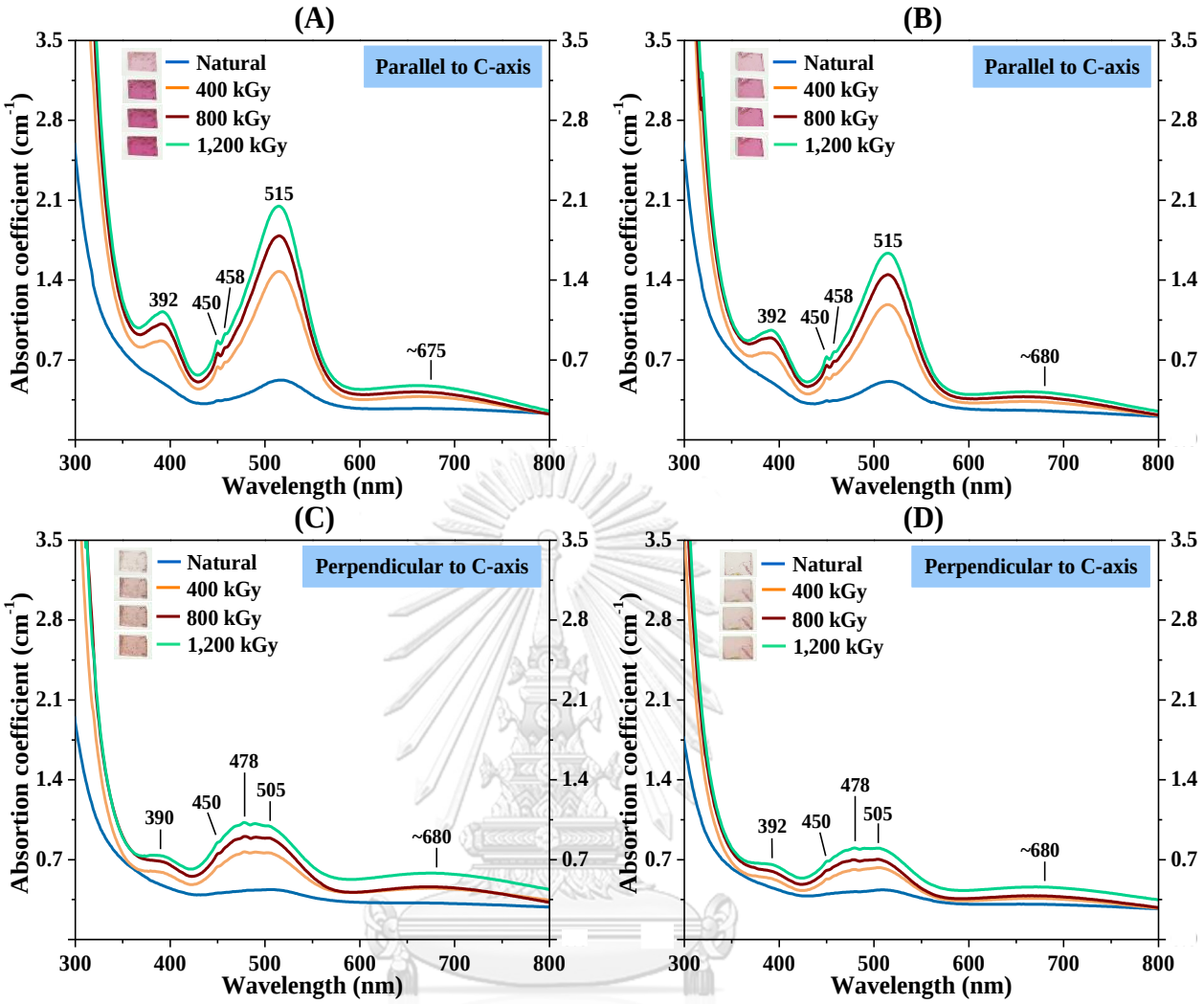

UV-Vis absorption spectra of Pk13 sample showing increasing absorption coefficients in oriented directions compared between natural and irradiated colors with different dosages: (A) e-beam irradiated color in //C-axis; (B) gamma irradiated color in //C-axis; (C) e-beam irradiated color in ⊥C-axis; (D) gamma irradiated color in ⊥C-axis.

จุฬาลงกรณ์มหาวิทยาลัย
CHULALONGKORN UNIVERSITY

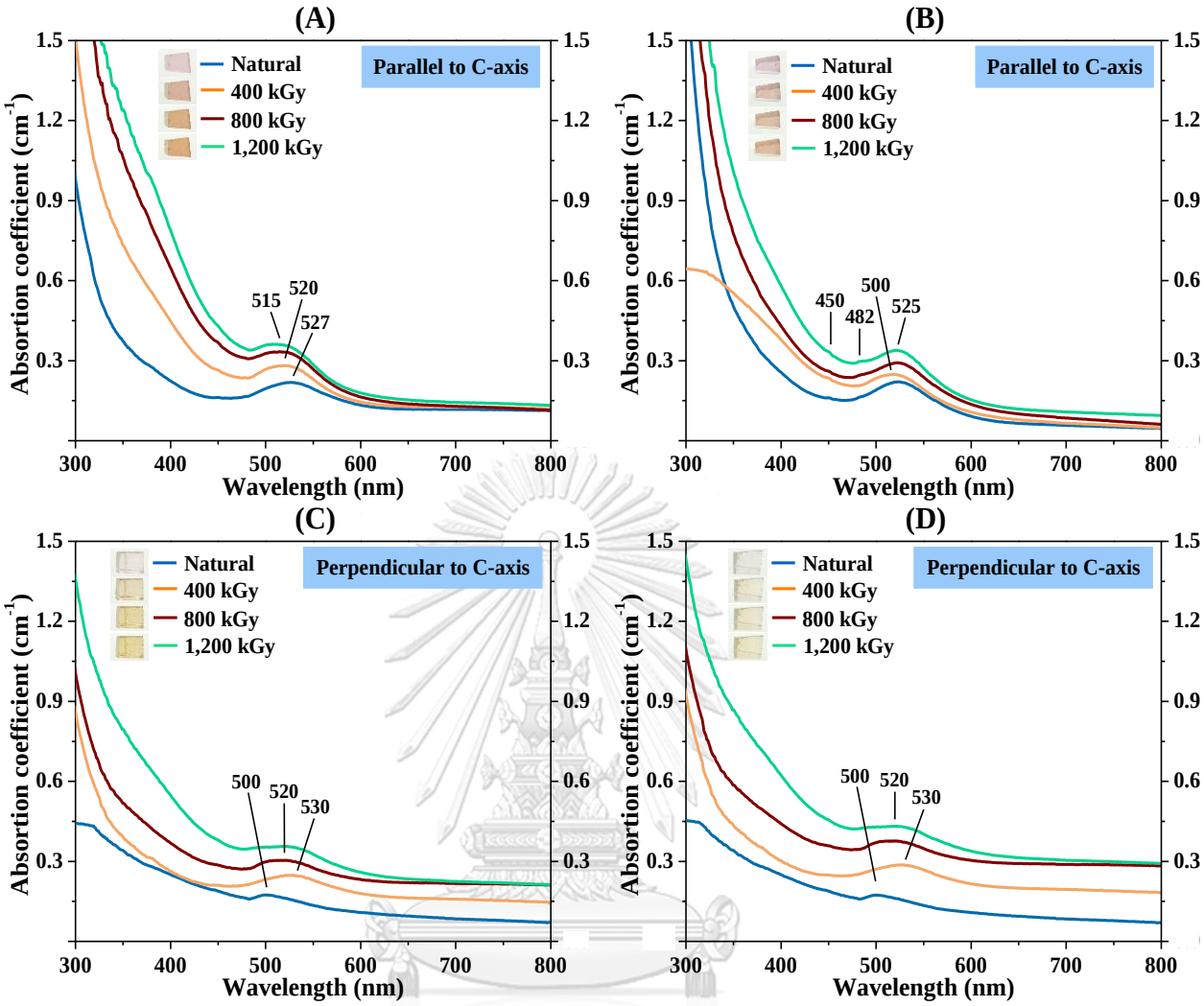

UV-Vis absorption spectra of Pk14 sample showing increasing absorption coefficients in oriented directions compared between natural and irradiated colors with different dosages: (A) e-beam irradiated color in //C-axis; (B) gamma irradiated color in //C-axis; (C) e-beam irradiated color in ⊥C-axis; (D) gamma irradiated color in ⊥C-axis.

จุฬาลงกรณ์มหาวิทยาลัย
CHULALONGKORN UNIVERSITY

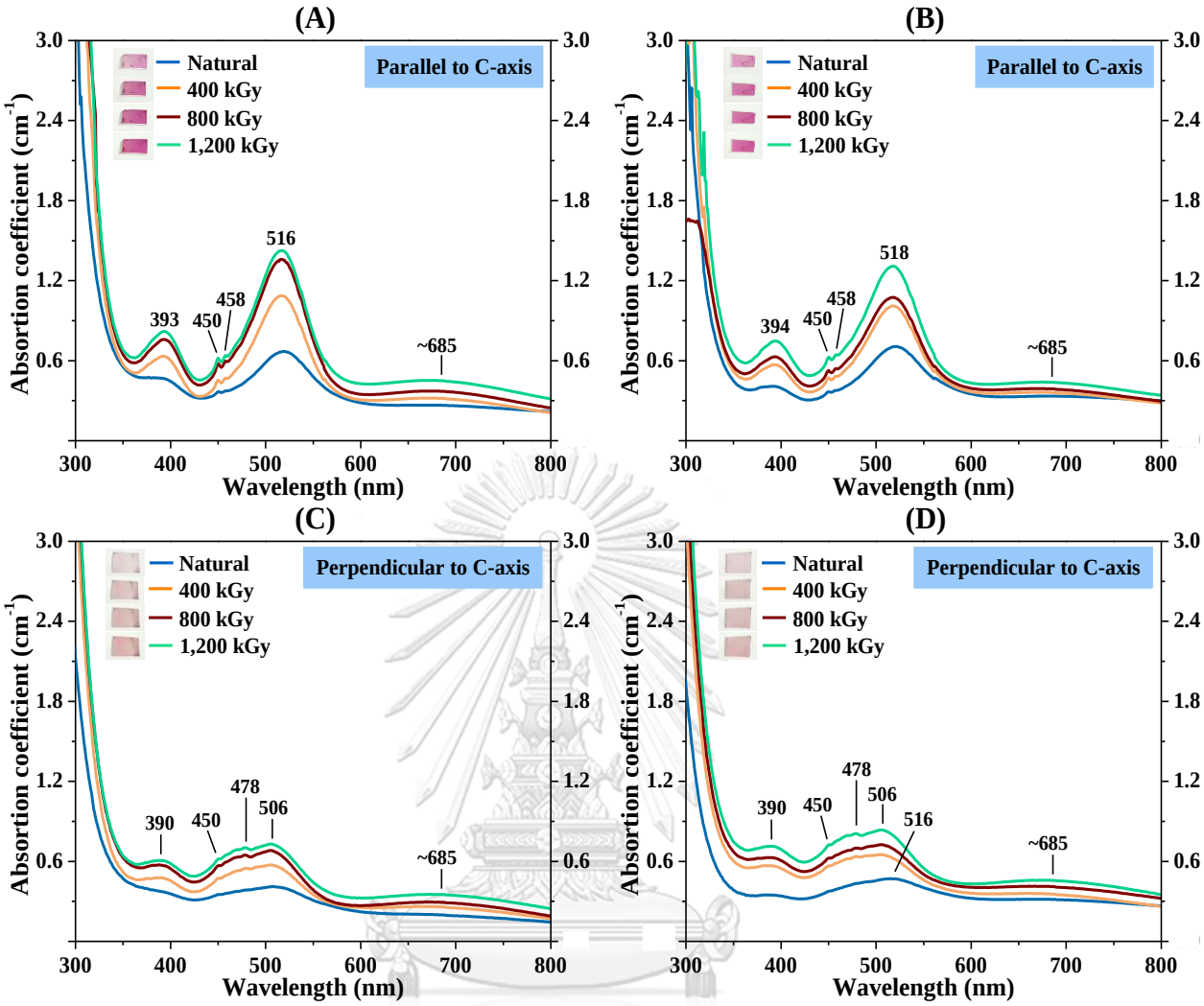

UV-Vis absorption spectra of Pk15 sample showing increasing absorption coefficients in oriented directions compared between natural and irradiated colors with different dosages: (A) e-beam irradiated color in //C-axis; (B) gamma irradiated color in //C-axis; (C) e-beam irradiated color in ⊥C-axis; (D) gamma irradiated color in ⊥C-axis.

จุฬาลงกรณ์มหาวิทยาลัย
CHULALONGKORN UNIVERSITY

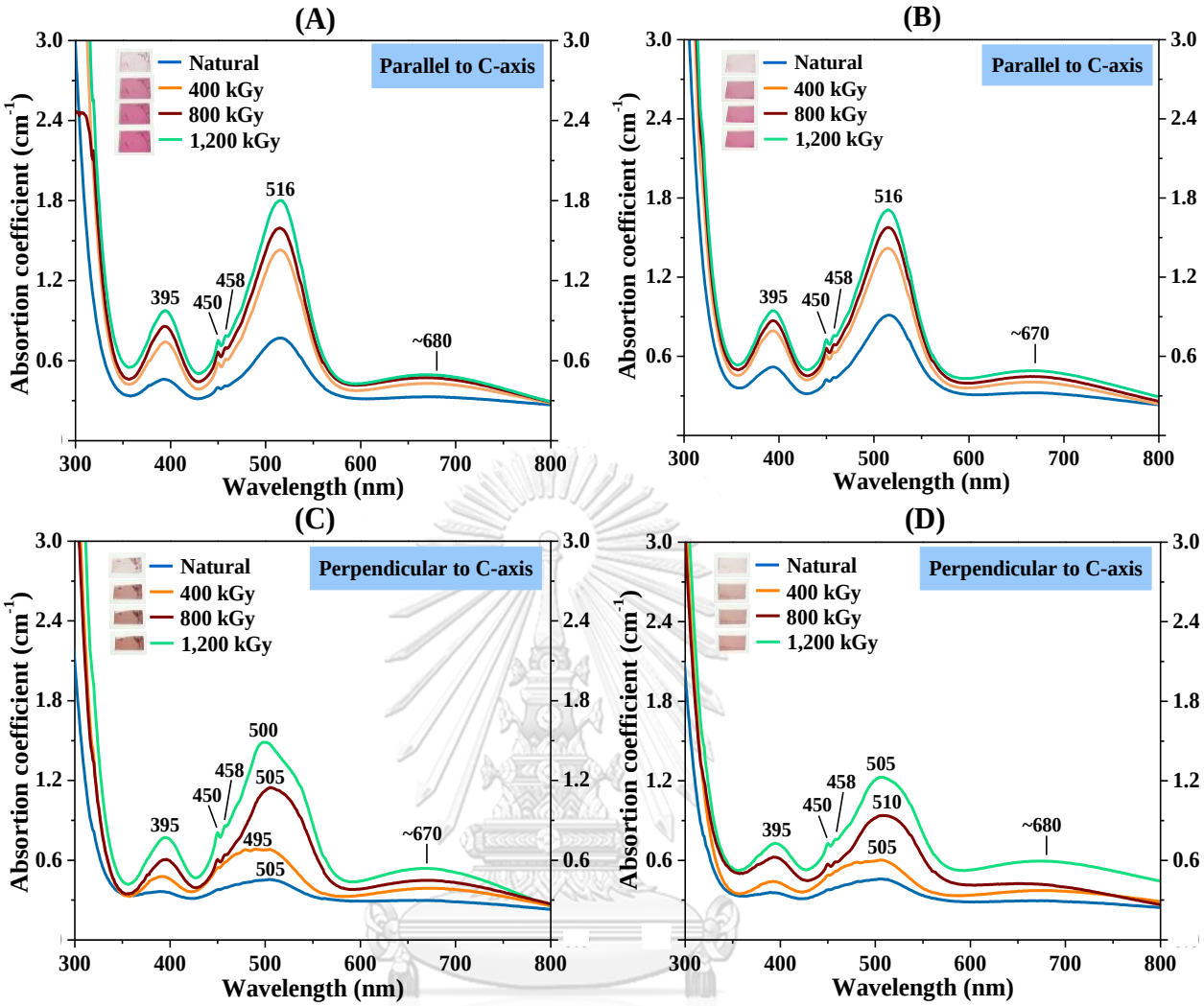

UV-Vis absorption spectra of Pk16 sample showing increasing absorption coefficients in oriented directions compared between natural and irradiated colors with different dosages: (A) e-beam irradiated color in //C-axis; (B) gamma irradiated color in //C-axis; (C) e-beam irradiated color in ⊥C-axis; (D) gamma irradiated color in ⊥C-axis.

จุฬาลงกรณ์มหาวิทยาลัย
CHULALONGKORN UNIVERSITY

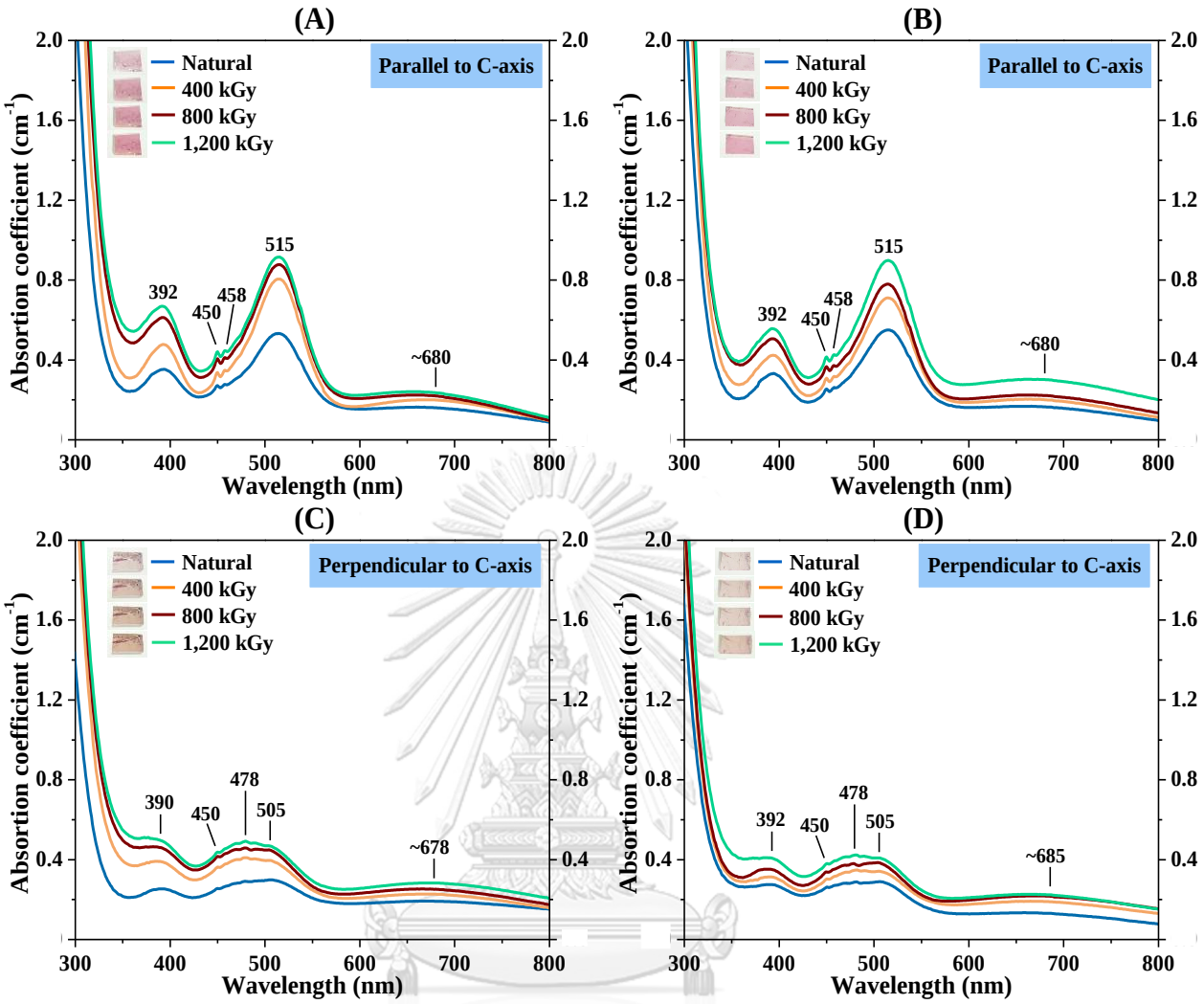

UV-Vis absorption spectra of Pk17 sample showing increasing absorption coefficients in oriented directions compared between natural and irradiated colors with different dosages: (A) e-beam irradiated color in //C-axis; (B) gamma irradiated color in //C-axis; (C) e-beam irradiated color in ⊥C-axis; (D) gamma irradiated color in ⊥C-axis.

จุฬาลงกรณ์มหาวิทยาลัย
CHULALONGKORN UNIVERSITY

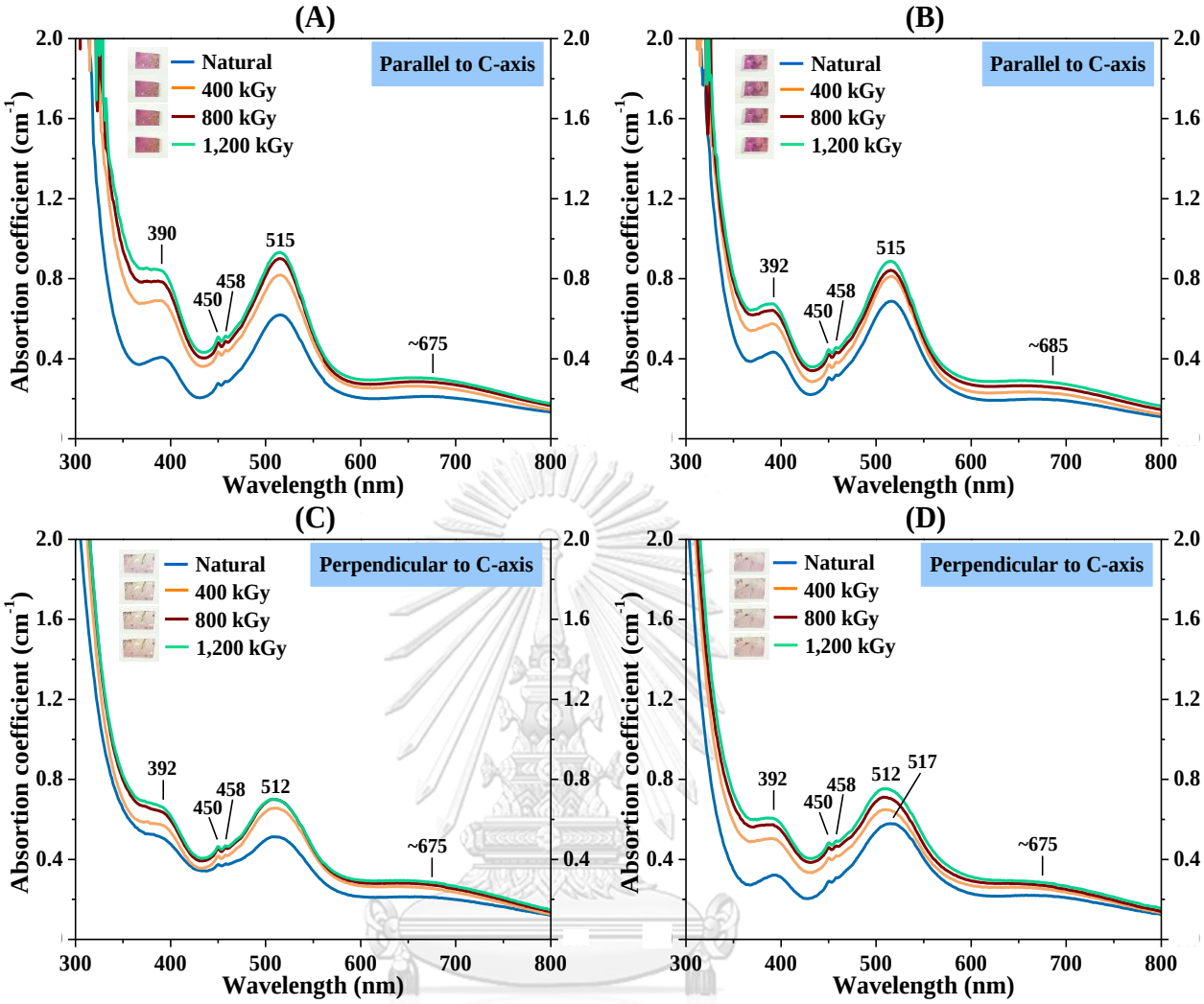

UV-Vis absorption spectra of Pk18 sample showing increasing absorption coefficients in oriented directions compared between natural and irradiated colors with different dosages: (A) e-beam irradiated color in //C-axis; (B) gamma irradiated color in //C-axis; (C) e-beam irradiated color in ⊥C-axis; (D) gamma irradiated color in ⊥C-axis.

จุฬาลงกรณ์มหาวิทยาลัย
CHULALONGKORN UNIVERSITY

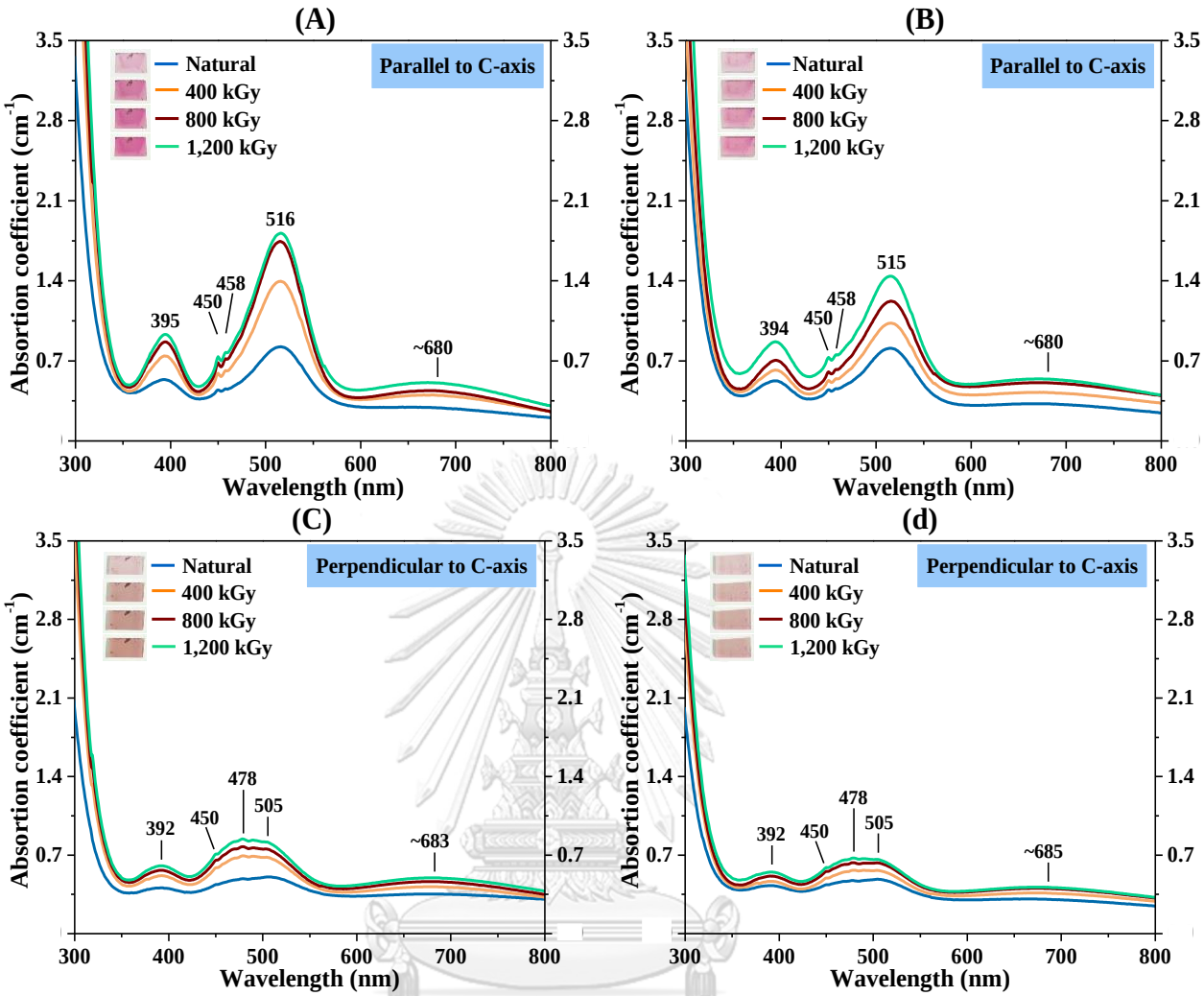

UV-Vis absorption spectra of Pk19 sample showing increasing absorption coefficients in oriented directions compared between natural and irradiated colors with different dosages: (A) e-beam irradiated color in //C-axis; (B) gamma irradiated color in //C-axis; (C) e-beam irradiated color in ⊥C-axis; (D) gamma irradiated color in ⊥C-axis.

จุฬาลงกรณ์มหาวิทยาลัย
CHULALONGKORN UNIVERSITY

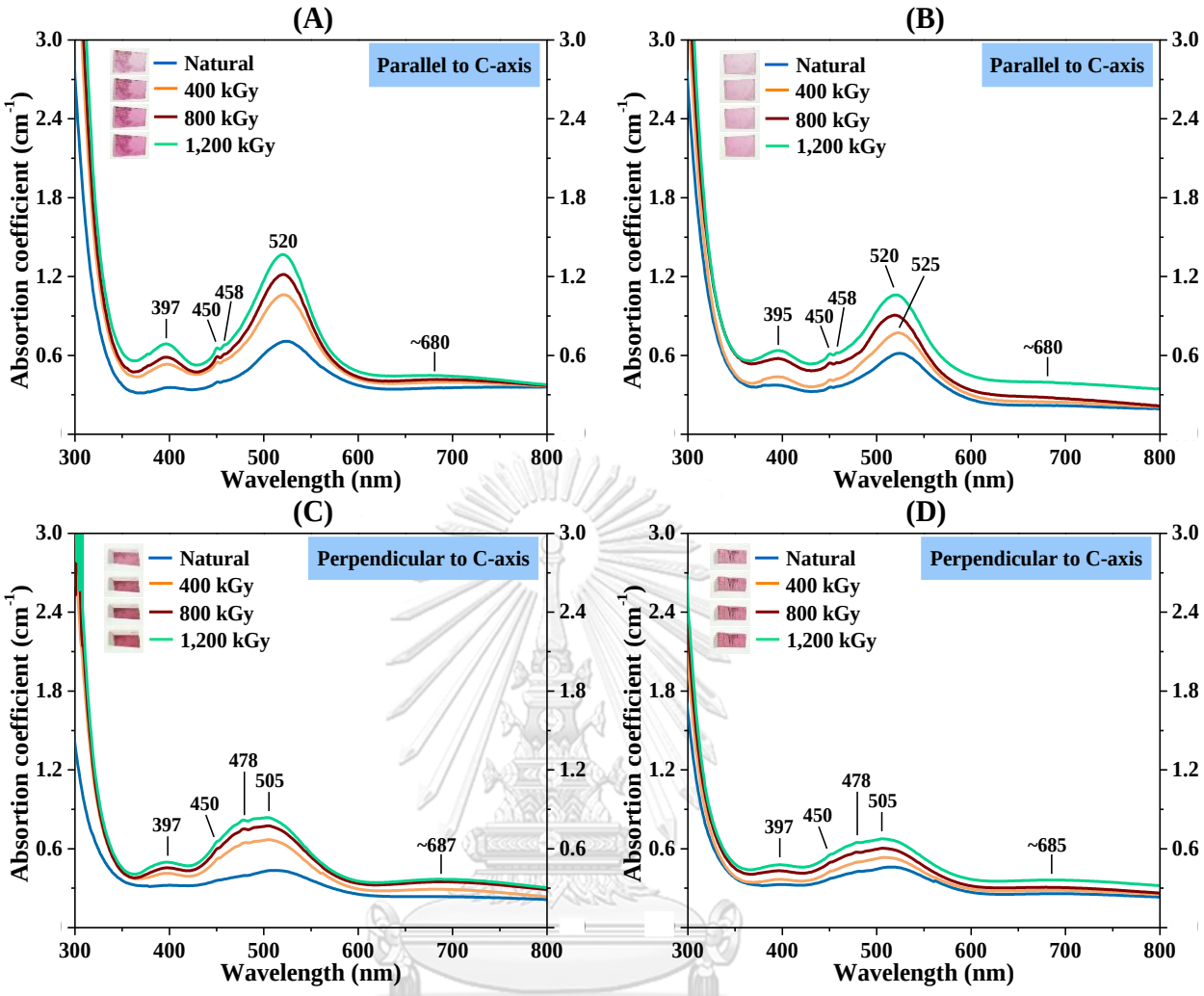

UV-Vis absorption spectra of Pk20 sample showing increasing absorption coefficients in oriented directions compared between natural and irradiated colors with different dosages: (A) e-beam irradiated color in //C-axis; (B) gamma irradiated color in //C-axis; (C) e-beam irradiated color in ⊥C-axis; (D) gamma irradiated color in ⊥C-axis.

จุฬาลงกรณ์มหาวิทยาลัย
Chulalongkorn University

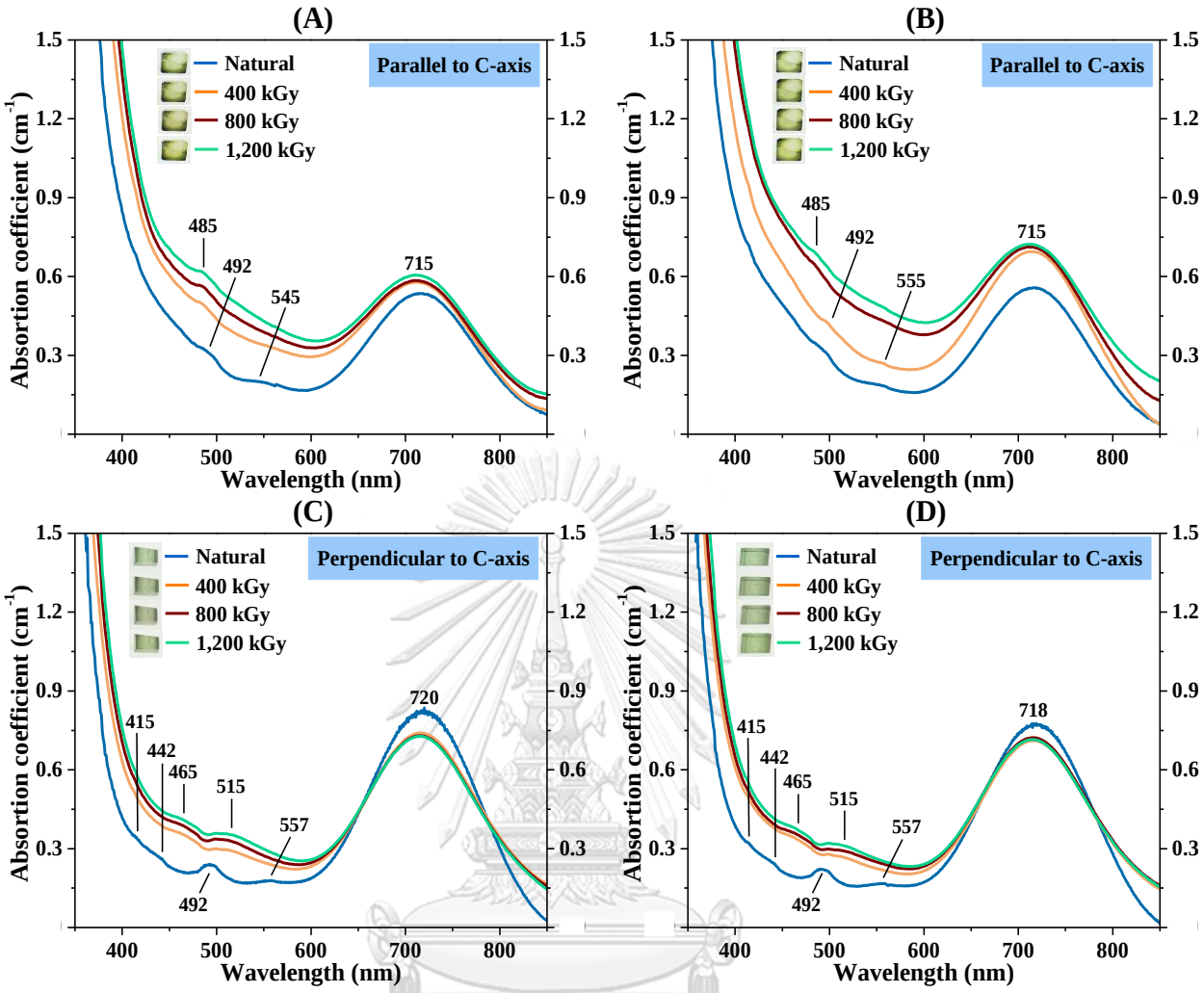

UV-Vis absorption spectra of DG01 sample showing increasing absorption coefficients in oriented directions compared between natural and irradiated colors with different dosages: (A) e-beam irradiated color in //C-axis; (B) gamma irradiated color in //C-axis; (C) e-beam irradiated color in ⊥C-axis; (D) gamma irradiated color in ⊥C-axis.

จุฬาลงกรณ์มหาวิทยาลัย
Chulalongkorn University

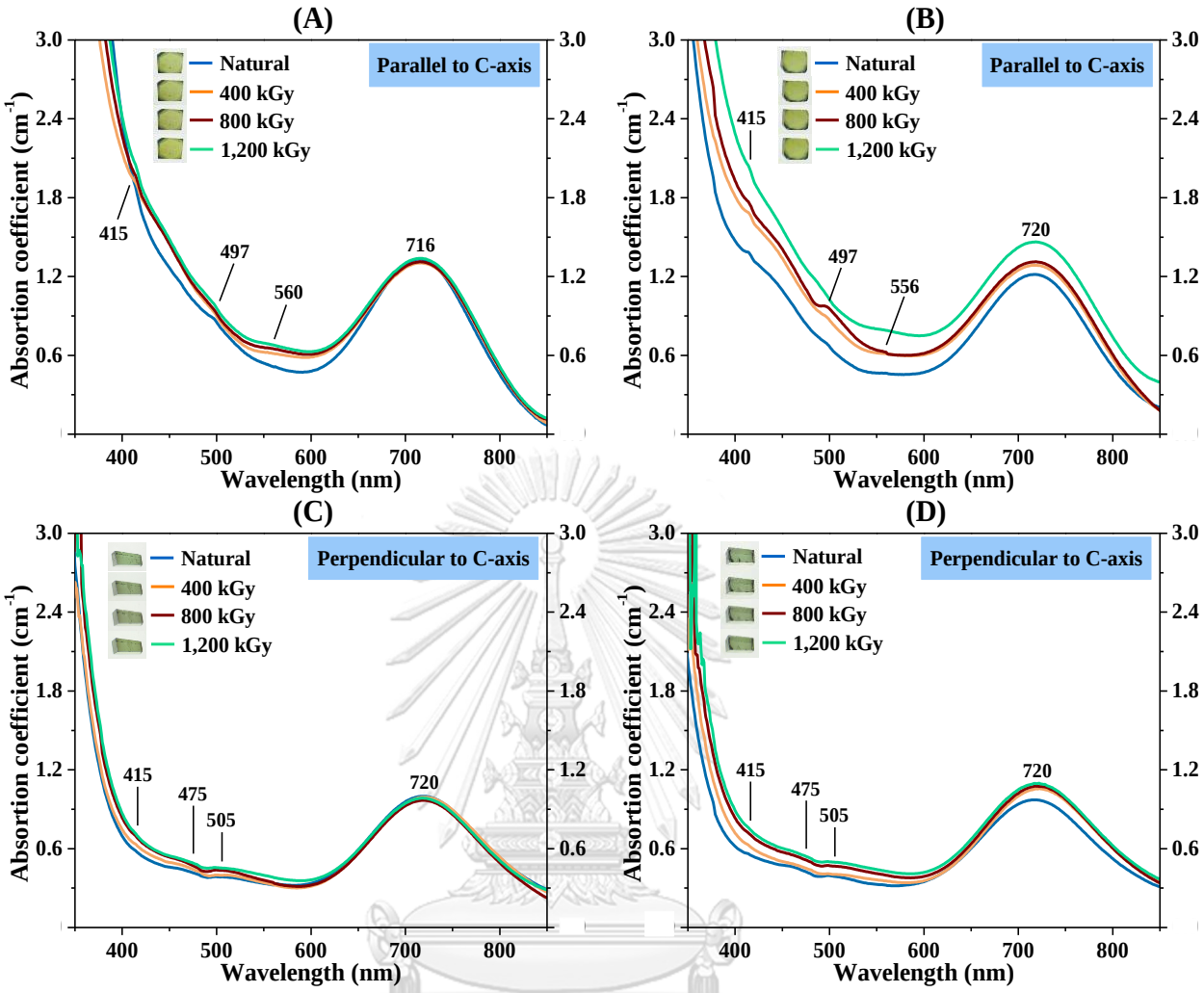

UV-Vis absorption spectra of DG03 sample showing increasing absorption coefficients in oriented directions compared between natural and irradiated colors with different dosages: (A) e-beam irradiated color in //C-axis; (B) gamma irradiated color in //C-axis; (C) e-beam irradiated color in ⊥C-axis; (D) gamma irradiated color in ⊥C-axis.

จุฬาลงกรณ์มหาวิทยาลัย
Chulalongkorn University

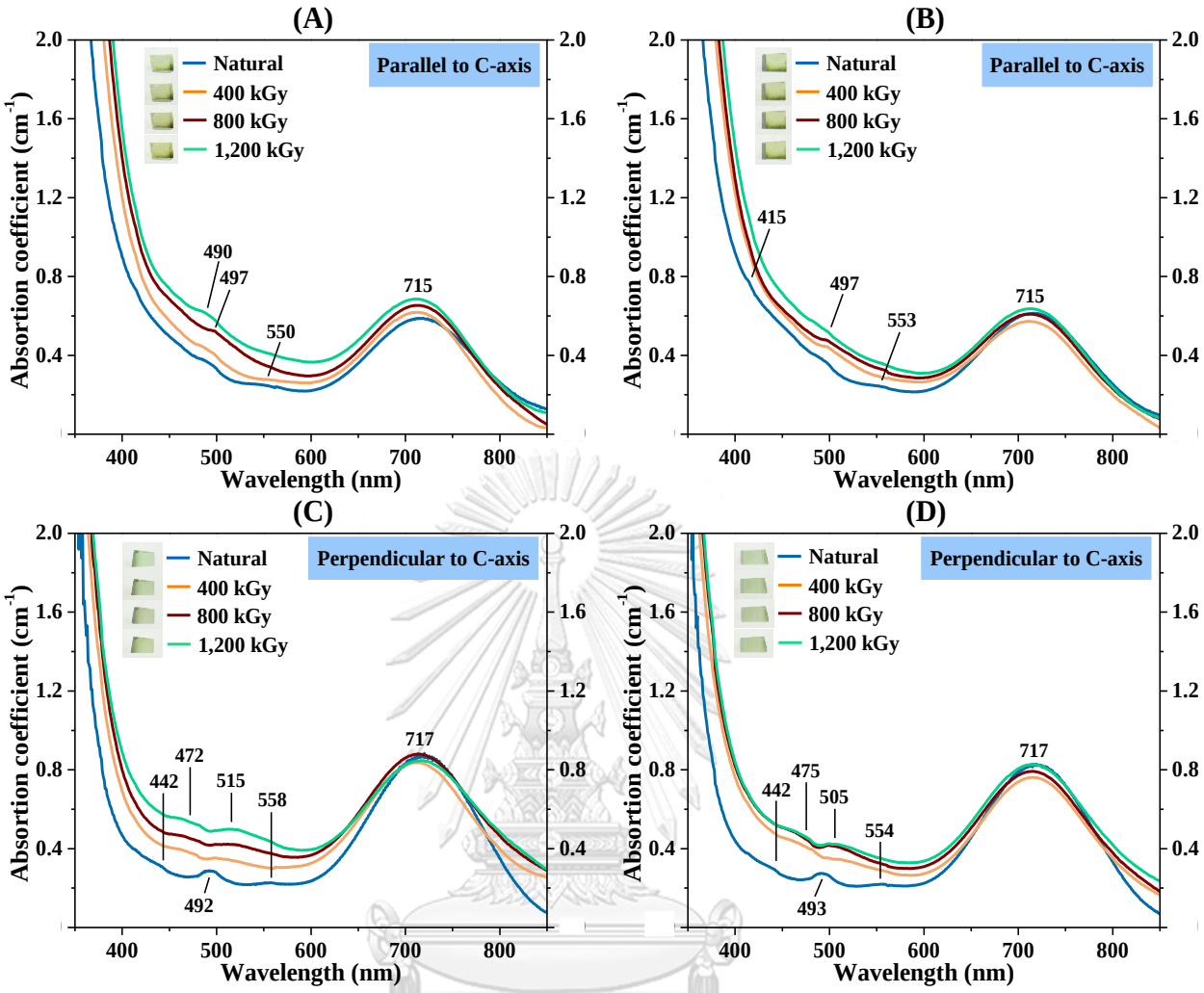

UV-Vis absorption spectra of DG04 sample showing increasing absorption coefficients in oriented directions compared between natural and irradiated colors with different dosages: (A) e-beam irradiated color in //C-axis; (B) gamma irradiated color in //C-axis; (C) e-beam irradiated color in ⊥C-axis; (D) gamma irradiated color in ⊥C-axis.

จุฬาลงกรณ์มหาวิทยาลัย
Chulalongkorn University

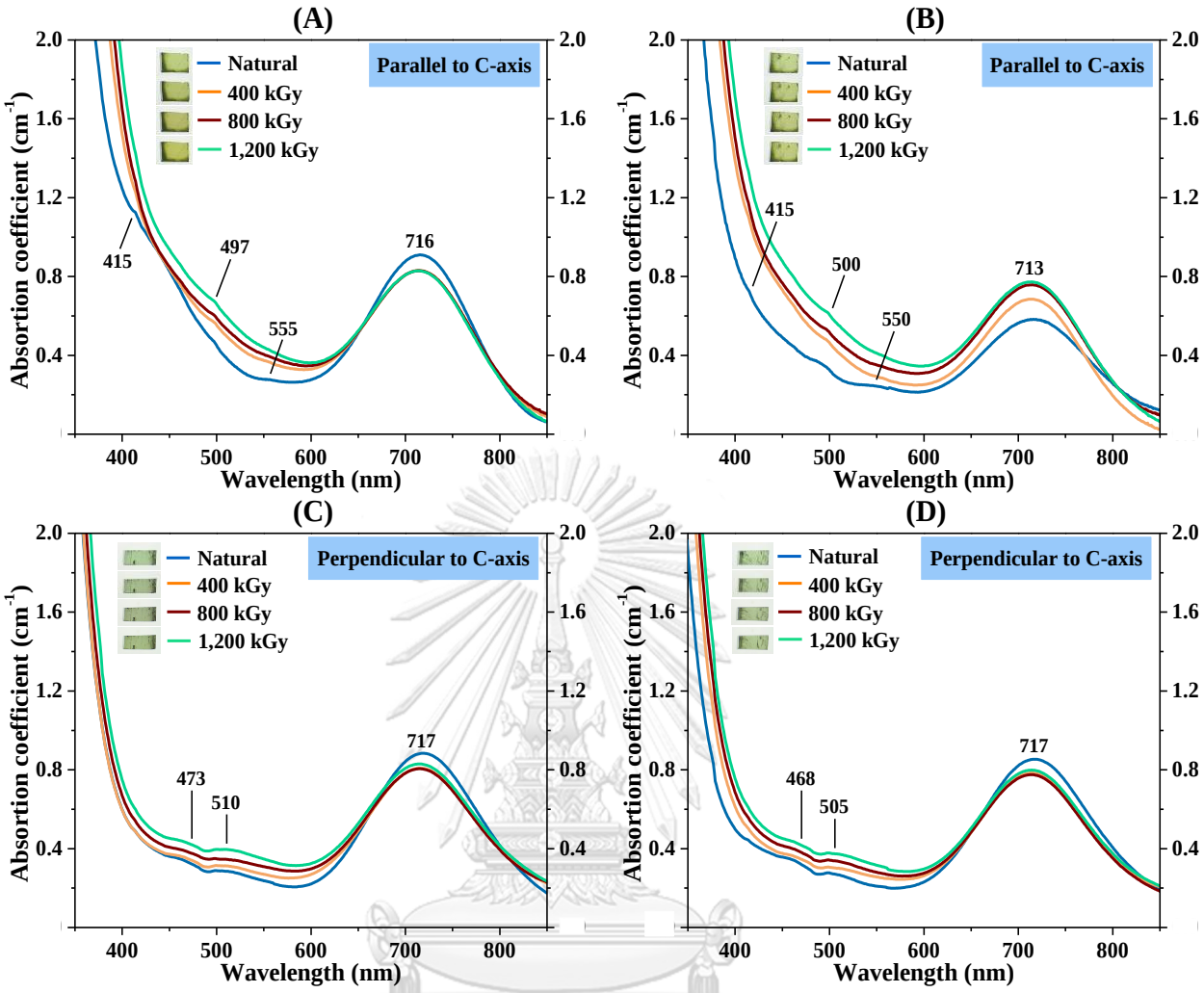

UV-Vis absorption spectra of DG05 sample showing increasing absorption coefficients in oriented directions compared between natural and irradiated colors with different dosages: (A) e-beam irradiated color in //C-axis; (B) gamma irradiated color in //C-axis; (C) e-beam irradiated color in ⊥C-axis; (D) gamma irradiated color in ⊥C-axis.

จุฬาลงกรณ์มหาวิทยาลัย
Chulalongkorn University

VITA

Miss Waratchanok Suwanmanee was born in Songkhla, Thailand on Feb 18,1995. She received Bachelor of Science degree (B.Sc.) in major of Gems and Jewelry, Faculty of Gems, Burapha University in 2017. She is currently studied in master's degree in Department of Geology at Chulalongkorn University. Nowadays, she works as research assistant at College of Creative Industry, Srinakarintrawirot University and she is also independent researcher.

จุฬาลงกรณ์มหาวิทยาลัย
CHULALONGKORN UNIVERSITY